Assessing the effect of using supercells instead of lattice blocks on multigroup cross sections of the MHTGR-350 reactor

TF Molokwane



orcid.org/ 0000-0002-1215-6200

Dissertation accepted in fulfilment of the requirements for the degree *Master of Science in Nuclear Engineering* at the North-West University

Supervisor:	Dr VV Naicker
Co-supervisor:	Ms SF Sihlangu
Co-supervisor:	Mr F Reitsma

Graduation ceremony : May 2020

Student number : 22619216

DECLARATION

I declare that the work contained in this research project is my own original work.

_____
Molokwane TF
Date: 17/12/2018

ACKNOWLEDGEMENT

I would firstly like to thank God for giving me the strength and persistence throughout this research study. Secondly, I would like to thank all my supervisors for the guidance and support throughout out this study. Your expertise and inputs made all goals reachable even in the most difficult times of this study. Special thanks also go to my family and friends for the support I have received throughout my studies.

Lastly, to the staff at NWU school of Mechanical and Nuclear Engineering, my colleagues and the NRF, all the support that I have received is acknowledged.

ABSTRACT

Uncertainty and sensitivity analysis methods are essential in nuclear reactor design and safety. These methods can be used to predict the probability distributions in output parameters, treat discreet events and handle large amounts of input data. The International Atomic Energy Agency (IAEA) initiated a co-ordinated research project (CRP) a few years ago to quantify the effect of modelling uncertainties on High Temperature Gas-cooled Reactors. This was done in parallel to a similar uncertainty analysis project on light water reactors overseen by the Nuclear Energy Agency of the Organisation for Economic Corporation and Development. The High Temperature Gas-cooled Reactors have unique features, for example the fuel comprises tri-structural-isotropic (TRISO) coated fuel particles, graphite is used as the moderator and structure material for the reactor core, and helium is used as the coolant. Thus, another important goal in addition to quantifying the uncertainty is to establish whether these differences influence the uncertainty and sensitivity propagation methodology significantly compared to those used for the Light Water Reactors cases.

In the International Atomic Energy Agency co-ordinated research project, two systems are defined based on the pebble bed design and the prismatic design. The prismatic reactor design is called the MHGTR-350.

In order to study the uncertainty quantification and associated sensitivities of the HTR, the IAEA CRP has been divided into a number of phases, with each phase in turn having a number of exercises. This dissertation is based only on exercise I-2c, which is concerned with the generation of groups constants using supercells. Other aspects of the IAEA CRP, for example, comparing the uncertainties propagated for the HTR with those of the LWRs are beyond the scope of this work.

In preparing collapsed group constants for nodal calculations, the traditional method is to use lattice calculations for the fuel blocks, in which single fuel blocks are modelled with reflective boundaries. However, the real environment of a fuel block is not an infinite array of fuel blocks, but rather has neighbouring blocks with different compositions, for example spent fuel or reflector blocks. The International Atomic Energy Agency Coordinated Research Project has an exercise (I-2c) based on modelling the fuel block within a mini-core (a supercell) to capture the uncertainties that can arise when modelling a fuel block in an infinite environment or otherwise.

In this study, the effect on the multiplication factor and the collapsed constants was studied using the definition in the benchmark document provided for exercise I-2c of the International Atomic Energy Agency Coordinated Research Project. The main sources of uncertainties

considered were the type of model (reflected fuel block or supercell), the library version (ENDF/B-VII.0 or ENDF/B-VII.1), the nuclear data uncertainties, modelling in continuous or multi-group mode and the code used.

The 4-group collapsed macroscopic cross sections of the MHTGR-350 supercells were obtained and were compared with equivalent MHTGR-350 fresh fuel block, and the difference was found to be significant. Furthermore, when comparing these differences with the uncertainties in the nuclear data, it was found that these differences were quite significant. It is therefore concluded that the model selected (fresh fuel block or supercell) generates a significantly larger uncertainty for the collapsed constants than that due to the uncertainties propagated by nuclear data uncertainties.

Keywords: supercell, fuel block, multigroup cross sections, modular high temperature gas-cooled reactor, uncertainty and sensitivity analysis, SCALE 6.2.1, KENO-VI, NEWT, TSUNAMI-3D, Sampler, multiplication factor, running average, sensitivity coefficients.

TABLE OF CONTENTS

DECLARATION ..... **I**

ACKNOWLEDGEMENT ..... **II**

ABSTRACT ..... **III**

CHAPTER 1 INTRODUCTION **1**

1.1 Background 1

1.2 The IAEA 1

1.3 The IAEA Coordinated Research Project (CRP) 2

1.4 The MHTGR-350 Reactor 2

1.5 Multigroup Cross Sections 4

1.5 Computer Codes Used in this Study 5

1.6 Uncertainty and Sensitivity Analysis 5

1.7 Research Problem Statement, Aim and Objectives 5

1.8 Layout of this Study 6

CHAPTER 2 BENCHMARK SPECIFICATIONS AND LITERATURE REVIEW **8**

2.1 Introduction 8

2.2 MHTGR-350 Reactor Core 8

2.3 The Fuel Block of the MHTGR-350 Reactor 11

2.3.1 The Fuel Particle of the MHTGR-350 Reactor 11

2.3.2 The Fuel Compact of the MHTGR-350 Reactor 12

2.3.3 Description of the MHTGR-350 Fuel Block 12

2.4 The Supercell of the MHTGR-350 Reactor 15

2.5 Unit Cell Definitions 18

2.6 Literature Studies 19

2.6.1 Results for Phase I of the IAEA Coordinated Research Project on HTGR Uncertainties [3] 19

2.6.2 Criticality Calculations of the Very High Temperature Reactor Critical Assembly Benchmark with Serpent and SCALE/KENO-VI [19] 21

2.6.3 Assessment of SCALE Capabilities for High Temperature Reactor Modelling and Simulation [20] 22

2.6.4 Uncertainty Quantification in the MHTGR-350 Fuel Compact and Block Using TSUNAMI-3D Clutch Method and Sampler [21] 22

2.6.5 Nuclear Data Uncertainty and Sensitivity Analysis of the VHTRC Benchmark using SCALE [22] 24

2.6.6 Quantifying Uncertainties of Aspects of the Neutronics modelling of the Kozloduy-6 System using Scale 6.2.1 [23] 26

2.6.7 Uncertainty and Sensitivity Analysis of Aspects of the Neutronics of a Prismatic Block-type HTGR [18]. 28

2.6.8 Neutronic Modeling of TRIGA Reactor at the University of Utah using AGENT, KENO6 and MCNP5 [27] 30

CHAPTER 3 THEORY AND CODES USED 32

3.1 Introduction 32

3.2 Nuclear Reactions and Cross Sections 32

3.2.1 Nuclear Reactions 32

3.2.2 Nuclear Cross Sections 33

3.2.3 Resonance Cross Section and Doppler Broadening 33

3.2.4 Evaluated Nuclear Data Libraries 37

3.3 Neutron Transport Equations 37

3.3.1 Boltzmann Transport Equation 37
3.3.2 Time-independent Boltzmann Transport Equation 38
3.3.3 The Extended Step Characterization method 39
3.3.4 The Multiplication Factor 42
3.3.5 Monte Carlo Methods 42
3.3.6 Convergence of Monte Carlo Methods 43
3.4 Collapsing of Cross Sections 44
3.4.1 Generation of Cross Sections 44
3.4.2 Collapsed Multigroup Cross Sections 45
3.5 The Concepts of Uncertainty and Sensitivity Analysis 46
3.5.1 General Statistics 47
3.5.2 Sensitivity Analysis Methods 48
3.5.3 Propagation of Uncertainties 49
3.5.3.1 The CLUTCH method 49
3.5.3.2 Statistical Sampling 52
3.6 Codes Used 54
3.6.1 KENO-VI 54
3.6.2 NEWT 55
3.6.3 TSUNAMI-3D 56
3.6.4 SAMS 56
3.6.5 Sampler 56

CHAPTER 4 RESEARCH METHODOLOGY 58

4.1 Introduction 58

4.2 Criticality Studies 58
4.2.1 Tools Used 58
4.2.2 Models used 58
4.2.3 Convergence Criteria 61
4.3 Self Shielding 61
4.4 Cross Section Collapsing 65
4.5 Uncertainty and Sensitivity Analysis Assessment 67
4.5.1 Computer Tools used 67
4.5.2 Models Used 67
4.5.3 Convergence criteria 67
4.6 Analysing of Results 68
4.6.1 Criticality Results 68
4.6.2 Self-shielding Results 69
4.6.3 Cross Section Collapsing Results 69
4.6.4 Uncertainty and Sensitivity Analysis Results 69

CHAPTER 5 RESULTS AND DISCUSSION 72
5.1 Introduction 72
5.2 Criticality Results 72
5.2.1 Criticality Results of the MHTGR-350 Fresh Fuel Block 72
5.2.2 KENO-VI Criticality Results of the MHTGR-350 Supercell Models 73
5.2.3 NEWT Criticality Results of the MHTGR-350 Supercell Models 76
5.2.4 Comparison of the Multiplication Factor Results of the KENO-VI MG and NEWT Models of the MHTGR-350 Supercells 77

5.3 Self-shielding Studies 78

5.4 Collapsed Cross Sections of the MHTGR-350 Supercell 79

5.4.1 The 4-Group Macroscopic Cross Sections of the NEWT MHTGR-350 Supercell Models 79

5.4.2 Comparison of the 4-group Macroscopic Cross Sections of MHTGR-350 Fresh Fuel Block and Supercell models 81

5.5 Results of Uncertainty and Sensitivity Analysis Assessment 93

5.5.1 TSUNAMI-3D Results of the MHTGR-350 Supercell Model 93

5.5.2 TSUNAMI-3D Results of the MHTGR-350 Fresh Fuel Block 96

5.5.3 Comparison of TSUNAMI-3D Results of the MHTGR-350 Fresh Fuel Block and Supercell 97

5.5.4 Sampler Results of the MHTGR-350 Fresh Fuel Block and Supercell Models 101

5.5.5 Comparison of TSUNAMI-3D and Sampler Results 102

5.5.6 Uncertainty in the Macroscopic Cross Sections 102

5.6 Contributors to Uncertainty in the Multiplication Factor 112

CHAPTER 6 CONCLUSION AND RECOMMENDATIONS 113

6.1 CONCLUSION 113

6.2 Recommendations 114

BIBLIOGRAPHY 116

APPENDIX A 121

LIST OF TABLES

Table 1: Characteristics of the MHTGR-350 reactor..... 4

Table 2: TRISO coated fuel particles and fuel block dimensions 13

Table 3: Number densities of the MHTGR-350 fresh fuel block 14

Table 4: Operating conditions of the MHTGR-350 fresh fuel block 15

Table 5: Number densities of the reflector region 17

Table 6: Operating conditions of the MHTGR-350 simplified supercell..... 18

Table 7: Reference CE results of the multiplication factor with Serpent 2.1.26..... 24

Table 8: The four-group energy structure 65

Table 9: Example of nuclide-reaction pairs applicable to this work 71

Table 10: Multiplication factor k results of the MHTGR-350 fresh fuel blocks..... 73

Table 11: Multiplication factor results of the of the KENO-VI MHTGR-350 supercell model 75

Table 12: MHTGR-350 supercell multiplication factor results obtained with NEWT..... 76

Table 13: KENO-VI MG and NEWT multiplication factor k results of the MHTGR-350 Supercell models 77

Table 14: Collapsed macroscopic cross sections of the MHTGR-350 supercells 80

Table 15: Macroscopic cross section of the MHTGR-350 fresh fuel block and supercell 81

Table 16: Uncertainty in multiplication results for the MHTGR-350 supercells 93

Table 17: Top seven contributors to uncertainty in multiplication factor for MHTGR-350 supercell using ENDF/B-VII.0 95

Table 18: Top seven contributors to uncertainty in multiplication factor for MHTGR-350 supercell using ENDF/B-VII.I 95

Table 19: Uncertainty in multiplication factor k results for the MHTGR-350 fresh fuel blocks 97

Table 20: Top seven contributors to uncertainty in multiplication factor k for MHTGR-350 fresh fuel blocks..... 97

Table 21: Uncertainty in multiplication factor results for the MHTGR-350 fresh fuel block and supercell..... 98

Table 22: Comparison of the order sensitivity coefficients of the ENDF/B-VII.0 nuclear data library 99

Table 23: Comparison or the order sensitivity coefficients of the ENDF/B-VII.I nuclear data library 100

Table 24: Uncertainty in multiplication factor results for the MHTGR-350 fresh fuel block and supercell..... 101

Table 25: Uncertainty in macroscopic cross section of the MGTGR-350 fresh fuel block and supercell..... 104

Table 26: Macroscopic cross section uncertainties due to nuclear data uncertainties . 105

LIST OF FIGURES

Figure 1: Axial unit layout of the MHTGR-350 reactor 3

Figure 2: MHTGR-350 reactor core layout (plane view) 9

Figure 3: MHTGR-350 reactor core layout (axial view) 10

Figure 4: The structure of the TRISO coated fuel particle 11

Figure 5: The fuel pin of the MHTGR-350 reactor 12

Figure 6: (a) The fresh fuel block with B_4C burnable poisons compacts and (b)depleted fuel block 13

Figure 7: The supercell of the MHTGR-350 reactor 16

Figure 8: Simplified representation of a supercell 17

Figure 9: Eigenvalue sensitivity to the capture cross section of graphite determined using TSUNAMI CE 25

Figure 10: Cross section of c-graphite (n,γ) for ENDF/B-VII.0 and ENDF/B-VII.1 nuclear data libraries 29

Figure 11: cross section of c-graphite (n,n') for ENDF/B-VII.0 and ENDF/B-VII.1 nuclear data libraries 29

Figure 12:Capture cross section of ^{238}U 34

Figure 13: Temperature broadening of the ψ function 36

Figure 14: A Typical rectangular cell used in the step characteristic approach 40

Figure 15: Orientation of the sides of a cell with respect to a given direction vector 42

Figure 16: Multigroup energy structure 45

Figure 17: Probability distributions for a discrete or continuous random variable X. 53

Figure 18: Cross Sectional view of the uniformly distributed (a) TRISO fuel particles in the fuel compact and (b) BP's in the BP compact 59

Figure 19: KENO-VI model of the MHTGR-350 supercell 61

Figure 20: a) TRISO fuel particle, b) fuel compact and c) the MHTGR-350 fresh fuel block 64

Figure 21: $F*(r)$ meshes for the MHTGR-350 supercell 68

Figure 22: Fission macroscopic cross section data set for the MHTGR-350 fuel 83

Figure 23: Scattering macroscopic cross section data set for the MHTGR-350 fuel compact 84

Figure 24: MHTGR-350 fresh fuel block showing unit cell numberings from 1 to 11 84

Figure 25: Flux distribution for the MHTGR-350 fresh fuel compact 86

Figure 26: Flux distribution for the MHTGR-350 supercell 86

Figure 27: Five individual fluxes from collapsed energy group-1 88

Figure 28: Five individual fluxes from collapsed energy group-2 89

Figure 29: Five Individual fluxes from collapsed energy group-3 90

Figure 30: Five individual fluxes from energy group-4 91

Figure 31: Individual fluxes for energy groups-142 to 153 92

Figure 32: Sensitivity plot of graphite (n,γ)/graphite n,γ reactions 96

Figure 33: sensitivity plot for $^{235}U(v)$/ $^{235}U(v)$ reactions 100

Figure 34: Sensitivity plot for $^{238}U(n,\gamma)$/ $^{238}U(n,\gamma)$ reactions 101

Figure 35: The running average of the multiplication factor and its associated standard deviation 106

Figure 36: The running average of group-4 $\Sigma fiss$ and its associated standard deviation 107

Figure 37: The running average of group-1 Σtot and its associated standard deviation 108

Figure 38: The running average of group-2 $\Sigma tot$and its associated standard deviation 109

Figure 39: The running average of group-3 Σtot and its associated standard deviation 110

Figure 40: The running average of group 4 Σtot and its associated standard deviation 111

Acronyms

1D	One dimensional
2D	Two dimensional
3D	Three dimensional
AC	Active Core
BISO	Bi-structural Isotropic
BONAMI	Bondarenko AMPX
BP	Burnable Poison
CE	Continuous Energy
CENTRM	Continuous Energy Transport Module
CRP	Coordinated Research Project
CSAS6	Criticality Safety Analysis Sequence
CZP	Cold Zero Power
EG	Energy Group
ENDF	Evaluated Nuclear Data File
FB	Fuel Block
GA	General Atomics
HPF	Hot Full Power
HTGR	High Temperature Gas-Cooled Reactor
IAEA	International Atomic Energy Agency
INL	Idaho National Laboratory
IPyC	Inner Pyrolytic Carbon
LBP	Lumped Burnable Poison
LWR	Light Water Reactor
MG	Multigroup
MHTGR	Modular High Temperature Gas-Cooled Reactor
MW	Megawatt
NEA	Nuclear Energy Agency
NEWT	New ESC-based Weighting Transport code
OECD	Organisation for Economic Corporation and Development
OPyC	Outer Pyrolytic Carbon
ORNL	Oak Ridge National Laboratory
RPV	Reactor Pressure Vessel
SAMS	Sensitivity Analysis Module of SCALE
SC	Supercell
SCALE	Standardized Computer Analyses for Licensing Evaluation
SiC	Silicon Carbide
TRISO	Tri-structural-Isotropic
TSUNAMI	Tool for Sensitivity and Uncertainty Analysis Implementation
UAM	Uncertainty Analysis in Modelling
UCO	Uranium Oxicarbide
VHTRC	Very-High Temperature Reactor Critical Assembly
XSProc	Material and Cross Section Processing

CHAPTER 1 INTRODUCTION

1.1 Background

The use of fossil fuels such as coal, oil and natural gases by the energy sector to produce electricity releases greenhouse gasses during combustion of these fossil fuels. As an attempt to reduce the greenhouse gasses in our environment, alternative ways of producing electricity are being implemented. Generating electricity from nuclear energy reduces pollution and can be taken as an alternative. However, the drawbacks of nuclear energy production need to be considered. These include long-term storage of nuclear waste, the fact that uranium is a non-renewable resource and the probability of a nuclear accident occurring [1] [2].

Currently South Africa has two nuclear reactors and produces approximately 5% of the country's electricity from the Koeberg nuclear power plant. Plans are underway to build other nuclear power plants, with possible construction sites being identified [1]. However, the date of implementation has recently become a discussion point. South Africa also has a long-term nuclear waste storage facility at Vaalputs in the Northern Cape Province.

As a result of nuclear accidents that have occurred in the past, for example Fukushima Daiichi in 2011 and Chernobyl in April 1986, nuclear power has lost favour in the general public's view. Despite this, it is worth noting that new generations of reactors are built with enhanced safety measures that give little or no room for an accident to occur. This has been achieved by conducting extensive research throughout the world on safety and design of nuclear reactors. This should eradicate the fear of the public.

This study is based on the International Atomic Energy Agency Coordinated Research Project (IAEA CRP) on High Temperature Gas-Cooled Reactor (HTGR) uncertainties [3]. This is an ongoing research project aimed at improving its ability to quantify the uncertainties in the safety and design analysis of HTGRs.

1.2 The IAEA

This section gives a brief discussion of the IAEA. The IAEA is a global organisation that was established in July 1957. It was established as an autonomous organisation, meaning it has the freedom to govern itself within the United Nations system. The IAEA, starting with 68 member states at the time of its establishment in 1957, has grown its membership over the years to around 150 member states in 2010 [4].

The IAEA is an organisation that seeks to actively encourage and promote peaceful uses of nuclear energy and has the objective of preventing the use of nuclear energy for military purposes [5]. To achieve the goal of the peaceful use of nuclear energy, the IAEA carries out the following functions, as authorised by its statute: (i) To promote and assist in the research, development and practical application of atomic energy for peaceful uses in the world (ii) To encourage the exchange of scientific and technical information throughout the world on the peaceful uses of atomic energy [4].

1.3 The IAEA Coordinated Research Project (CRP)

The IAEA CRP is an important tool for organising research work to achieve a specific objective consistent with the IAEA programmes. The CRP is developed on the basis that different institutions agree to work together on a well-defined research topic in line with the IAEA framework, thereby presenting an effective way of bringing researchers from different countries together to allow comparison and assessment to solve problems and give recommendations for furthering the development of these solutions [6]. The goal for developing the CRP is to research, gather and provide information for current and new generations of nuclear plants (facilities) [3].

In February 2009, the technical working group on gas cooled reactors of the IAEA recommended the implementation of the CRP on High Temperature Gas-Cooled Reactor (HTGR) Uncertainty Analysis in Modelling (UAM) [3]. The IAEA CRP on HTGR UAM is a tool that continues from the previously established IAEA and Organisation for Economic Corporation and Development/ Nuclear Energy Agency (OECD/NEA) international activities on validation and verification using the analysis abilities of HTGR simulations for safety and design evaluations. The CRP is divided into four phases and within each phase there are detailed descriptions of exercises to be done. These exercises are performed by considering all sources of uncertainty [7].

This study is based on exercise I-2c of phase I, which is titled, “Supercell (mini-core) lattice calculation”, of the IAEA CRP on HTGR uncertainties [3]. This exercise involves modelling of the MHTGR-350 supercell, which shall be defined later in this study.

1.4 The MHTGR-350 Reactor

The Modular High Temperature Gas-Cooled Reactor (MHTGR-350) is a General Atomics (GA) generation-IV reactor design which was developed in the 1980s, with a thermal power of 350 MW. This prismatic modular reactor consists of the annular configured core within the reactor vessel with inlet and outlet core temperatures of 259^{o}C and 687^{o}C respectively. Prismatic

hexagonal blocks fuelled with Uranium Oxycarbide (UCO) in compacts make up the reactor core, and helium is used as a coolant [8]. The reflectors, neutron control system, shutdown cooling heat exchanger and core support structures are also contained in the reactor vessel. The helically coiled steam generator, together with the motor-driven circulator, is housed in the steam generator vessel. Figure 1 shows an axial unit layout of the MHTGR-350 reactor, and Table 1 provides the main characteristics of the MHTGR-350 reactor. The MHTGHR-350 reactor is the reference reactor for this study.

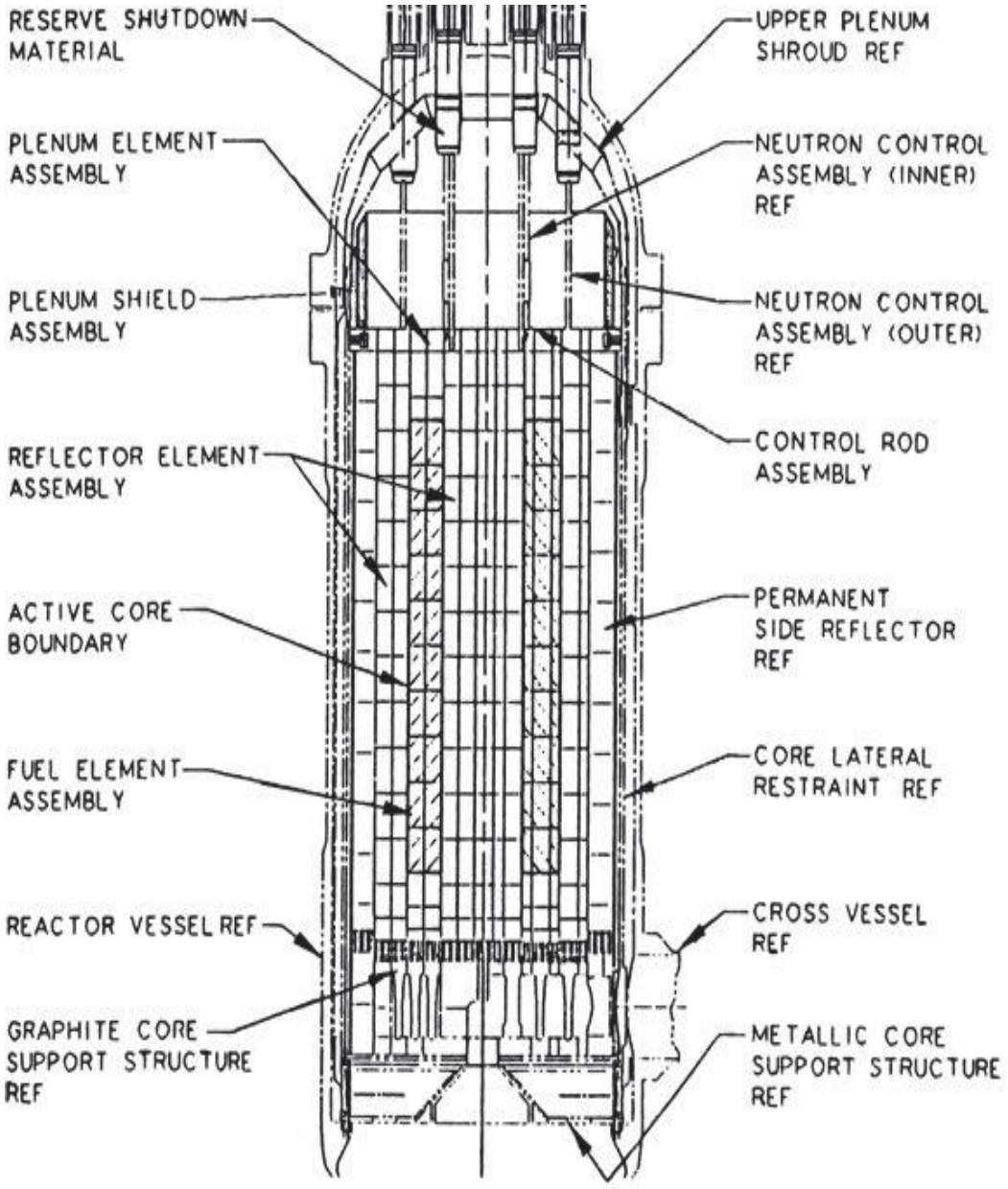


Figure 1: Axial unit layout of the MHTGR-350 reactor

Source: [9]

Table 1: Characteristics of the MHTGR-350 reactor

Characteristic	Value
Thermal capacity	350 MW
Electric capacity	165 MW
Core configuration	Annular
Fuel	Prismatic hexagonal block fuelled with UCO fuel compacts of 15.5 wt% enriched Uranium (average)
Control rods	B_4C granules uniformly dispersed in graphite matrix formed into annular shapes
Primary Coolant	Helium
Primary coolant pressure	6.39 MPa
Moderator	Graphite
Core outlet temperature	687^oC
Core inlet temperature	259^oC
Mass flow rate	157.1 kg/s
Reactor vessel height	22 m
Reactor vessel outside diameter	6.8 m

1.5 Multigroup Cross Sections

In reactor physics, the multigroup neutron cross sections are the basis for the probability information on nuclear interactions for most deterministic codes, which include discrete ordinates, diffusion theory and nodal diffusion theory codes. Normally the so-called continuous energy libraries are used to obtain fine-group cross sections considering at most only unit cell geometries. In subsequent lattice calculations, the geometry of the lattice (for example the fuel assembly) is considered by condensing the fine-group cross sections into a few group cross sections that are homogenised over particular regions [10].

In Monte Carlo codes, multigroup cross sections can also be used to decrease the running time of the calculations and perform adjoint calculations, although such solutions would not have the same high fidelity as a calculation that could be performed in continuous energy (CE) Monte-Carlo mode.

In this study, multigroup cross sections of the MHTGR-350 supercell models will be assessed relative to the single MHTGR-350 fresh fuel block multigroup cross sections utilising the New ESC-based Weighting Transport (NEWT) code and Sampler [11] mentioned in Section 1.6.

1.5 Computer Codes Used in this Study

The MHTGR-350 supercell models are developed using KENO-VI, NEWT, Tool for Sensitivity and Uncertainty Analysis Implementation (TSUNAMI-3D) and Sampler. In this study, these are codes within the Standardised Computer Analyses for Licensing Evaluation (SCALE6.2.1) code package [11]. KENO-VI is a Monte Carlo code. NEWT is a multigroup discrete-ordinate transport code. TSUNAMI-3D is a code that facilitates the application of uncertainty and sensitivity analysis theory to criticality safety analysis. Sampler is a code that performs general uncertainty analysis by using statistical treatment.

1.6 Uncertainty and Sensitivity Analysis

Uncertainty and sensitivity analysis methods can be used to assess the predictive capability of coupled neutronics/thermal-hydraulics and depletion simulations of the reactor design analysis and safety analysis. Thus, uncertainty and sensitivity analysis must be considered as an essential component of coupled code methods [12]. Uncertainty analysis tries to give a detailed account of the entire set of possible model outcomes (outputs), together with their associated probabilities of occurrence. Uncertainties originate from errors in physical data, modelling, computational algorithms and manufacturing. Sensitivity analysis measures the change in the model output in an assigned region of interest of the space of inputs [3] [8].

Uncertainty and sensitivity analysis calculations are performed in this study as a requisition from the benchmark. TSUNAMI-3D and Sampler are used for uncertainty and sensitivity models.

1.7 Research Problem Statement, Aim and Objectives

Research problem statement:

In recent uncertainty and sensitivity studies, it has been shown that the uncertainty due to the nuclear data on the multiplication factor is significant. However, other uncertainties must also be considered. One such uncertainty is due the environment considered when calculating the group constants used in core calculations. The group constants are macroscopic cross sections and other associated parameters.

These groups constants are calculated in so called lattice calculations. The lattice calculation is traditionally a single block calculation with reflective boundary conditions. This is effectively an

infinite lattice of identical fuel blocks. However, the fuel blocks in a real reactor core is not an infinite radial system. The neighbourhood of each fuel block will change, depending on its position in the core, and burnup history. In the literature it is proposed that supercells be used rather than single fuel blocks to calculate these group constants. The supercell consists of fresh fuel blocks, depleted fuel blocks and graphite reflector blocks. The fuel block in which group constants need to be calculated is then placed at the centre of the supercell.

It is therefore necessary to investigate whether the environment of the fuel blocks significantly influences calculation of the group constants.

As mentioned above, when these parameters together with their uncertainties are passed to subsequent core calculations, and the effect on the resulting core calculations can then be assessed.

The study will therefore aim to quantify the uncertainty propagated on the group constants in terms of the nuclear data against that due the uncertainty of using different environments for the lattice calculations.

Research aim:

To investigate the effect of neighbouring blocks on a typical lattice calculation and address uncertainties due to the basic nuclear data on these two models.

Research objectives:

- Build lattice supercell models using KENO-VI (CE and MG) and NEWT;
- Calculate and compare multiplication factors;
- Extract cross sections and compare;
- Build uncertainty models and propagate the associated uncertainties;
- Analyse results.

1.8 Layout of this Study

CHAPTER 2- Benchmark Specifications and Literature Review

This chapter presents the benchmark specifications followed in achieving the goals of this study. Previously conducted studies that are in line with this study are also presented.

CHAPTER 3- Theory

This chapter presents the theory that formed the basis of this study and a description of the SCALE 6.2.1 code package.

CHAPTER 4- Methodology

This chapter presents the steps which were followed in building the MHTGR-350 supercell models using the SCALE 6.2.1 code package.

CHAPTER 5 -Results and Discussion

This chapter presents all results obtained in this study and a discussion thereof.

CHAPTER 6 -Conclusion and Recommendations

This chapter concludes all the work done in this study and outlines the recommendations for future work related to this study.

CHAPTER 2 BENCHMARK SPECIFICATIONS AND LITERATURE REVIEW

2.1 Introduction

This chapter presents the IAEA CRP on HTGR uncertainties benchmark specifications for the reference MHTGR-350 reactor design. Since this study is mainly focused on the MHTGR-350 supercell and fresh fuel block, the specifications for the fresh fuel block and supercell are further presented for the development of models, simulations and evaluation processes. Studies which were conducted by other researchers that are in line with this study, are also presented in this chapter, for comparison and to show relevance to this study.

2.2 MHTGR-350 Reactor Core

The MHTGR-350 reactor core is annular and designed to provide 350 MW at an average power density of 5.9 MW/m^3. Figure 2 shows the plane view of the MHTGR-350 core layout and Figure 3 shows the axial view. From Figure 2, it is observed that the reactor core is made up of an array of hexagonal fuel blocks and graphite replaceable blocks. The centre of the core consists of hexagonal replaceable graphite blocks. These hexagonal blocks, which are identical in size, are arranged cylindrically and are surrounded by a ring of solid permanent graphite reflector blocks. All these blocks are within the Reactor Pressure Vessel (RPV). Within the permanent reflector elements, a 10 cm thick borated region is contained at the outer boundary, next to the core barrel. The core barrel is located adjacent to the outermost boundary of the permanent graphite reflector blocks. The borated region contains boron carbide (B_4C) particles in the shape of spheres. B_4C is a neutron absorber and can absorb neutrons without resulting in radionuclides of longer half-lives [8] [9].

The Active Core (AC) is made of hexagonal graphite fuel blocks, with each graphite fuel block containing blind holes for fuel compacts and full-length channels for the flow of helium, which is the coolant. The hexagonal fuel blocks are stacked to form columns, each column consisting of ten hexagonal fuel blocks and resting on support structures. The columns of the active core form a three-row annulus with the hexagonal graphite columns in the inner and outer regions as shown in the axial view of the MHTGR-350 core layout in Figure 3. Thirty graphite reflector columns contain control rod channels and twelve other columns in the core contain reserve shut-down material channels. This can be seen in Figure 2. The annular shaped active core radial thickness is specified to ensure that all shutdown and operating control rods are located in the reflector regions surrounding the active core or in the central graphite part of the core only. The active core has an effective outer diameter of 3.5 m, which is sized to maintain a

minimum of 1 m reflector thickness within the diameter of the reactor vessel of 6.55 m. The height of the core with the ten blocks stacked in each element is 7.9 m.

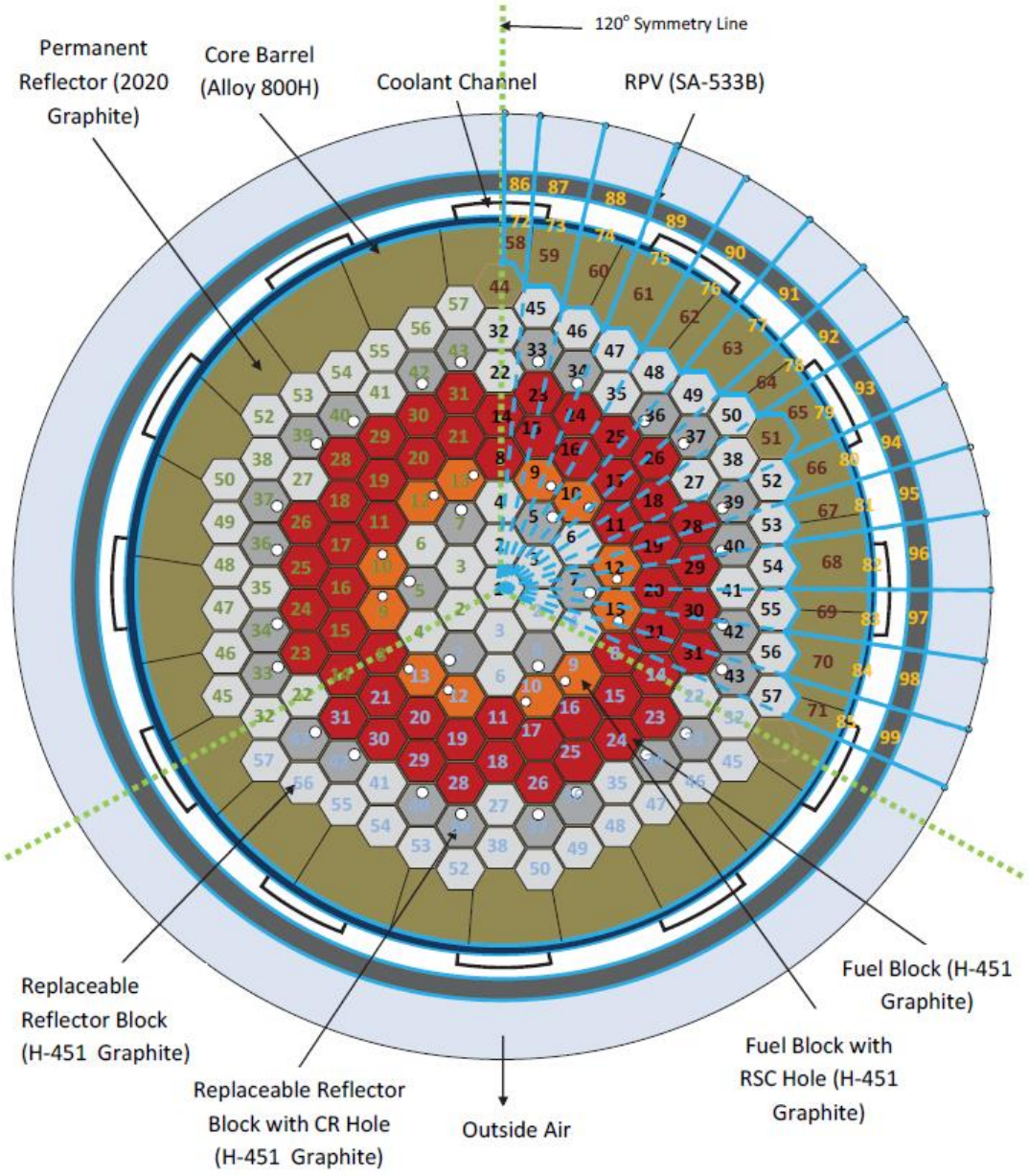


Figure 2: MHTGR-350 reactor core layout (plane view)

Source: [9]

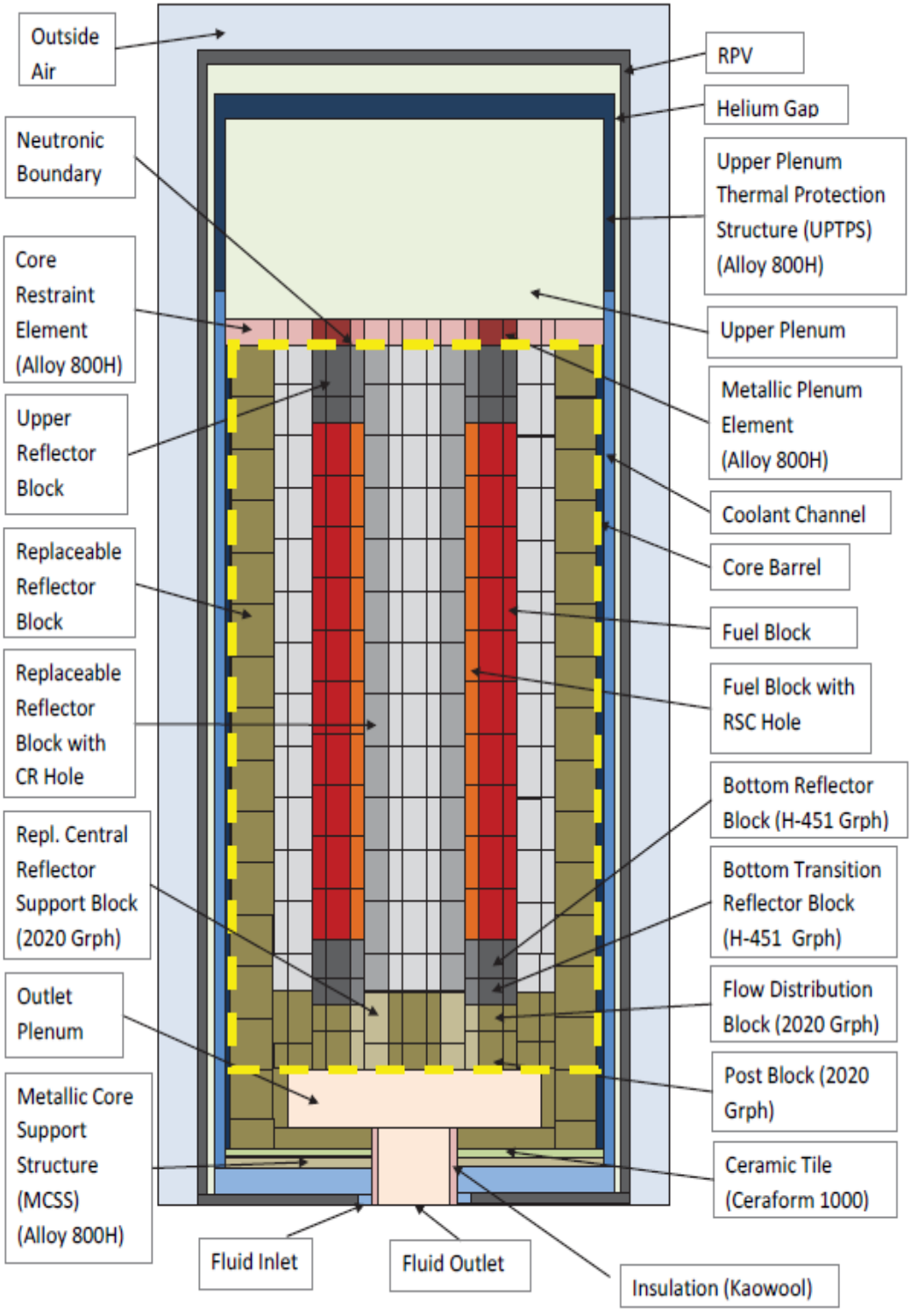


Figure 3: MHTGR-350 reactor core layout (axial view)

Source: [9]

2.3 The Fuel Block of the MHTGR-350 Reactor

In this section a general description of the MHTGR-350 fuel block, the tri-structural-isotropic (TRISO) coated particles and the fuel compact is given.

2.3.1 The Fuel Particle of the MHTGR-350 Reactor

The fuel particle of the MHTGR-350 reactor comprises of Tristructural-Isotropic (TRISO) coated fuel particles, which are very important components of the fuel elements of this reactor. The TRISO coated fuel particles consist of the fuel kernel surrounded by layers of ceramic that act as protection barriers and keep the fission products contained. The fuel kernel is surrounded by a porous carbon layer (buffer layer), followed by an inner pyrolytic layer (IPyC), followed by a silicon carbide (SiC) layer, and an outer pyrolytic carbon layer (OPyC) [13]. The material composition of the TRISO coated particles is outlined in Table 2. The TRISO coated particles are spherical in shape and have a diameter of less than 1 mm. These particles can withstand temperatures of up to 1800^{o}C [8]. Figure 4 shows the structure of the TRISO coated fuel particle.

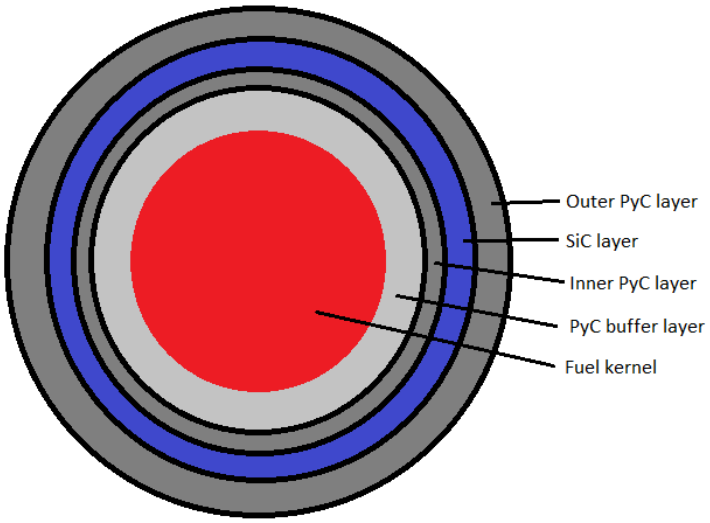


Figure 4: The structure of the TRISO coated fuel particle

Source: [14]

2.3.2 The Fuel Compact of the MHTGR-350 Reactor

The fuel compact of the MHTGR-350 reactor consists of TRISO coated fuel particles that are embedded in a cylindrical graphite matrix to form a compact. Figure 5 shows a single unit cell of the MHTGR-350 fuel block in which the compact matrix graphite which houses the TRISO coated particles is surrounded by the helium gap within the hexagonal block graphite.

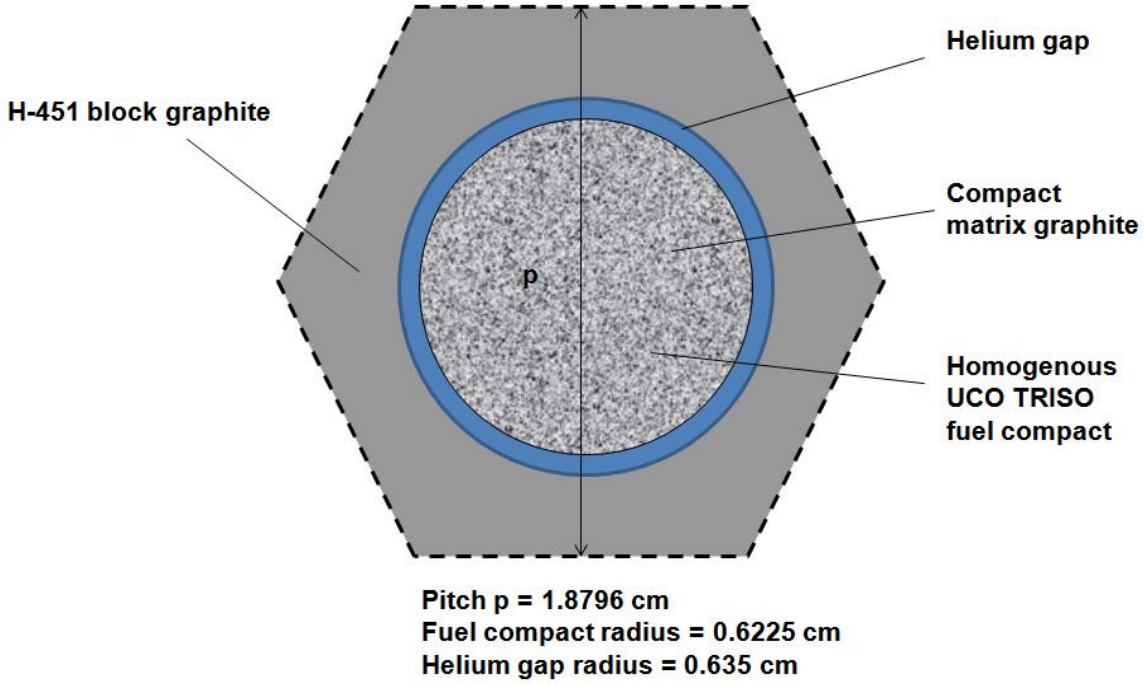


Figure 5: The fuel pin of the MHTGR-350 reactor

Source: [15]

2.3.3 Description of the MHTGR-350 Fuel Block

Figure 6 shows how the fuel pin, coolant channels, burnable poisons and block graphite are arranged in a lattice structure to form the fuel block. The fuel pin is an axial stack of fuel compacts. A helium gap is present between the fuel pin and the surrounding graphite of the block. A fuel unit cell can therefore be considered to consist of the compact, which is in the central region, surrounded by the helium gas, and the two of them are surrounded by graphite (which makes up the block) to form a fuel pin of a hexagonal structure [15], as shown in Figure 5. It is noted that the unit cell treated as a single hexagonal entity is a mathematical construct to aid with the modelling.

This unit cell does not extend from the bottom to the top of the fuel block, since there are graphite caps at the bottom and the top of the unit cell to prevent to compacts from falling out of

the fuel block. However, the benchmark definition did not take this into account, and the unit cell is defined from the bottom to the top of the graphite block.

The small and large coolant channels shown in Figure 6 are holes in the graphite block to allow the coolant (helium) to flow through the block.

Note that the fuel block in Figure 6(a) with six B_4C burnable poison compacts in the corners of the block represents a fresh fuel block and Figure 6(b) with no B_4C burnable poison compacts in the corners represents a depleted fuel block [3]. The B_4C burnable poison compact consists of B_4C particles embedded in a graphite matrix.

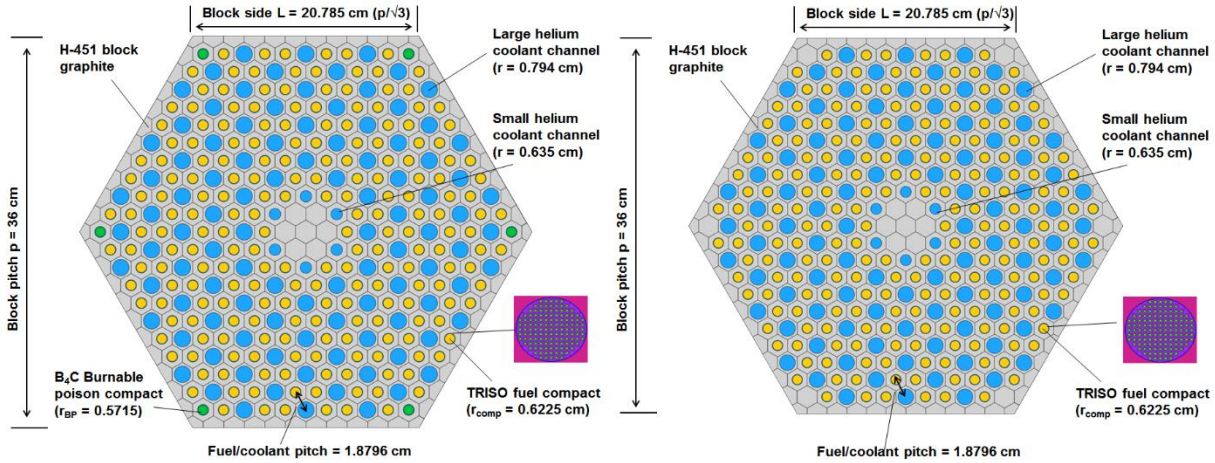


Figure 6: (a) The fresh fuel block with B_4C burnable poisons compacts and (b)depleted fuel block

Source: [3]

The following tables present the dimensions of the TRISO coated fuel particles and the fuel block, the number densities for the fuel block and the operating conditions.

Table 2: TRISO coated fuel particles and fuel block dimensions

Parameter		Value	Units
TRISO	$UC_{0.5}O_{1.5}$ kernel radius	0.02125	cm
	Porous carbon buffer outer radius	0.03125	cm
	IPyC outer radius	0.03525	cm
	SiC outer radius	0.03875	cm

	OPyC outer radius	0.4275	cm
TRISO packing fraction		0.35	
Fuel compact radius		0.6225	cm
Gap radius		0.6350	cm
Number of fuel compacts per block		210	
Lumped burnable poison particle	Kernel radius	0.0100	cm
	Porous carbon buffer outer radius	0.0118	cm
	PyC outer radius	0.0141	cm
Burnable poison particle packing fraction		0.1090	
Burnable poison compact radius		0.5715	cm
Large coolant channel radius		0.7940	cm
Number of large coolant holes		102	
Small coolant channel radius		0.6350	cm
Number of small coolant channel holes		6	
Pitch of the pin		1.8796	cm
Block flat to flat width		36.0	cm
Compact height		4.9280	cm

Table 3: Number densities of the MHTGR-350 fresh fuel block

Parameter		Nuclide	Number density(at/b.cm)
TRISO	$UC_{0.5}O_{1.5}$ kernel	^{235}U	3.6676E-03
		^{238}U	1.9742E-02
		^{16}O	3.5114E02
		Graphite	1.1705E-02
	Porous carbon buffer	Graphite	5.2646E-02
	IPyC	Graphite	9.5263E-02
	SiC	^{28}Si	4.4159E-02

		^{29}Si	2.2433E-03
		^{30}Si	1.4805E-03
		Graphite	4.7883E-02
	OPyC	Graphite	9.5263E-02
BP particle	Kernel	^{10}B	2.1400E-02
		^{11}B	8.6300E-02
		Graphite	2.6900E-02
	Buffer	Graphite	5.0200E-02
	PyC	Graphite	9.3800E-02
Fuel compact matrix		Graphite	7.2701E-02
BP compact matrix		Graphite	7.2701E-02
Coolant in coolant channel		^{4}He	2.4600E-05
H-451 Block graphite		Graphite	9.2756E-02

Table 4: Operating conditions of the MHTGR-350 fresh fuel block

Parameter	Value
Temperature of all the materials in fuel compact	1200 K
Temperature of helium in gap	1200 K
Temperature of H-4-51 block graphite	1200 K
Temperature of all materials in the BP compact	1200 K
Reactor power	350 MW

2.4 The Supercell of the MHTGR-350 Reactor

The supercell (or mini-core) of the MHTGR-350 reactor consists of a fresh fuel block at the centre (block number 26 from Figure 7), surrounded by two depleted fuel blocks and one fresh fuel on the left and lower boundaries. On the right and top boundaries, the centred fresh fuel is surrounded by a graphite reflector block [16], as shown in Figure 7. The block numbering is taken from Figure 2 in Section 2.2.

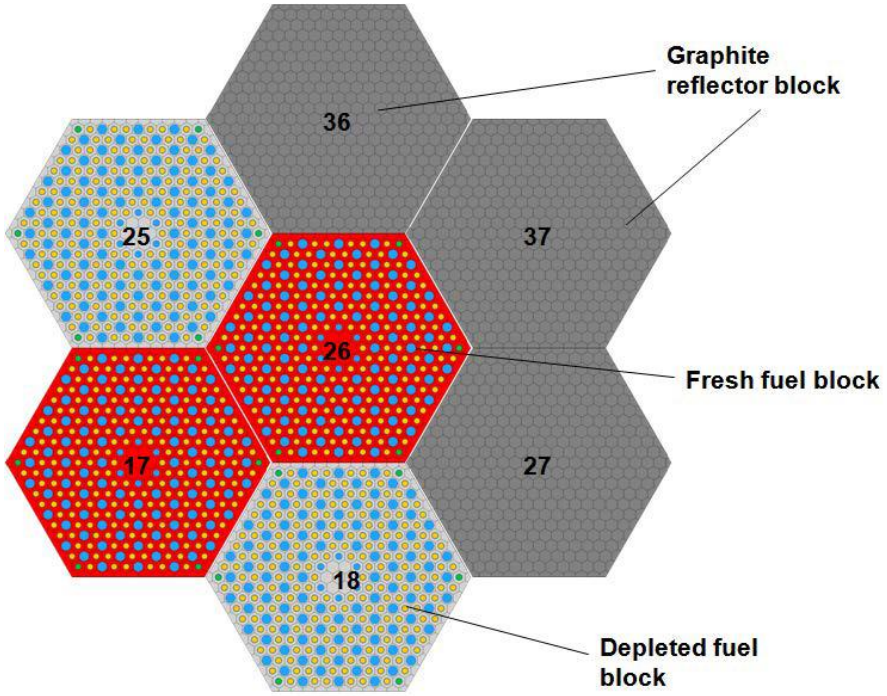


Figure 7: The supercell of the MHTGR-350 reactor

Source: [3]

In the benchmark, an assumption is made to relax the significant memory and computational resources required to model the supercell in all its details, therefore a simplified representation of the same supercell is investigated using reflective boundary conditions. The simplified MHTGR-350 supercell consists of a centred fresh fuel block of the hexagonal cell surrounded by the lumped reflector blocks on the one side and lumped depleted fuel blocks on the other side, as shown in Figure 8. In this simplification of the supercell, only the centred fuel block is modelled in its heterogeneous detail (LBP and TRISO compacts). The reflector blocks and depleted fuel blocks (together with one fresh fuel block, block 17) are homogenised into two regions respectively. The Hot Full Power (HFP) reactor conditions at a temperature of 1200 K are imposed [3].

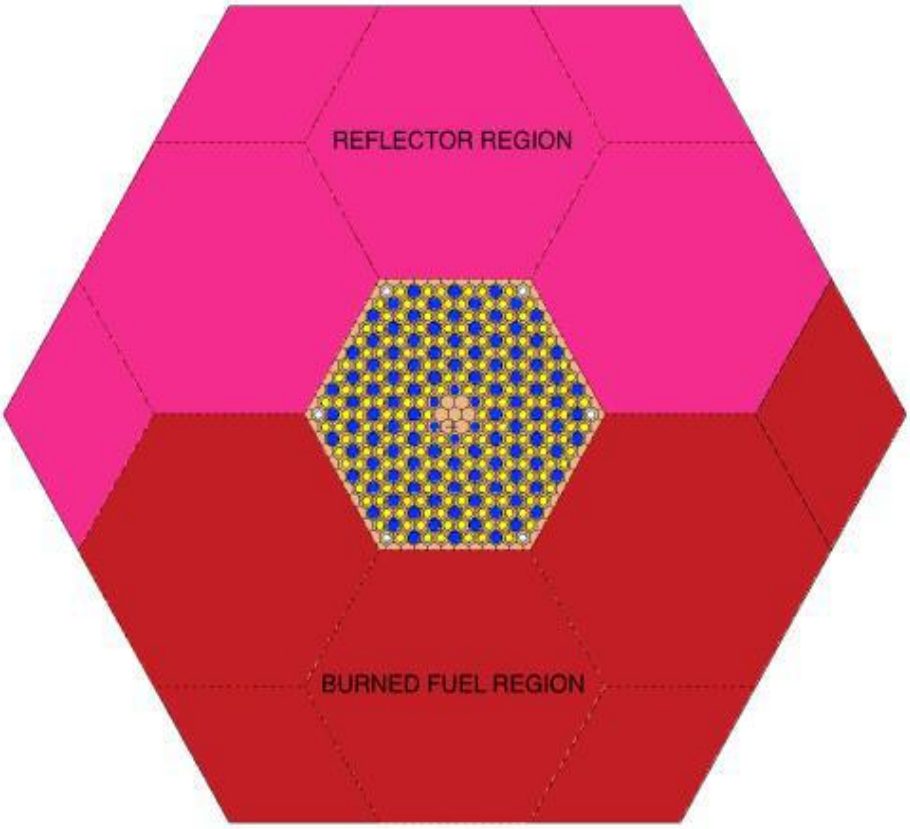


Figure 8: Simplified representation of a supercell

Source: [3]

The dimensions of the centred fresh fuel block are given in Table 2, and the block pitch and block (compact) height of the reflector region block and depleted region block is equal to that of the fresh fuel outlined in the same table. Table 5 and 6 outline the specifications of the supercell's material composition, dimensions and operating conditions, the HFP operating conditions, and number densities of the simplified representation of the supercell, as given in the IAEA Coordinated Research Project (CRP) on HTGR uncertainties [3]. Only number densities of the reflector blocks are given, the number densities of the depleted blocks can be extracted from Appendix A.

Table 5: Number densities of the reflector region

Block	Nuclide	Number density(at/b.cm)
Reflector block	Graphite	9.2756E-02
	^{10}B	2.7600E-08

Table 6: Operating conditions of the MHTGR-350 simplified supercell

Block	Parameter	
Fuel block	Temperature of all material in fuel compact	1200 K
	Temperature of helium gap	1200 K
	Temperature of H-451 block	1200 K
	Temperature of all material in BP	1200 K
Temperature of the homogenised depleted fuel block		1200 K
Temperature of H-451 graphite reflector block		1200 K
Reactor power		350 MW

The above-mentioned benchmark specifications of the MHTGR-350 supercell were used to model the supercells using KENO-VI, NEWT and TSUNAMI (codes in SCALE 6.2.1 code package). The methodologies used to model the supercells are described in Chapter 4.

2.5 Unit Cell Definitions

In general, the High Temperature Gas-cooled Reactor (HTGR) systems consists of unique fuel elements, with large quantities of graphite in the reactor core, and operates at high temperatures (i.e. 1200K at hot full power), etc., when compared with Light Water Reactors (LWR's) and Pressurized Water Reactors (PWR's). HTGR's uses the advanced coated fuel particle design (i.e. TRISO fuel particles), which can envelop fission products in order to enhance radiation safety features if an accident is to occur. The design of the fuel element of HTGR's is distinguished from the fuel elements of water reactors and forms what is known as a doubly heterogeneous system, which requires advanced simulation methods and models [17]. In this study the TRISO fuel particles of the MHTGR-350 supercell models and fresh fuel blocks were designed using the DOUBLEHET treatment for the multigroup analysis.

The DOUBLEHET Treatment uses a specialized calculational approach to treat resonance self-shielding in systems that are doubly heterogeneous. The fuel of the systems that are doubly heterogeneous, typically consists of small spherical fuel particles that are heterogeneous, which are embedded in a moderator matrix to form a fuel compact. This constitutes the first level of heterogeneity. The cylindrical, spherical, or slab fuel elements that are composed of the compact material are arranged in a moderating medium to form a lattice (regular or irregular lattice), constituting the second level of heterogeneity. Advanced reactor systems that consist of fuel designs that use TRISO fuel particle require the DOUBLEHET treatment to account for both levels of heterogeneities in the self-shielding calculations [11]. According to the SCALE 6.2.1 manual [11], if the double-heterogeneity of the system is simply ignored by volume weighting the fuel particles and moderator matrix material into a homogenized compact mixture, a large reactivity bias can result in the simulation.

The fuel of the MHTGR-350 reactor, consists of TRISO fuel particles that are heterogeneous (i.e. the kernel and layers surrounding it as described in Section 2.3.1), which are embedded in a cylindrical graphite matrix to form a compact, this constitute the first level of heterogeneity, as per definition of DOUBLEHET treatment given above. The cylindrical fuel element that consists of fuel compact material arranged in graphite matrix to form a lattice, constitute the second level of heterogeneity.

In this present study, the fuel designs of the MHTGR-350 fresh fuel block and supercell models are design using DOUBLEHET treatment for Multigroup (MG) calculations (i.e. KENO-VI MG and NEWT calculations).

Continuous energy (CE) calculations do not require the DOUBLEHET treatment since self-shielding (for the group constants) is not required.

2.6 Literature Studies

This section presents studies that are in line with this study, which are later used for comparison. In these studies, the differences in multiplication factors are presented in units of pcm, which is the difference in multiplication factors multiplied by the factor 10^{-5}. Further details regarding this unit is given in Chapter 4.

2.6.1 Results for Phase I of the IAEA Coordinated Research Project on HTGR Uncertainties [3]

The purpose of this section is to provide an overview of the phases and exercises defined for the IAEA CRP on HTGR uncertainties, which is a benchmark project.

Phase I consists of exercise I-1 and I-2 (cell physics and lattice physics respectively) and exercise I-3 and I-4 for thermal hydraulics. Of interest is exercise I-1 and I-2.

In exercise I-1, two basic unit cells are defined based on the MHTGR-350 design parameters at Cold Zero Power (CZP) and Hot Full Power (HPF). Exercise I-1a investigates a homogeneous fuel region of the fuel pin cell and exercise I-1b investigates the double-heterogeneity of the fuel region. Exercise I-2 consists of three sub-cases at hot full power (HPF), which all require a lattice calculation to be performed. Exercise I-2a requires a lattice calculation to be performed on a single MHTGR-350 fresh fuel block. Exercise I-2b specifies the same problem, but with the MHTGR-350 depleted fuel block at 100 MWd/kg-U burnup and exercise I-2 requires a lattice calculation to be performed on the MHTGR-350 supercell.

Monte Carlo codes Serpent, KENO-VI AND NEWT were utilised for the simulation of the MHTGR-350 fresh fuel block and supercell, classified under exercise I-2, with Evaluated Nuclear Data File (ENDF) nuclear data libraries, ENDF/B-VII.0 and ENDF/B-VII.I.

Reference results:

Serpent multiplication factor results with random particle distribution and ENDF/B-VII.0 nuclear data library calculations were used as reference for the MHTGR-350 fresh fuel block calculations. The relative difference between KENO-VI CE and Serpent multiplication factors was at most 492 pcm and that of KENO-MG (utilising DOUBLEHET treatment) was at most 360 pcm when compared to Serpent. The effect of homogenisation of BP compacts led to a significant multiplication factor underestimation (more than 1%).

For the MHTGR-350 supercell, Serpent multiplication results with random and regular particle distributions with a difference of 206 pcm were used as reference. The KENO-VI results were at most 350 pcm different to Serpent and 220 pcm between various KENO-VI models. When NEWT was utilised, a significantly large difference of 3336 pcm was obtained at most for the supercell calculation when compared to Serpent and other KENO-VI results, while the single MHTGR-350 fresh fuel block produced a difference of 400 pcm at most.

Conclusion:

- The KENO-VI CE multiplication factor for the MHTGR-350 fresh fuel block exceeds equivalent Serpent calculations except for the supercell.
- An underestimation of the multiplication factor results is observed in the KENO-VI MG calculation when compared to the equivalent KENO-VI calculation, except for the supercell case.

- The supercell showed the smallest multiplication factor difference for the KENO-VI MG and CE calculations

The MHTGR-350 supercell calculations are carried out in this present study, while the calculations for the MHTGR-350 fresh fuel block were carried out by Sihlangu S.F. [18].

2.6.2 Criticality Calculations of the Very High Temperature Reactor Critical Assembly Benchmark with Serpent and SCALE/KENO-VI [19]

The purpose is to validate the cell and lattice calculation of exercises I-1 and 1-2 in phase I of the study discussed in Section 2.5.1 using the Very-High Temperature Critical Assembly (VHTRC).

Simulations were performed using Monte Carlo codes, Serpent 2 and SCALE/KENO-VI to model the VHTRC, which served as a reference to the MHTGR-350 single block calculations. The VHTRC experiments were performed in three loading patterns, which were different in the type and number of control rods. In the HP experiment the assembly was brought to criticality at 25^0C, while in the HC-1 and HC-2 core experiments criticality was reached at 80^0C and 200.3^0C respectively. Results from the actual experiment and simulations performed were compared. Regular and random BISO particle arrangements were investigated within the double heterogeneity of BISO particles in the fuel.

The Serpent results showed an agreement with 2σ (error bars) between regular and random BISO particle distributions for ENDF/B-VII.0 and ENDF/B-VII.I nuclear data libraries. Only the ENDF/B-VII.1 nuclear data library showed a slight increase in multiplication factors (less than 50 pcm) for the HC-2 experiment. Comparison of Serpent calculations utilising the ENDF/B-VII.0 nuclear data library and the experimental results showed a difference of up to 100 pcm, while the corresponding ENDF/B-VII.I calculations showed results significantly closer to the experimental results.

The difference between the ENDF/B-VII.0 KENO-VI MG calculation and Serpent random particle distribution calculations was less than 150 pcm, while the corresponding ENDF/B-VII.I nuclear data library showed a difference of less than 182 pcm.

Conclusion:

- All ENDF/B-VII.0 nuclear data library simulations were approximately 1% higher than the experimental data
- The ENDF/B-VII.I nuclear data library produced results significantly closer to the experimental values.

2.6.3 Assessment of SCALE Capabilities for High Temperature Reactor Modelling and Simulation [20]

The purpose is to provide the results of verification and validation for CE and MG modelling methods for double-heterogeneous systems and to examine the effect of ENDF/B-VII.0 and ENDF/B-VII.I nuclear data libraries.

Comparisons of the results between four Monte Carlo codes were carried out: KENO-VI, beta version of SCALE6.3, Serpent 2, and MCNP using a single fuel pebble and HTR-10 full core initial critical configuration. In KENO-VI, the random-mesh model was used, and the other three codes used truly random models. The random models were compared with corresponding array models.

All four codes showed consistent eigenvalue results for CE calculations when utilising the ENDF/B-VII.I nuclear data library, with differences below 100 pcm. The differences between random and array models were between 150 pcm and 250 pcm for various calculations. For MG calculations, the ENDF/B-VII.I nuclear data library underestimated the reference by up to 280 pcm. When utilising the ENDF/B-VII.0 nuclear data library, the difference of 280 pcm was increased to 380 pcm.

The differences in the eigenvalue results for the HTR-10 fuel pebble between ENDF/B-VII.0 and ENDF/B-VII.I were higher, with a maximum of 440 pcm.

Conclusion:

- The SCALE code package provides capabilities for neutronic analysis of HTGRs. The random distribution of the TRISO coated particles can be modelled using a lattice or random distribution for CE calculations.
- Double-heterogeneous systems can be modelled with the SCALE code.

2.6.4 Uncertainty Quantification in the MHTGR-350 Fuel Compact and Block Using TSUNAMI-3D Clutch Method and Sampler [21]

The purpose is to calculate sensitivity coefficients and propagate uncertainties for the MHTGR-350 fuel compact and fresh fuel block fuel block specified in [3], using TSUNAMI-3D and Sampler.

KENO-VI and NEWT were used to simulate the MHTGR-350 heterogeneous fuel compact and fuel block at CZP and HFP, utilising ENDF/B-VII.I. Convergence and optimisation parameters

for both codes were studied. The sensitivity and uncertainty analysis codes used were TSUNAMI-3D and Sampler, while the transport solver used for TSUNAMI-3D was KENO-VI and for Sampler it was NEWT.

The convergence of KENO-VI results was performed to ensure that the fission source was well distributed over all volumes containing fissile material and to achieve adequate statistical accuracy of the multiplication factor (k_∞), by setting NPG to 50000, NSK to 50 and the statistical error to 15 pcm. For convergence of NEWT, the parameters epsilon and epseigen were set to values of 5.0E-08.

The CE calculations for the fuel compact showed differences in k_∞ of 115 pcm and 639 pcm at CZP and HFP respectively, between SCALE 6.2.1 and SCALE 6.2.2. Comparison of the results of SCALE 6.2.1 with the corresponding Idaho National Laboratory (INL) results showed differences of 186 pcm and 29 pcm at CZP and HFP, respectively. MG calculations of KENO-VI using SCALE 6.2.1 and SCALE 6.2.2 yielded identical results and compared well with the INL results of SCALE 6.2. beta3 (33 pcm and 26 pcm respectively).

CE results for the MHTGR-350 fuel compact using TSUNAMI-3D at CZP yielded comparable Δk and $\%\Delta k/k$ results, with differences of 8 pcm and 0.006 between SCALE 6.2.1 and SCALE 6.2.2 codes. At HFP, the differences were 19 pcm and 0.013 respectively. The MHTGR-350 fuel block at HPF yielded differences of 4 pcm and 0.005, for comparable Δk and $\%\Delta k/k$ values respectively between the two versions of SCALE. TSUNAMI-3D was only used for CE calculations.

Sampler/NEWT and Sampler/KENO calculations using 100 samples compared well, with differences of 5 pcm and 2 pcm for Δk, and the difference in $\%\Delta k/k$ was zero for both cases. With a changed number of samples from 100 to 1000, $\Delta k/k$ decreased by $\sim$75% for CZF and HFP. Comparing TSUNAMI-3D CE calculations with Sampler/KENO-VI and Sampler/NEWT for 100 samples, differences of 63 and 58 pcm were observed. Comparing TSUNAMI CE calculation with Sampler NEWT over 100 samples yielded a difference in Δk of 3 pcm for both CZP and HFP.

Uncertainty contributors for the MHTGR-350 fuel compact and fuel block were presented and compared.

Conclusion:

- The use of DBRC=1 seems to yield a higher k_∞value.
- Using larger sample sizes in Sampler results in better agreement with TSUNAMI-3D CE calculations

2.6.5 Nuclear Data Uncertainty and Sensitivity Analysis of the VHTRC Benchmark using SCALE [22]

The purpose is to analyse the uncertainties due to basic nuclear data as well as the effect of processing cross-sections and covariance data.

Simulations were performed with KENO-VI and Serpent using both ENDF/B-VII.0 and ENDF/B-VII.I nuclear data libraries for the sub-models of the VHTRC. These were the fuel compact cell, the fuel unit cell and the fuel compact. The uncertainties and sensitivities analyses were determined using either the random sampling approach or perturbation theory. The Sampler module, in combination with the KENO-VI code, performed the random sampling-based nuclear data uncertainty analysis. Linear perturbations were performed with the continuous energy (CE) TSUNAMI code. The analyses were performed to determine the uncertainty in the multiplication factor k, due to uncertainties in nuclear data and the main contributing cross-sections for several criticality states. The effect of moderator-to-fuel ratio and double-heterogeneity modelling were assessed, as well as the nuclear data libraries.

The model that was using random particle distributions was considered as the closest to reality and served as reference for all calculations. This reference model was modelled with Serpent using both nuclear data libraries as shown in Table 7:

Table 7: Reference CE results of the multiplication factor with Serpent 2.1.26

	Fuel compact	Fuel unit cell	Fuel block
ENDF/B-VII.0	1.33490	1.33472	1.45953
ENDF/B-VII.I	1.33089	1.32319	1.44342

The differences between the results obtained using ENDF/B-VII.0 and ENDF/B-VII.I nuclear data library was almost exclusively caused by an update in the carbon capture cross section in the ENDF/B-VII nuclear data library, when comparing simulation results of the two nuclear data libraries. To study the influence of nuclear data libraries, the models were simulated using ENDF/B-VII.0 nuclear data library but changing the cross sections of graphite to ENDF/B-VII.I nuclear data library (which is possible with Serpent). An agreement within two statistical standard deviations with the ENDF/B-VII.I nuclear data library was obtained. Figure 9 presents the eigenvalue sensitivity to the carbon capture cross sections for the models that were investigated. These models were obtained using TSUNAMI CE with ENDF/B.VII.0 nuclear data

library, and the HC-1 core was the additionally model with ENDF/B-VII.I nuclear data library. For better comparison, the output was collapsed into the 252-group structure.

If more graphite was present in the system, the eigenvalue sensitivity was larger and therefore the difference of the eigenvalues between the calculations with the two nuclear data library releases was increased. It was further observed that the absolute sensitivity to carbon capture in the case of ENDF/B-VII.1 nuclear data library compared to ENDF/B-VII.0 nuclear data library was increased, this was because of the increased cross section in the thermal energy range in the ENDF/B-VII.1 nuclear data library. Due to reasons of legibility, this comparison was only presented for the core (HC-1). This effect was visible for other models, but smaller with the decreasing ratio of the moderator-to-fuel.

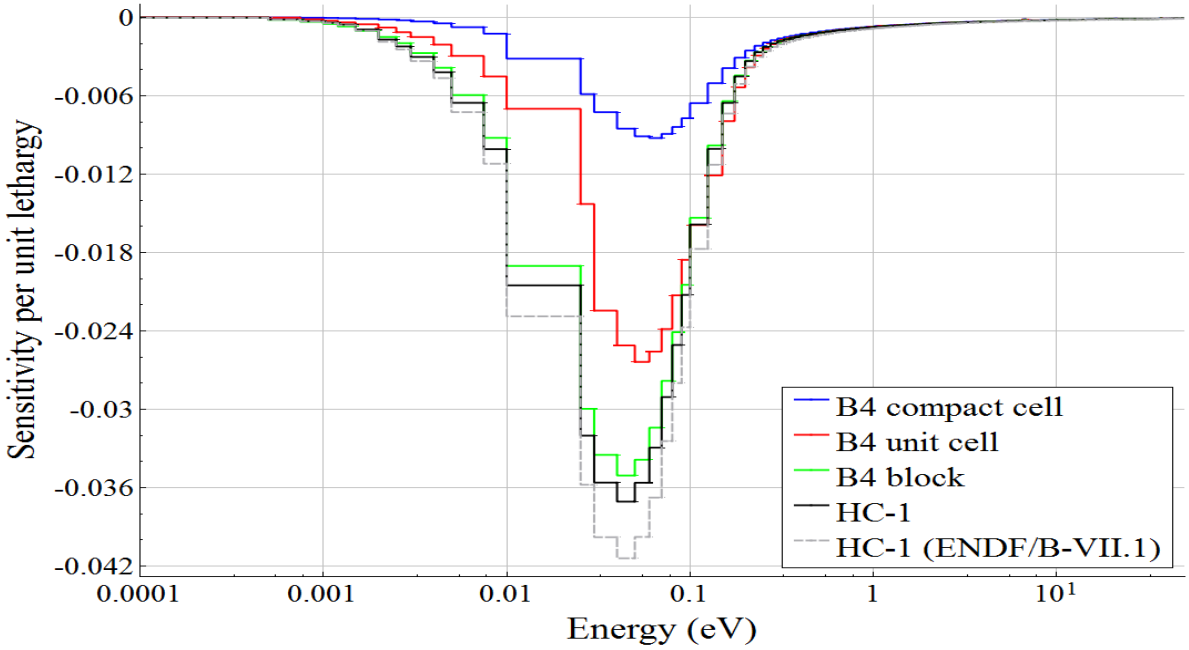


Figure 9: Eigenvalue sensitivity to the capture cross section of graphite determined using TSUNAMI CE

Source [22]

The influence of the applied covariance nuclear data library used was assessed by comparing the corresponding TSUNAMI-CE and Sampler calculations. It was observed that the eigenvalue uncertainty increased by between 7% and 18% when comparing the result obtained using the ENDF/B-VII.I nuclear data library with those obtained by utilising the ENDF/B-VII.0 nuclear data library. It was determined that this increase of the eigenvalue uncertainty was caused by an increase of the uncertainty of the neutron multiplicity $\bar{\nu}$ of U-235 in the ENDF/B-VII.I nuclear data library. According to [22], the $\bar{\nu}$ uncertainty in the thermal energy range was increased from

0.311% in the ENDF/B-VII.0 nuclear data library to approximately 0.385% in the ENDF/B.VII.1 nuclear data library.

After comparison of the criticality, uncertainty and sensitivity results, the findings were as follows:

- The influence of particle distributions was very small and was therefore neglected for all the models.
- If there is more graphite in the system (i.e. better neutron moderation because of the moderator-fuel-ratio) the eigenvalue sensitivity becomes larger, resulting in an increase in the difference of the eigenvalues between the two libraries.
- The increase of uncertainty of the neutron multiplicity $\bar{\nu}$, of U-235 in the ENDF/B-VII.I nuclear data library causes an increase in the eigenvalue uncertainty.

According to the SCALE 6.2.1 manual [11], the ENDF/B-VII.0 nuclear data library is unchanged from earlier releases of SCALE code package prior to SCALE 6.2.1 version, except for changes in the identifications of the nuclides. Several enhancements and improvements (which are outlined in the SCALE 6.2.1 manual) were made to produce the ENDF/B-VII.I nuclear data library.

2.6.6 Quantifying Uncertainties of Aspects of the Neutronics modelling of the Kozloduy-6 System using Scale 6.2.1 [23]

The purpose of this study is to formulate an uncertainty quantification of the Kozloduy-6 VVER-1000 models for the neutronic analyses. This study is based on the benchmark for Uncertainty Analysis in Modelling of light water reactors [24].

This benchmark [24], comprises of three phases and each phase comprises three exercises. The systems specified for this benchmark are the pressurised water reactor (PWR), the boiling water reactor (BWR) and the VVER which is a pressurized light water reactor, with hexagonal symmetry for the fuel assembles.

In this study [23], the propagation of uncertainties in terms of Exercise I-2 of Phase 1 of the benchmark, which was the lattice physics modelling, was investigated. The study was performed using the SCALE-6.2.1 code package to develop the fuel pin and assembly model of the Kozloduy-6 VVER-1000 reactor system. The criticality calculations were performed using KENO-VI and NEWT. The nuclear data uncertainties were propagated by TSUNAMI-2D and 3D

as well Sampler. The importance of this study in terms of the current study is that the IAEA CRP Benchmark [3] follows similar general strategies for propagating the uncertainties.

Comparison of the multiplication factor results from NEWT of the fuel pin and fuel assembly models were about 150 pcm and 180 pcm compared with their equivalent KENO-VI (MG) solutions, respectively. The effect of nuclear data uncertainties on the multiplication factor results of the fuel pin and the fuel assembly were about 780 and 760 pcm respectively using both TSUNAMI-3D and TSUNAMI-2D.

The highest sensitivity was about 200 pcm, while for the NEWT parameters tested this was about 283 pcm. The uncertainty due to nuclear data uncertainties was not significantly affected by the change in the code parameters in the optimisation tests. A good agreement was obtained between the NEWT results (with optimised parameters) and the KENO-VI results.

Worth noting is that the water based reactor is different to the HTGR in three main areas:

1. Water vs graphite as the moderator. This means that the neutrons are more effectively moderated to thermal energies in the PWR against the HTGR. So two energy groups are required for most cases, whereas the HTGR needs four or more groups.
2. The environment of the FA assembly in the water reactor also is different, due to different burnups of FAs and fuel enrichments. However, related to point one, the mean free path of the neutrons in water is shorter than that of HTGRS, so the effect of the environment might be weaker in the water moderated reactor.
3. PWRs do not have double heterogeneity. HTGRs do. The selfshielding treatment requires an additional homogenization step. This complicates the code development for uncertainty treatment. Direct evidence of this is in SCALE 6.2.1. TSUNAMI 3D using the General Perturbation Theory has not been developed for doubly heterogenous system.

As stated above, the two reactor systems are quite different from each other, especially from a physics point of view. Other than following the general methodology, (as was done, since the HTR benchmark follows the general methodology for the LWR UAM benchmark fairly closely), there will most probably not be much similarity in terms of specific aspects of the physics, especially in terms of self-shielding, since the HTRs system must also consider the further step associated with the double heterogeneity. Given this, the LWR uncertainty analysis will not be discussed further, since it is also not part of the scope of the project in terms of time constraints.

2.6.7 Uncertainty and Sensitivity Analysis of Aspects of the Neutronics of a Prismatic Block-type HTGR [18].

The purpose of this study is to propagate uncertainties for prismatic type HTGRs. This study is based on the IAEA CRP on HTGR uncertainties [3].

The computer codes used to develop these models were KENO-VI, NEWT, TSUNAMI-3D and Sampler (codes within the SCALE 6.2 code package) utilising both ENDF/B-VII.0 and ENDF/B-VII.I nuclear data libraries. Other nuclear data libraries that are in existence includes the Joint Evaluated Fission and Fusion file (JEFF), the Russian Evaluated Nuclear Data File (BROND) and the Cross-section Evaluated Working Group (ENDF/B) from several nuclear data agencies that collect international published and theoretical results on the neutron-nuclear reactions for computerization [25]. However, these other libraries were not used in this study. Since the present study only uses SCALE 6.2.1 code package, which utilises ENDF/B-VII.0 and ENDF/B-VII.I nuclear data libraries. . This is carried out so that the scope does not become very large, and thus dilute the depth required for the study due to the time constraints. Comparisons in terms of cross sections from other data agencies can be carried out in further studies.

In this work, the models were studied in terms of criticality (i.e. multiplication factor), cross section collapsing and uncertainty and sensitivity analysis. The methodology for the convergence of the $F^*(r)$ function was also developed using both the MHTGR-350 fuel compact and the fuel block models, this methodology was followed for the MHTGR-350 supercell models used in the present study. The methodology used for uncertainty and sensitivity analysis (i.e. the CLUTCH method and statistical sampling) in this study [18] are the same as the methodologies that were followed in the present study, since both studies use the same modules of SCALE 6.2.

The graphite cross section of ENDF/B-VII.0 and ENDF/B-VII.I nuclear data libraries were also studied. Figure 10 and 11 shows the effect of an update of c-graphite (n, γ) and c-graphite (n, n') cross sections in the ENDF/B-VII.I nuclear data library compared to the ENDF/B-VII.0 nuclear data. (n, γ) and (n, n') denote radiative capture and inelastic scattering reactions. The data that was used to plot these figures was obtained from the IAEA Nuclear Data Services [26]. It can be seen that there is a distinct difference between the ENDF/B-VII.0 and ENDF/B-VII.I nuclear data libraries.

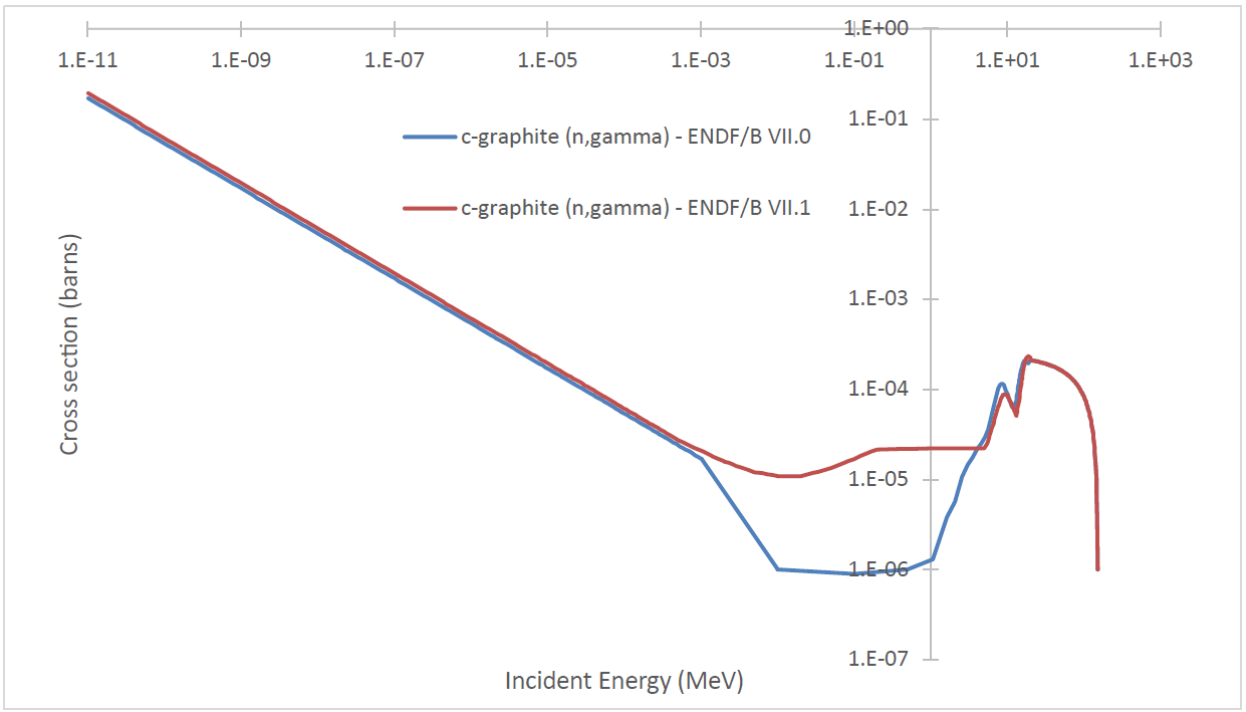


Figure 10: Cross section of c-graphite (n, γ) for ENDF/B-VII.0 and ENDF/B-VII.1 nuclear data libraries

Source [18]

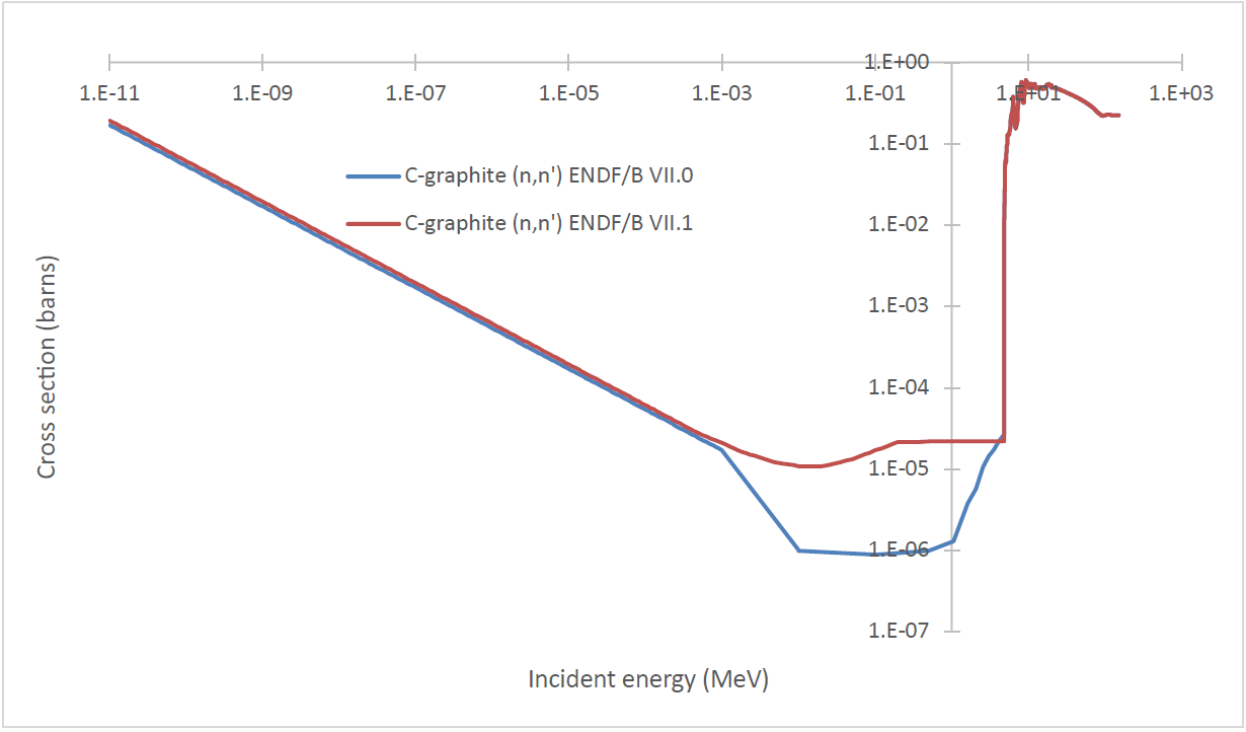


Figure 11: cross section of c-graphite (n, n') for ENDF/B-VII.0 and ENDF/B-VII.1 nuclear data libraries

Source [18]

The MHTGR-350 fresh fuel blocks that are used in this present study are based on this study [18], the results thereof are presented in Chapter 5.

2.6.8 Neutronic Modeling of TRIGA Reactor at the University of Utah using AGENT, KENO6 and MCNP5 [27]

The purpose of this study is to study the effect of different fuel configurations in developing practical educational exercises for reactor physics students. This study is based on modelling of the 100 kW TRIGA reactor at the University of Utah. The TRIGA (Training, Research, Isotopes, General Atomics) reactor is designed for research and testing purposes. The computer codes that were used in this study are DRAGON, AGENT, KENO-VI and MCNP5.

DRAGON contains various methods to simulating fuel assemblies, which includes the collision probability, method of characteristics and discrete ordinates methods [28]. However, its primary method is the collision probability method [25]. In this study, DRAGON was used as the lattice physics code to produce broad group cross sections for AGENT. A 172 group library (known as WLUP) was used for the collapsing of the cross sections to the seven groups for the AGENT calculation. The WLUP stands for WIMS-D Library Update Project, WIMS-D (Winfrith Improved Multigroup Scheme-D) is a software packages for reactor lattice calculations [29] .

It is also reported that DRAGON was used for the self shielding calculations. AGENT is the core solver, and the method that AGENT employs is based on the method of characteristics.

KENO-VI is a Monte-Carlo code and was used in multi-group mode as an alternate to AGENT. The library used was the 238 group ENDF/B-VI library.

MCNP5 is also a Monte Carlo code. However, it was used in continuous energy format. The continuous energy ENDF/B-VI nuclear data library was used for the MCNP5 calculation.

The multiplication factors obtained with AGENT and KENO-VI were 1.02188 and 1.02182 respectively, which showed a difference of 6 pcm, which was considered very small. The multiplication factor result obtained with MCNP5 was 1.02575, of which comparison with both AGENT and KENO-VI showed an underestimation in multiplication factor of 0.40% (390 pcm) by AGENT and KENO-VI to MCNP5 results. (The definition for pcm is given in Section 4.6.1)

It was shown that the results of the codes that uses resonance corrected cross sections based on multigroup cross section library are consistent with each other (i.e. AGENT and KENO-VI)

The much bigger difference between MCNP5 results and the other two codes, AGENT and KENO-VI, when compared with the difference between AGENT and KENO-VI, was attributed to

way in which the cross sections were treated in terms of self shielding and collapsing. The use of different nuclear data libraries was also presented as a reason for the differences.

CHAPTER 3 THEORY AND CODES USED

3.1 Introduction

This chapter presents the relevant theory needed to conduct this research study on multigroup (MG) cross sections of the MHTGR-350 lattice fuel blocks and supercells with the aid of the SCALE 6.2.1 code package. A brief description of the SCALE 6.2.1 modules that were used in this study is also presented.

3.2 Nuclear Reactions and Cross Sections

In nuclear engineering studies it is very important to determine the type of nuclear reactions that take place in the reactor system as well as their associated cross sections. This section describes nuclear reactions that can take place in a reactor system as well as the cross sections associated with them.

3.2.1 Nuclear Reactions

A nuclear reaction results from interaction of two nuclear particles producing two or more nuclear particles. A gamma ray could also be emitted. Equation (3-1) below is a simple representation of a nuclear reaction, where A and B denotes initial nuclei, the product nuclei and (or) a gamma ray is denoted by C and D (with the assumption that there are only two products) [30].

$$A + B \rightarrow C + D \tag{3-1}$$

There are different nuclear reactions that can occur when a neutron interacts with the nucleus of an atom, for example scattering (elastic or inelastic), absorption, radiative capture (a type of absorption), fission (also a type of absorption), etc.

Let's consider an incident neutron that strikes the nucleus at its ground state (state of its lowest energy). If the neutron reappears and the nucleus remains in its ground state, the process is known as elastic scattering. Inelastic scattering is identical to the process of elastic scattering, except that in this process the nucleus is left in an excited state (more energy than its ground state). If the incident neutron gets captured by the nucleus and one or more γ-rays are emitted, this process is known as radiative capture, since the neutron is basically absorbed by the nucleus, this is an example of the class of interactions known as absorption. If the incident neutron causes the nucleus to split apart, then the process is known as a fission reaction.

3.2.2 Nuclear Cross Sections

Nuclear cross sections are quantities that describe the extent to which particles or gamma rays interact with nuclei and are denoted by the symbol σ. Cross sections are measured in terms of area and are normally expressed in terms of units called barn, 1 barn = 10^{-24} cm^2 [25]

Each of the nuclear reactions described in Section 3.2.1 is denoted by a characteristic nuclear cross section. That is to say, the elastic scattering is described by the elastic scattering cross section σ_e, the inelastic scattering is described by inelastic scattering cross section σ_i (the scattering cross section σ_s is the sum of elastic and inelastic cross sections), radiative capture is described by the capture cross section σ_γ and fission is described by the fission cross section σ_f. Equation (3-2) is a representation of the total cross section denoted by σ_t, which is the sum of the cross sections for all possible interactions [30].

$$\sigma_t = \sigma_e + \sigma_i + \sigma_\gamma + \sigma_f + \cdots \tag{3-2}$$

3.2.3 Resonance Cross Section and Doppler Broadening

Cross sections are quantities that characterise the probability of a certain type of nuclear reaction taking place and are measured in units called barn, as mentioned in the previous section. When an incident neutron is captured by the nucleus of an atom to form a compound nucleus, energy is produced due to binding energy. Binding energy is the amount of energy required to disassemble the nucleus into separate nucleons. If the relative energy of an incident neutron and the nucleus plus the binding energy equals the energy of the compound nucleus to be formed upon capturing of the neutron, then the probability of the neutron being captured is large, and thus the resonance phenomena will be achieved [25]. Figure 12 shows the capture cross section of ^{238}U.

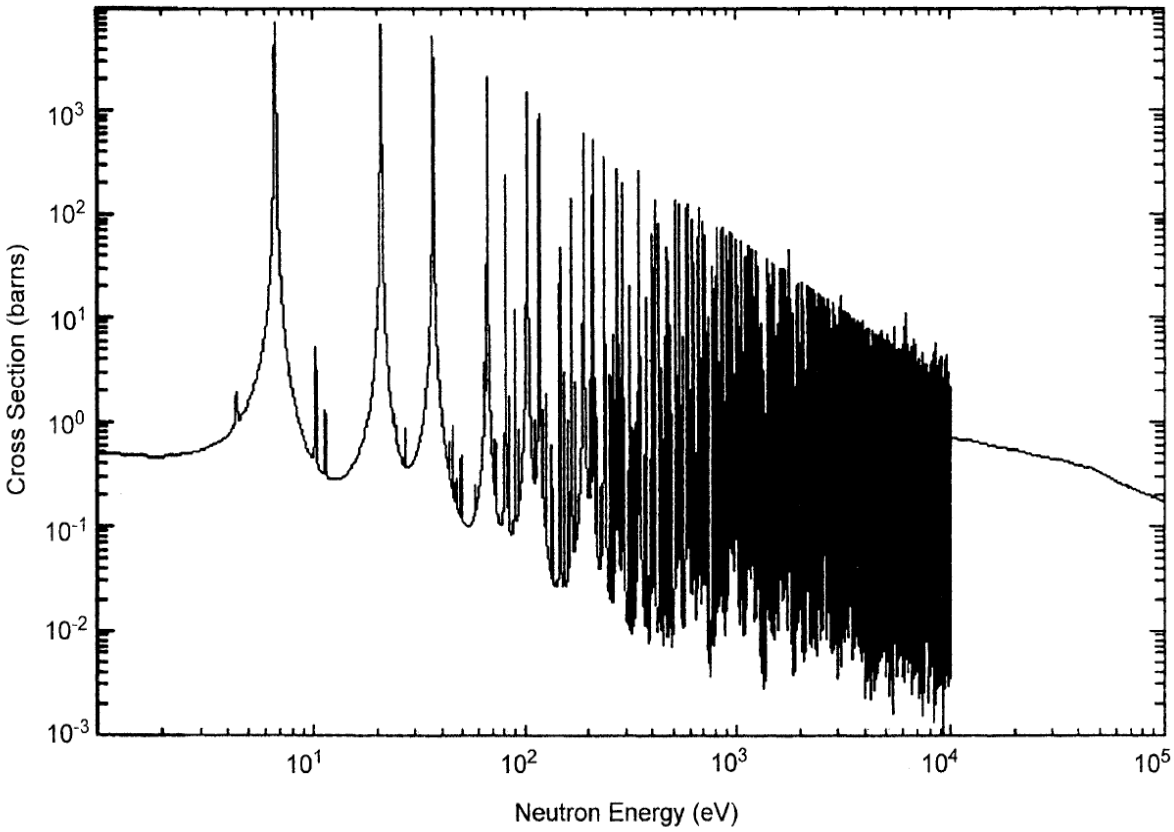


Figure 12:Capture cross section of ^{238}U

Source: [25]

The lowest excited energy states are a fraction of 1 eV above the ground state and go up to 100 keV for intermediate to heavy mass fuel nuclei (fissile and fertile materials). However, they start at around 10 eV for intermediate mass nuclei and at around 10 keV for lighter mass nuclei. The heavier mass isotopes have many relatively low excited states of energy, and this gives rise to resonance in the absorption and scattering cross section of the neutrons, as shown in Figure 12 above. The region where the peaks are visible, that is the region between neutron energies 10^0 eV and 10^4 eV from the figure, is known as the resonance region.

The (n,γ) capture cross section averaged in terms of the motion of the nucleus is given by:

$$\sigma_\gamma(E,T) = \sigma_0 \frac{\Gamma_\gamma}{\Gamma}\left(\frac{E_0}{E}\right)^{\frac{1}{2}} \psi(\xi,x) \tag{3-3}$$

where:

σ_0 is the peak value of the cross section,

E_0 is the neutron energy at which it occurs in the centre-of-mass co-ordinate system,

Γ is the resonance width, and

Γ_γ is the partial width for neutron capture.

The total scattering cross section including resonance and potential scattering and the interference between the two can be written as:

$$\sigma_\gamma(E,T) = \sigma_0 \frac{\Gamma_\gamma}{\Gamma}\left(\frac{E_0}{E}\right)^{\frac{1}{2}} \psi(\xi,x) + \frac{\sigma_0 R}{\lambda_0} x(\xi,x) + 4\pi R^2 \tag{3-4}$$

where:

λ_0 is the DeBroglie wavelength, and

R is the nucleus radius,

with the assumption made that the motion can be characterised by a Maxwellian distribution with temperature T and energy E of the neutron in the laboratory system. The functions

$$\psi(\xi,x) = \frac{\xi}{\sqrt{\pi}} \int_{-\infty}^{\infty} e^{-1/4(x-y)^2\xi^2} \frac{dy}{1+y^2} \tag{3-5}$$

and

$$\chi(\xi,x) = \frac{\xi}{\sqrt{\pi}} \int_{-\infty}^{\infty} e^{-1/4(x-y)^2\xi^2} \frac{ydy}{1+y^2} \tag{3-6}$$

are integrals over the relative motion of the neutron and the nucleus with $x = 2(E - E_0)/\Gamma$.

The temperature characterising the nuclear motion is contained in parameter ξ,

$$\xi = \frac{\Gamma}{\left(4E_0 kT/A\right)^{1/2}} \tag{3-7}$$

where:

k is the Boltzman constant, and

A is the atomic mass in (amu).

Figure 13 below indicates the general dependence of the ψ function on temperature. When the temperature increases, the peak height decreases and the width increases (broadens). This is the broadening of cross sections and is known as Doppler broadening [25].

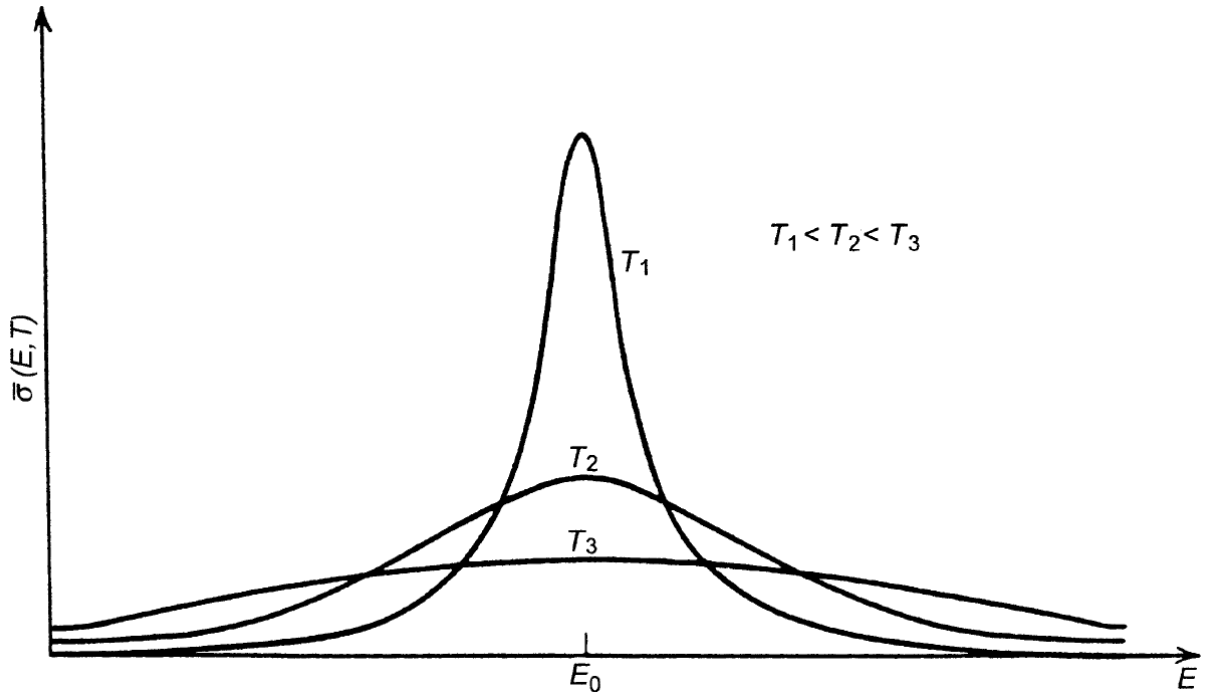


Figure 13: Temperature broadening of the ψ function

Source: [25]

For the multigroup resonance cross sections, the resonances within a given energy group in a multigroup can be treated as a group capture cross section as follows (assuming that the flux behaves as 1/E):

:

$$\sigma_\gamma^g = \frac{\int_{E_g}^{E_{g-1}} dE\sigma_\gamma(E)\phi(E)}{\int_{E_g}^{E_{g-1}} dE\phi(E)} = \frac{\sum_{i\in g} I_i}{In(E_{g-1}/E_g)} \quad (3\text{-}8)$$

where I_i is the resonance integral for isotope i.

3.2.4 Evaluated Nuclear Data Libraries

The probability of different neutron-nuclear reactions (e.g. scattering, absorption, capture, fission etc.) occurring is characterised by cross sections. Evaluated nuclear data libraries provide the measured probabilities of different neutron-nuclear reactions that can occur. Examples are the Evaluated Nuclear Data File, version B (ENDF/B), the Joint Evaluated Fission and Fusion File (JEFF) and the Russian Evaluated Nuclear Data File (BROND).

There are several nuclear data agencies, such as the Cross-section Evaluated Working Group that collect international published and theoretical results on the neutron-nuclear reactions and compile these nuclear data libraries [25]. These nuclear data libraries are used for input models and simulations.

In this study the ENDF/B-VII.0 (238-group) and ENDF/B-VII.I (252-group) nuclear data library files are used for providing nuclear data input to the MHTGR-350 fresh fuel block and supercell models developed by the different SCALE 6.2.1 codes.

3.3 Neutron Transport Equations

In reactor core physics, it is important to understand neutron transport and interactions with matter, in order to determine the distribution of neutrons in the reactor system. Knowing the distribution allows the determination of reaction rates and analysis of fission power in the reactor system. For this, the neutron transport equation is used. The neutron transport equation may be presented in many forms, depending on the problem. Sections 3.3.1 and 3.3.2 presents the neutron transport equations used by KENO-VI and NEWT, respectively [11].

3.3.1 Boltzmann Transport Equation

The Boltzmann transport equation can be written as [11]:

$$\frac{1}{v}\frac{\partial \psi}{\partial t}(\vec{r},E,\hat{\Omega},t)+\hat{\Omega}\cdot\vec{\nabla}\psi(\vec{r},E,\hat{\Omega},t)+\Sigma_t(\vec{r},E,\hat{\Omega},t)\psi(\vec{r},E,\hat{\Omega},t) = S(\vec{r},E,\hat{\Omega},t) + \int_{E'}\int_{\hat{\Omega}'}\Sigma_s\left(\vec{r},E'\rightarrow E,\hat{\Omega}'\rightarrow\hat{\Omega},t\right)\psi\left(\vec{r},E',\hat{\Omega}',t\right)d\hat{\Omega}'dE' \quad (3\text{-}9)$$

where :

$\psi(\vec{r},E,\hat{\Omega},t)$ is the neutron flux per unit energy at energy E along direction $\hat{\Omega}$ at position $\vec{r}$ and time t,

$\Sigma_t(\vec{r}, E, \hat{\Omega}, t)$ is the total macroscopic cross section of the media at position $\vec{r}$, energy E, direction $\hat{\Omega}$ and time t,

$\Sigma_s(\vec{r}, E' \to E\hat{\Omega}' \to \hat{\Omega}, t)$ is the scattering macroscopic cross section of the media per unit energy E at energy E' along direction $\hat{\Omega}$ at position $\vec{r}$ and time t, for scattering of neutrons to energy E and direction $\hat{\Omega}$, and

$S(\vec{r}, E, \hat{\Omega}, t)$ is the neutron source term, neutrons born at position $\vec{r}$ and time t per unit energy at energy E along direction $\hat{\Omega}$.

3.3.2 Time-independent Boltzmann Transport Equation

For steady state situations, the first term of Equation (3-9) becomes zero, and the equation then be written (without time dependence) as [11]:

$$\hat{\Omega} \cdot \vec{\nabla}\psi(\vec{r}, \hat{\Omega}, E) + \Sigma_t(\vec{r}, E)\psi(\vec{r}, \hat{\Omega}, E) = Q(\vec{r}, \hat{\Omega}, E) \tag{3-10}$$

The terms in the equation are defined as follows:

$\psi(\vec{r}, \hat{\Omega}, E)$ is the angular flux at position $\vec{r}$ per unit volume in direction $\hat{\Omega}$ per unit solid angle and energy E per unit energy,

$\Sigma_t(\vec{r}, E)$ is the total macroscopic cross section at position $\vec{r}$ and energy E,

$Q(\vec{r}, \hat{\Omega}, E)$ – is the source at position $\vec{r}$ per unit volume in direction $\hat{\Omega}$ per unit solid angle and energy E per unit energy.

1) The source Q consists of three terms, the scattering source, the fission source and an external or fixed source. The scattering source is defined as:

$$S(\vec{r}, \hat{\Omega}, E) = \int_{4\pi} d\hat{\Omega} \int_0^\infty dE' \Sigma_s(\vec{r}, \hat{\Omega}' \to \hat{\Omega}, E' \to E)\, \psi(\vec{r}, \hat{\Omega}', E')$$

where:$\Sigma_s(\vec{r}, \hat{\Omega}' \to \hat{\Omega}, E' \to E)$ is the macroscopic scattering cross section at position $\vec{r}$ from initial energy E' and direction $\hat{\Omega}'$ to the final energy E and direction $\hat{\Omega}$.

2) The fission source is defined as

$$f(\vec{r}, \hat{\Omega}, E) = \chi(\vec{r}, E) \int_0^\infty dE' \nu(\vec{r}, E')\Sigma_f(\vec{r}, E')\psi(\vec{r}, \hat{\Omega}, E')$$

where:

$\chi(\vec{r}, E)$ is the fraction of neutrons that are born at position $\vec{r}$ and energy E,

$\nu(\vec{r}, E')$ is the number of neutrons produced per fission event at position $\vec{r}$ and energy E',

$\Sigma_f(\vec{r}, E')$ - is the macroscopic fission cross section at position $\vec{r}$ and energy E', assumed to be isotropic.

3) The external or fixed source:

$S(\vec{r}, E)$ which is the neutron source born at position $\vec{r}$ with energy E.

When $\nu(\vec{r}, E')$ is integrated over an energy range (of the neutron), it is known as "nubar", $\bar{\nu}$ [11].

3.3.3 The Extended Step Characterization method

Using discrete-ordinates method (which is based on finite differencing approximations for spatial derivatives) is difficult when dealing with complex non-orthogonal geometries due to the nature of the finite differencing approximations. A method that can be used is the method of characteristics, which solves the neutron transport equation, Equation (3-10), analytically along characteristic directions within a computational cell [11].

Since the angular flux $\psi(\vec{r}, \hat{\Omega}, E)$ in direction $\hat{\Omega}$ is of concern, the streaming term, i.e. the first term in Equation (3-10), is then written along the s-axis that is oriented along the characteristic direction $\hat{\Omega}$ to give:

$$\hat{\Omega} \cdot \vec{\nabla}\psi(\vec{r}, \hat{\Omega}, E) = \frac{d\psi(s, E)}{ds} \tag{3-11}$$

Hence Equation (3-11) above can be written in the characteristic form as:

$$\frac{d\psi(s)}{ds} + \Sigma_t(s)\psi(s) = Q(s) \tag{3-12}$$

E is omitted from the equation for purposes of clarity and $Q(s)$ is the source. The solution for Equation (3-12) above then becomes:

$$\psi(s) = \psi_0 e^{-\Sigma_t s} + e^{-\Sigma_t s} \int_0^s Q e^{\Sigma_t s'} ds' \tag{3-13}$$

where s symbolizes the distance along the characteristic direction $\hat{\Omega}$, and ψ_0 is the known angular flux at $s = 0$. The value for angular flux ψ_0 is given from boundary conditions for known

cell sides. Methods which are used for the determination of an appropriate value for the angular flux ψ_0 and for evaluation of the integral term vary in different techniques of solution.

One scheme is the step characteristic method developed by Lathrop [11]. In this method, the source Q and the total macroscopic total cross section Σ_t, are assumed to be constant within a computational cell and the angular flux is also assumed to be constant on the cell boundaries of the incoming direction. The integration of Equation (3-13) can then be performed to obtain:

$$\psi(s) = \psi_0 e^{-\Sigma_t s} + \frac{Q}{\Sigma_t}(1 - e^{-\Sigma_t s}) \tag{3-14}$$

Figure 14 is an example of a rectangular computational cell in which the step characteristic method can be applied. For the characteristic direction $\hat{\Omega}$ shown in Figure 14, the unknown flux ψ_T at the top may be computed as a linearly weighted average of contributions from known fluxes (sides with ψ_B and ψ_L). The fluxes ψ_B and ψ_L sides are taken to be constant along the length of each side, representing the average angular flux in direction $\hat{\Omega}$. Knowing the lengths of the sides of this rectangular cell (that is Δx and Δy) and the cosines of direction $\hat{\Omega}$ in the $x - y$ plane, a function for the length s can be determined. The solution for $\psi(s)$ in Equation (3-14) can then be integrated along the length of each side to determine the average angular flux for the unknown sides. Once the angular flux is known on all four sides, a neutron balance on the cell can be used to determine the cell's average angular flux.

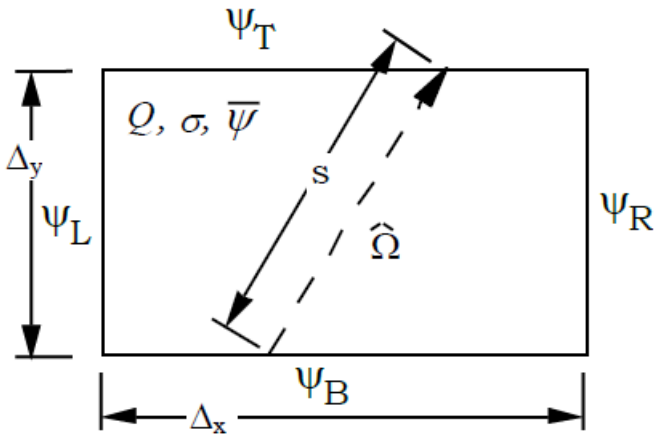


Figure 14: A Typical rectangular cell used in the step characteristic approach

Source: [11]

The method described above is the step characteristic method of the rectangular cell. The derivation of Equation (3-14) makes no assumptions about the shape of the cell. It merely requires knowledge of the relationship between edges of the cell along the direction of

characteristic. When this method is applied to generalized geometries, the method is referred to as the Extended Step Characteristic method.

The Extended Step Characteristic is therefore an extension of the step characteristic method developed for igeneralized geometries. The extended step characteristic method is based primarily on two assumptions, which are, all properties (i.e. Σ_t and Q) are uniform within a computational cell and that the cell boundaries are defined by straight lines.

Given a characteristic direction, each side of a cell can have one of three possible attributes relative to the flow of the particle, as show in Figure 15. Flow can enter the cell when crossing a side (as shown by sides E and F), flow can leave (exit) from the cell when crossing a side (shown by B and C), and flow may be parallel to the orientation of a given side (shown by sides A and D). This can be mathematically expressed as:

	$\hat{\Omega}_k \cdot \hat{n}_i < 0$	Flow entering
	$\hat{\Omega}_k \cdot \hat{n}_i > 0$	Flow exiting
	$\hat{\Omega}_k \cdot \hat{n}_i = 0$	Parallel flow

where $\hat{n}_i$ is the unit vector in the cell's outward direction normal to side i, and $\hat{\Omega}_k$ is the k^{th} discrete element of the set of characteristic directions. The side with flow entering is termed the incoming side with respect to direction $\hat{\Omega}_k$. The side with flow exiting is termed the outgoing side with respect to direction $\hat{\Omega}_k$. With parallel flow included as a special case of the incoming side, the equations can be mathematically expressed as

Side i is incoming with respect to $\hat{\Omega}_k$:	$\hat{\Omega}_k \cdot \hat{n}_i \leq 0$
Side i s outgoing with respect to $\hat{\Omega}_k$:	$\hat{\Omega}_k \cdot \hat{n}_i > 0$

To solve the flow (fluxes) on the outgoing sides, the flow all incoming sides must be known.

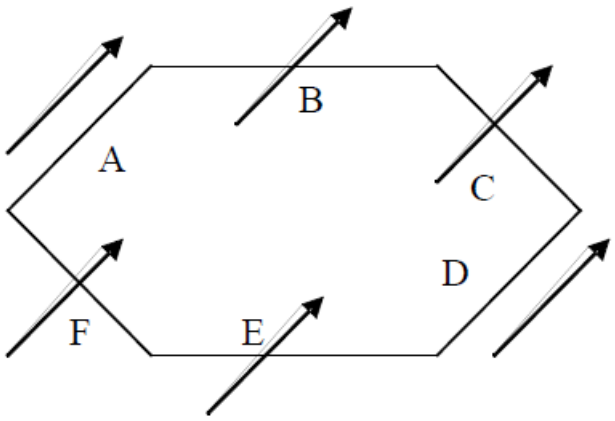


Figure 15: Orientation of the sides of a cell with respect to a given direction vector

Source: [11]

3.3.4 The Multiplication Factor

One of the most important aspects of operating a reactor is to achieve a controlled sustainable nuclear chain reaction. The nuclear chain reaction is a sequential splitting of atomic nuclei (nuclear fission), where each reaction in the chain is started by a neutron that is produced in the previous fission reaction. To achieve the sustainability of the chain reaction, the ratio of the number of neutrons of a current generation to the next generation must be kept constant [25]. The ratio is presented in Equation (3-15) below:

$$k_{eff} = \frac{fission\ neutrons\ in\ generation(i+1)}{fission\ neutrons\ \ in\ generation(i)} \tag{3-15}$$

This ratio is referred to as the multiplication factor. There are also other ways of defining k_{eff}. k_{eff} can be adjusted by changing the geometry of the reactor, changing the material densities (most importantly the absorber materials), or by withdrawal or insertion of the control rods.

3.3.5 Monte Carlo Methods

A Monte Carlo method is a statistical sampling technique that uses probability laws to describe the behaviour of a neutron and to trace the step by step events of a particle's lifetime until death, in that way creating a series of histories of the neutron's (particle) life. Monte Carlo techniques are based on statistical concepts, hence the results of Monte Carlo methods are an estimation and should lie on some confidence interval relating to the true answer [32].

In Monte Carlo methods, neutrons are produced or born randomly, except for the first cycle where the neutron source needs to be specified. The total macroscopic cross section Σ_t

characterises the path lengths of the neutrons and probabilistic methods to be used to determine whether the neutron undergoes leakage or collisions. At each collision point, different types of reactions are randomly selected according to the relevant cross sections. The direction and energy of the neutron is changed by different scattering events while it is transported in the system. If either fission or capture occurs, the particle is killed by “roulette” or terminated completely depending in the code being used. If leakage occurs, the history of the neutron is terminated.

3.3.6 Convergence of Monte Carlo Methods

Monte Carlo calculations of systems containing fissile materials are based on iteration methods, where random walks of a single generation of neutron population are carried out for each cycle of neutrons to estimate the value of the effective multiplication factor (k_{eff}) and the fission source distribution of the next generation. The iteration method is repeated until the fission source distribution is converged. Hence, the active and inactive neutron cycles are specified. Inactive cycles are those where the fission source distribution has not converged, and active cycles are where the fission source distribution has converged, that is when uniformity of the fission source distribution within the statistical nature is reached, and tallies are accumulated.

In a study performed by Brown F.B. [33], it was noted that the fission distribution converges slower than k_{inf}, hence the fission distribution and k_{inf} must be assessed simultaneously for convergence to ensure correct results. The Shannon entropy is used for characterising the convergence of the fission distribution.

The Shannon entropy (H_{src}) is a well-known phenomenon from information theory that provides a number for each neutron cycle to assist in characterising the convergence of the fission source distribution [34]. When calculating H_{src}, the three-dimensional (3D) grid geometry is superimposed on a problem domain encompassing all the fissionable regions, and the number of fission sites is tallied in each of the grid boxes in each cycle. The tallies can be used to create a discretised estimate of the fission source distribution, (P_j, j=1, N_S), given that N_S is the number of grid boxes in the superimposed mesh, and P_j is equal to the number of source sites in the j-th grid box over the total number of source sites. The H_{src} is computed as follows [33]:

$$H_{src} = -\sum_{j=1}^{N} P_j ln_2(P_j) \tag{3-16}$$

The Shannon entropy H_{src} varies between zero for a point distribution and $ln_2(N_S)$ for a uniform distribution.

3.4 Collapsing of Cross Sections

3.4.1 Generation of Cross Sections

Cross sections in multigroup energy calculations are generated by using the flux as a weighting function, mathematically defined as [15]:

$$\sigma_{z,r,g}^{j} = \frac{\int_{\Delta E_g} \sigma_{z,r}^{j}(E)\phi_z(E)dE}{\int_{\Delta E_g} \phi_z(E)dE} \tag{3-17}$$

where:

$\sigma_{z,r,g}^{j}$ is the region averaged group cross section,

$\phi_{z,g}$ is the multigroup flux in a particular region,

ΔE_g is the discrete energy interval.

If it is also required to consider the spatial dependence of the cross section and the angular and spatial dependence of the flux, then the collapsed cross section can be calculated as given in the next section specifically for the form used in NEWT. NEWT is a neutron transport solver code in SCALE which can also perform cross section collapsing.

In NEWT the few-group cross sections are calculated after the fluxes in the fuel assembly have been calculated for a single isotope using Equation (3-18) below [18]:

$$\Sigma_x^{i,g} = \frac{\int_{E_g}^{E_{g-1}} \int_V \int_{4\pi} dE dV d\widehat{\Omega} N_i(\vec{r}) \sigma_x^i(E) \psi(\vec{r}, \widehat{\Omega}, E)}{\int_{E_g}^{E_{g-1}} \int_V \int_{4\pi} dE dV d\widehat{\Omega} \psi(\vec{r}, \widehat{\Omega}, E)}, \tag{3-18}$$

where $\psi(\vec{r}, \widehat{\Omega}, E)$ is the angular flux at position $\vec{r}$, the direction at which the neutron travels is $\widehat{\Omega}$ and the energy of the neutron is E. The integral over dV is over the volume for which the few-group cross section is calculated. The energy is discretized into the fine group structure. The integral involving $d\widehat{\Omega}$ will be performed using an angular quadrature scheme. The cross section σ_x^i is defined for the nuclide under consideration at position $\vec{r}$ for reaction x and the index i denotes the nuclide. When all the nuclides in the volume V are considered, a summation over all these nuclides is required, and the Equation (3-18) becomes [18]:

$$\Sigma_x^g = \frac{\int_{E_g}^{E_{g-1}} \int_V \int_{4\pi} dE dV d\hat{\Omega}\ \sum_i \left(N_i(\vec{r})\sigma_x^i(E)\right) \psi(\vec{r}, \hat{\Omega}, E)}{\int_{E_g}^{E_{g-1}} \int_V \int_{4\pi} dE dV d\hat{\Omega}\ \psi(\vec{r}, \hat{\Omega}, E)}. \quad (3\text{-}19)$$

3.4.2 Collapsed Multigroup Cross Sections

The multigroup method is widely used for the neutron flux characterisation in terms of energy. To develop a multigroup calculation method for energy distribution, the energy structure is divided into energy intervals of interest, for example, dividing the energy structure into G groups, from zero to 10 MeV. Figure 16 below shows the division of the energy structure into G groups [25] [35].

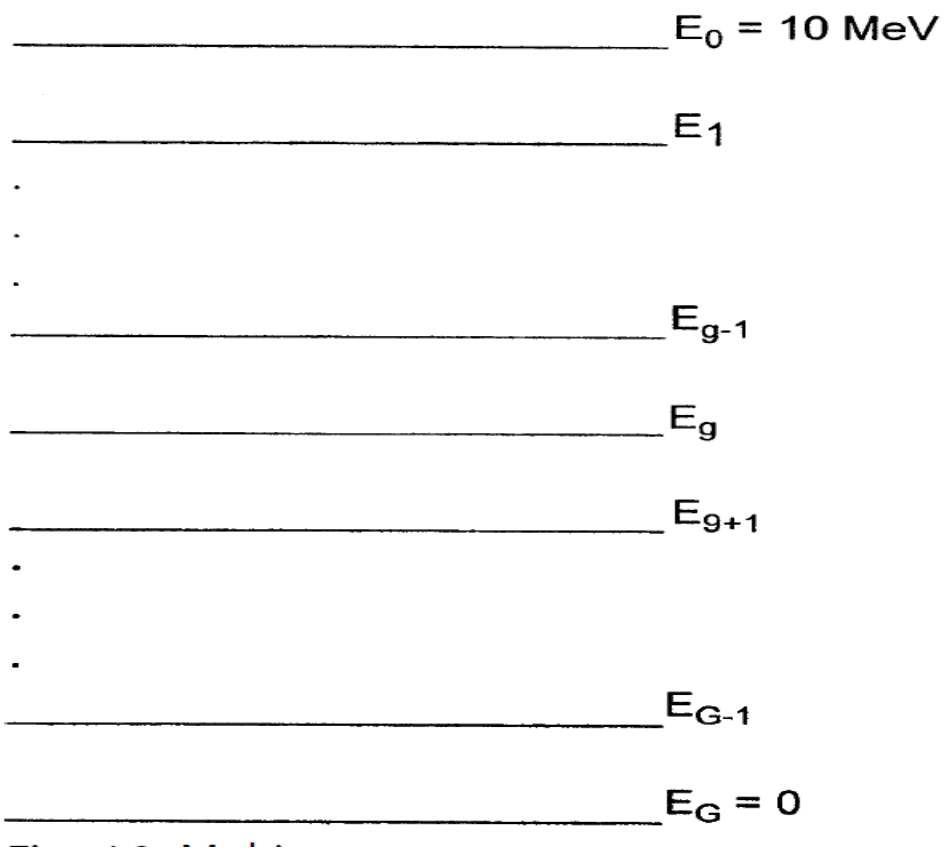


Figure 16: Multigroup energy structure

Source: [25]

where:

E_0 is the upper energy,

E_G Is the lowest energy,

E_{g-1} is the energy higher than E_g,

E_g to E_{g-1} are energies contained in energy group g, and

G is the total number of energy groups.

The formalism described in the previous section is then used to generate the collapsed multigroup cross sections according to these energy groups.

For continuous energy (CE) calculations, there is no need to collapse the cross section data set into groups.

3.5 The Concepts of Uncertainty and Sensitivity Analysis

Uncertainty and sensitivity analysis methods are essential for identifying valuable processes in safety and design, providing quantifiable biases for neutronic validation of criticality safety, and quantifying the impacts of uncertainties in nuclear data and physical parameters for safety analysis [11].

Uncertainty analysis is a method that seeks to describe the entire set of possible model outcomes together with their associated probabilities of occurrence [36]. This method is valuable for identifying potential sources of computational biases and highlighting important parameters for code validation. When applying uncertainties in the cross section data, the sensitivity of the cross section data can be used to propagate uncertainties in cross section data to an uncertainty in a system response.

Sensitivity analysis is the method that aims to describe how much the model output values are impacted by variations in the input values. It investigates the importance of uncertainty in input values (uncertainties are normally associated with input values). This method gives insight into the system's performance in that the anticipated response of the system to an adjustment in some input process is quantified. Essential processes can be distinguished as those that cause the biggest changes in the response per unit change in the input. In the numerical simulations of neutron transport, calculating essential responses such as reaction rates, the effective multiplication factor and reactivity coefficients require many input parameters (such as material composition, geometry, temperature, etc. These parameters are described in Appendix A. Due to the complexity of nuclear data and their corresponding evaluation procedures, the response of models to cross section data is very important for analysis.

The input parameters that cause the uncertainties in output parameters for the MHTGR-350 fresh fuel block and supercell include the nuclear parameters that are propagated using the multigroup cross section covariance matrix and manufacturing uncertainties [3]. Methods and modelling approximations such as the DOUBLEHET and self-shielding treatment can also contribute to the uncertainty.

The computational tools for uncertainty and sensitivity analysis used in this study are TSUNAMI-3D and Sampler. Both are part of the SCALE 6.2.1 code system. KENO-VI and NEWT are transport solvers used in this study for TSUNAMI-3D and Sampler respectively.

3.5.1 General Statistics

Uncertainty and sensitivity analysis studies uses general statistics, these includes the mean, standard deviation, covariance and variance. A general statistical definition of those is given in this section.

Suppose there are N separate measurement of a single quantity x denoted by $x_1, \dots, x_N$. Then the mean and standard deviation are mathematically expressed in Equation (3-20) and (3-21), respectively [37].

$$\bar{x} = \frac{1}{N}\sum_{i=1}^{N} x_i \tag{3-20}$$

$$\sigma_x = \sqrt{\frac{1}{N-1}\sum (x_i - \bar{x})^2} \tag{3-21}$$

The term covariance is used to indicate the relation of two variables. Suppose values of an output function $Q(x, y)$ that only depends on x and y variables are obtained by measuring pairs of such variables N times yielding the set (x_i, y_i)... (x_N, y_N). Then the covariance is mathematically expressed as [15]:

$$cov(x, y) = \sigma_{xy} = \frac{1}{N}\sum_{i=1}^{N} (x_i - \bar{x})(y_i - \bar{y}) \tag{3-22}$$

Variance is a parameter that measures how far a set of numbers are distributed and is expressed when the variables are identical [15].

$$VAR = COV(x,x) = \frac{1}{N}\sum_{i=1}^{N}(x_i - \bar{x})^2 \tag{3-23}$$

3.5.2 Sensitivity Analysis Methods

In this study sensitivity coefficients are used to measure sensitivity. Sensitivity coefficients are a measure of sensitivity (which is the derivative of a model output variable with respect to the input parameter or variable) [36]. Equation (3-24) shows a change in the system's multiplication factor k response due to change in nuclear data parameters (i.e. capture, fission, etc.), which defines the sensitivity coefficient [11].

$$S_{k,\Sigma_x} = \frac{dk/k}{d\Sigma_x/\Sigma_x} \tag{3-24}$$

Equation (3-25) is used to calculate the relative uncertainty of the multiplication factor k response [23].

$$\frac{dk}{k} = \mu_i = S^T_{k,\Sigma^i_{x,g}} COV_{\Sigma\Sigma} S_{k,\Sigma^i_{x,g}} \tag{3-25}$$

Where $COV_{\Sigma\Sigma}$ denotes the covariance matrix (which contains the cross-section relative covariance data evaluated for all reactions in all energy groups) measured in relative units of $(\%)^2$ and the subscript T denotes the transpose of the matrix.

It is noted that Equation (3-25) is written in energy group format, and Equation (3-24) is not. For such as case which would be in continuous energy mode, the sensitivity results must be edited so that they are written in energy group format, i.e. the sensitivity coefficients computed in CE mode must be stored in a multigroup sensitivity data file.

Sensitivity coefficients are used in several sensitivity analysis methods. In this study sensitivity coefficients are determined by the making use of the CLUTCH method.

3.5.3 Propagation of Uncertainties

The methodologies used in this study to propagate uncertainties are the CLUTCH method and statistical sampling. The CLUTCH method is the method that calculates sensitivity coefficients, which is based on contribution theory. Statistical sampling involves the notion of randomness and the use of probability distribution functions.

3.5.3.1 The CLUTCH method

The CLUTCH method, developed by Perferti in 2012 [38], calculates eigenvalue sensitivity coefficients in a single forward Monte Carlo calculation using the importance of events during a particle's lifetime by examining how many fission neutrons arise after those events have occurred [11]. Consider a neutron source Q, which is equal to the fission source of the system of interest:

$$Q = \lambda F\psi \tag{3-26}$$

where ψ is the neutron flux, $\lambda = 1/k$ and F is the neutron production term.

Multiplying Equation (3-26) by the adjoint flux ψ^* and integrating over phase space we get

$$\langle \psi^* Q \rangle = \lambda \langle \psi^* F\psi \rangle \tag{3-27}$$

The adjoint flux ψ^* can be physically interpreted as the importance of events that occur during the lifetime of particle histories.

The importance of a neutron in phase space τ_s is calculated from Equation (3-28), that is deduced from Equation (3-27) [18]:

$$\psi^*(\tau_s) = \frac{\lambda}{Q_s}\int_V G(\tau_s \to \vec{r})F^*(\vec{r})d\vec{r}, \quad \textit{equation} \tag{3-28}$$

where

Q_s is the neutron source in phase space, such that $Q_s = Q_s(\tau_s \to \vec{r})$ and $G(\tau_s \to \vec{r})$ is the transfer function and is defined as the expected number of fission neutrons generated in all energies and directions due to a neutron emitted in phase space and can be expressed as:

$$G(\tau_s \to \vec{r}) = \frac{1}{Q_s}\int_V \int_{\hat{\Omega}} \nu\, \Sigma_f(\vec{r},\ E)\psi(\vec{r},E,\hat{\Omega}|G(\tau_s \to \vec{r})Q(\tau_s))d\hat{\Omega}dE, \quad (3\text{-}29)$$

where

$\psi^*(\vec{r},E,\hat{\Omega}|G(\tau_s \to \vec{r})$ is the flux created in phase space $(\vec{r},E,\hat{\Omega})$ given the source $Q(\tau_s)$.

$$F^*(\vec{r}) \ = \int_E \int_{\hat{\Omega}} \frac{\chi(\vec{r},E)}{4\pi}\psi^*(\vec{r},E,\hat{\Omega})d\hat{\Omega}dE, \quad \textbf{(3-30)}$$

where $F^*(\vec{r})$ is the weighting function and is defined as the expected importance of a fission neutron emitted at $\vec{r}$.

The definition of the unconstrained fission spectrum sensitivity coefficients is given by:

$$S_{k,X}(r) = \frac{1}{D}\frac{1}{k}\int_0^\infty \int_{4\pi} \overline{\nu}\,\Sigma_f(r,E)\psi(\mathrm{r,E},\Omega)\mathrm{d\Omega dE} \int_0^\infty \int_{4\pi} \frac{\chi(\mathrm{r,E'})}{4\pi}\ \psi^*(\mathrm{r,E',\Omega')d\Omega' dE'} \quad (3\text{-}31)$$

where the adjoint-weighted fission source is denoted by D and $\int_0^\infty \int_{4\pi} \frac{\chi(\mathrm{r,E'})}{4\pi}\ \psi^*(\mathrm{r,E',\Omega')d\Omega' dE'}$ is the definition of the weighting function $F^*(r)$. Rearranging Equation (3-57) gives:

$$F^*(r) = \frac{D \times\ S_{k,\chi}(r)}{\int_0^\infty \int_{4\pi} \frac{\overline{\nu}\,\Sigma_f\,(r,\ \ E,)\,\psi\,(r,\ \ E,\ \ \Omega)}{k}\,d\Omega dE} \quad (3\text{-}32)$$

where $\int_0^\infty \int_{4\pi} \frac{\overline{\nu}\,\Sigma_f\,(r,\ \ E,)\,\psi\,(r,\ \ E,\ \ \Omega)}{k}\,d\Omega dE$ is the total weight of the fission neutron in each of the $F^*(r)$ mesh regions.

The $F^*(r)$ spatial dependence is accounted for by calculating and storing the $F^*(r)$ on a spatial mesh, where the $F^*(r)$ mesh only covers the regions of all fissionable materials in the system.

The unconstrained chi-sensitivity in the numerator of Equation (3-58) is tallied during the inactive generations to estimate $F^*(r)$ for the active generation sensitivity coefficient calculations.

Using this formulation for $F^*(r)$, [18] has shown, that the sensitivity coefficients can then be calculated using:

$$S_{k,\Sigma_x} = \frac{C_s + C_f + C_x}{D} \quad (3\text{-}33)$$

Where

Σ_x is the macroscopic cross section for reaction x

C_s is the scattering contribution which describes the correlation of the forward and adjoint fluxes in energy and in direction, mathematically expressed in Equation (3-34).

C_f is the fission source contribution which describes how the forward and adjoint fluxes are uncorrelated in direction, mathematically expressed in Equation (3-35).

C_x is the collisional contribution for the reaction x which contains the forward and adjoint fluxes that are completely correlated, mathematically expressed in Equation (3-36).

D in the denominator is the adjoint weighted fission source term integrated over all regions and nuclides, define in Equation (3-37).

$$C_s(z, E \to E') = \int_{V_z} \int_{4\pi} \int_{4\pi} \psi(\vec{r}, E, \hat{\Omega}) \Sigma_S \left(\vec{r}, E \to E', \hat{\Omega} \to \hat{\Omega}'\right) \psi^*\left(\vec{r}, E', \hat{\Omega}'\right) d\hat{\Omega}' d\hat{\Omega} dV \tag{3-34}$$

$$C_f(z, E \to E') = \int_{V_z} \int_{4\pi} \bar{\nu} \Sigma_f(\vec{r}, E)(\vec{r}, E, \hat{\Omega}) d\hat{\Omega} \int_{4\pi} \frac{\chi(\vec{r}, E')}{4\pi} \psi^*\left(\vec{r}, E', \hat{\Omega}'\right) d\hat{\Omega}' dV \tag{3-35}$$

$$C_x(z, E) = \int_{V_z} \int_{4\pi} \Sigma_x(z, E) \psi(\vec{r}, E, \hat{\Omega}) \psi^*\left(\vec{r}, E, \hat{\Omega}\right) d\hat{\Omega} dV \tag{3-36}$$

$$D = \lambda \int_V \int_0^\infty \int_{4\pi} \bar{\nu} \Sigma_f(\vec{r}, E) \psi(\vec{r}, E, \hat{\Omega})\, d\hat{\Omega} \mathrm{dE} \int_0^\infty \int_{4\pi} \frac{\chi(\vec{r}, E')}{4\pi} \psi^*\left(\vec{r}, E', \hat{\Omega}'\right) d\hat{\Omega}' dE' dV. \tag{3-37}$$

In the above equations,

Σ_s is the macroscopic scattering cross section

z is the represent a region and V_z is the volume of region z

E' and $\hat{\Omega}'$ represent the neutrons from the fission reactions having random directions and energies

Σ_f is the macroscopic fission cross section

$\bar{\nu}$ is a parameter called nubar, which denoted the average number of fission neutronsχ is a parameter called the unconstrained chi, which is the fission neutron energy spectrum (e.g. $\chi(E)dE$ is defined as the number of fission neutrons emitted with energy E in $E + dE$ per fission neutron [18])

The following expressions are of sensitivity coefficients according to reaction types [18]:

- The capture reaction sensitivity coefficient

$$S_{capture}(z,g) = -\int_g \frac{C_{x=capture}(z,E)}{D}\,dE \tag{3-38}$$

- The fission reaction sensitivity coefficient

$$S_{fission}\,(z,g) = \int_g [\lambda \int_0^\infty \frac{C_{fission}(z,E\rightarrow E')}{D}\,dE' - \frac{C_{x=fission}(z,E)}{D}]dE \tag{3-39}$$

- Scattering reaction sensitivity coefficient

$$S_{scattering}\,(z,g) = \int_g [\int_0^\infty \frac{C_{scattering}(z,E\rightarrow E')}{D}\,dE' - \frac{C_{x=scattering}(z,E)}{D}]dE \tag{3-40}$$

- The sensitivity coefficient for a nubar ($\bar{\nu}$) reaction

$$S_{\bar{\nu}}(z,g) = \int_g [\int_0^\infty \frac{C_{fission}(z,E\rightarrow E')}{D}]\,dE' \tag{3-41}$$

- The sensitivity coefficient for the unconstrained chi (χ) reaction

$$S_{\chi}(z,g) = \lambda \int_g [\int_0^\infty \frac{C_{fission}(z,E\rightarrow E')}{D}]\,dE' \tag{3-42}$$

For more detail on the derivation of the CLUTCH method from the contribution theory, the reader is referred to [38].

3.5.3.2 Statistical Sampling

This method involves the notion of randomness. For example, let's consider a value of performance measure like the depth of water at a location which varies, and this variation over space and time cannot be predicted with certainty, it is called a random variable. In such a case, one cannot specify with certainty what the value of a random variable will be but can only provide the likelihood or probability of occurrence within some specified range of values. The likelihood or probability of observing particular ranges of values of a random variable are characterized by what is called a probability distribution. There are multiple probability distributions that are in existence for observing a selected range of values for a random variable [36].

Consider a random variable X that can only have discrete sets of values, then its probability distribution can be described by a histogram, Figure 17 a). From Figure 17 a), the function

$P_X(X)$ ascribe probability to a random variable for having a specific value. When summing up the probabilities for all possible outcomes, the sum must be equal to one. Figure 17 b). shows an expression of the probability distribution of X as a continuous distribution, that is when the random variable is a continuous variable that can assume any real value over a range of values. The shaded area (blue) under the curve in Figure 17 b) is 1. Figure 17 c) shows the probability that the value of x of X will be within the range of values between u and v (i.e. the shaded area between u and v). The probability distributions shown in Figure 17 b) and Figure 15 c) are called probability density functions (pdf) and are characterized by the function $f_X(X)$. The subscript X on the functions P_X(X) and $f_X(X)$ represents the random variable, and the variable X in the brackets is some value of that random variable X.

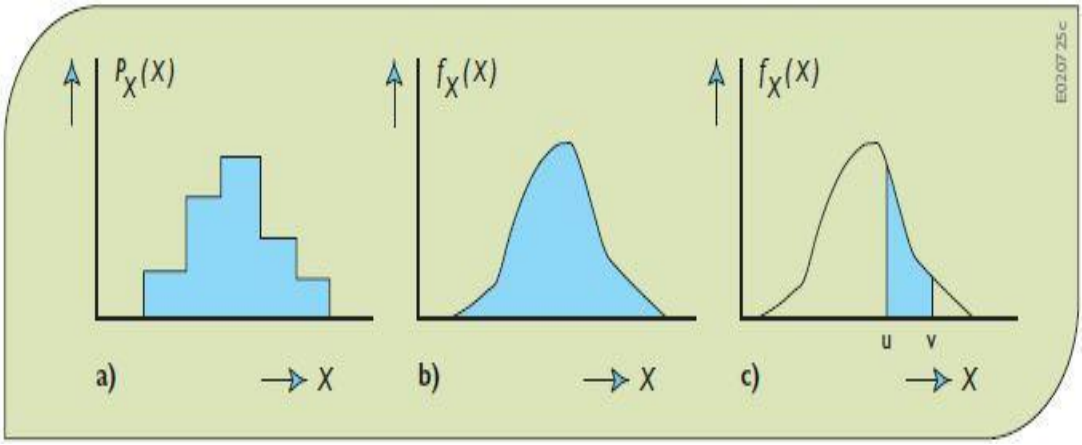


Figure 17: Probability distributions for a discrete or continuous random variable X.

Source: [36]

In order to accomplish a complete uncertainty quantification, all sources of uncertainties in terms of probability distributions for each input in a model must be identified.

A number of calculations (say *N*) can then be performed. For each calculation, values for the input parameters are chosen randomly from the probability distributions. The *N* calculations then produce as set of *N* values for each response considered.

For example, consider the multiplication factor k chosen as a response. The uncertainty in the multiplication factor k response due to uncertainties in the input data is then interpreted from the standard deviation (described in Section 3.5.1) estimated using Equation (3-43). The relative uncertainty in the multiplication factor k response can then be obtained using Equation (3-44) [23].

$$dk = \sqrt{\frac{1}{N-1}\sum_{n=1}^{N}(k_n - \bar{k}_n)^2} \tag{3-43}$$

$$\mu_i = 100\% \times \frac{dk}{k} \tag{3-44}$$

3.6 Codes Used

The Standardised Computer Analyses for Licensing Evaluation (SCALE 6.2.1) code package is used in this study. It is a modelling and simulation code developed, maintained and tested at the Oak Ridge National Laboratory (ORNL). It provides a user-friendly tool that can perform criticality safety calculations, radiation shielding applications, reactor and lattice physics, and uncertainty and sensitivity analysis. SCALE 6.2.1 is equipped with different computational modules. Some of these are deterministic and Monte Carlo transport solvers which are selected according to the solution strategy of choice. The nuclear data libraries included in SCALE 6.2.1 are the latest for continuous energy (CE) and multigroup (MG) neutronics [11] [15] [39].

The computational modules in SCALE 6.2.1 consist of a class of functional modules and control modules. A functional module performs calculations for reactor studies such as criticality, depletion and uncertainty and sensitivity analysis. A control module manages data transfer in between functional modules and provides guidance for the calculations that are performed by functional modules [15] [39].

For this study, the SCALE 6.2.1 code package is used to perform criticality calculations, self-shielding studies, generate cross sections and analyse uncertainty and sensitivity studies of the MHTGR-350 fresh fuel block and supercell.

3.6.1 KENO-VI

KENO-VI is a functional module of SCALE 6.2.1 that is executed by using the control module CSAS6. It is a Monte Carlo criticality transport code which can be used as a standalone code or as part of a sequence such as TSUNAMI-3D, TRITON or CSAS. KENO-VI is a three-dimensional (3D) code, hence it has the capability of modelling 3D systems with complex geometries. KENO-VI performs continuous energy (CE) or multigroup (MG) criticality calculations using either ENDF/B-VII.0 or ENDF/B-VII.1 nuclear data files, which are included in the SCALE 6.2.1 code package [11] [15].

The geometry package in KENO-VI can model any volume that can be constructed by using quadratic equations. The shapes that can be constructed with KENO-VI are cubes, spheres, cuboids, cylinders and hexagonal prisms. Arrays of these shapes can also be constructed.

Additional geometry features include body rotations and dodecahedral arrays to make the code more flexible [11] [39].

For KENO-VI MG calculations, the cross sections used must first be collapsed into the group structure required. To carry this out, the control module CSAS6 uses the Material and Cross Section Processing module (XSProc) to automatically call on BONAMI and CENTRM modules to prepare the group cross sections for the KENO-VI MG calculation.

The Continuous Energy Transport Module (CENTRM) is the module that computes sets of pointwise continuous fluxes and prepares self-shielded cross sections based on the unit cell and pointwise continuous energy cross section library. Bondarenko AMPX (BONAMI) is the module that provides resonance corrected cross sections when called in support of CENTRM in those regions not explicitly treated by CENTRM.

For KENO-VI CE calculations, the self-shielding treatment carried out in BONAMI and CENTRM is not required, although the CE cross sections must be broadened due to the temperature broadening.

3.6.2 NEWT

NEWT is a 2D deterministic radiation transport code that uses multigroup discrete-ordinates with flexible meshing capabilities that allow 2D neutron transport calculations. The transport equation is solved using the method of characteristics (the extended step characterization method, described in Section 3.3.3), in which the transport equation is solved along characteristic directions within a computation cell. Further details of the method are given in [11]. Like KENO-VI, NEWT can be used as a standalone code or as part of a sequence in a calculation. It has the capability of modelling a 2D system with complex geometry models.

The geometry package of NEWT can model shapes such as the cylinder, cuboid, hexaprism, rotated hexaprism, wedge and polygon, however in 2D. NEWT allows a computational mesh based on arbitrary polygons. This scheme is capable of closely approximating curved or irregular surfaces providing NEWT with the capability of modelling problems that were formerly impractical to model directly using discrete-ordinates [11].

The control module used in NEWT is TRITON. TRITON first reads the composition and cell data blocks, loads the specified library to be self-shielded, and performs MG self-shielding calculations for all compositions by calling on the BONAMI and CENTRM modules through XSProc, thereby preparing a cross section data set for use in the multigroup transport calculation. Thereafter, NEWT is executed.

3.6.3 TSUNAMI-3D

TSUNAMI-3D is a control module that is used to facilitate the implementation of uncertainty and sensitivity analysis theory for criticality safety calculations. Hence its primary function is to guide a sequence of calculations performed by other modules of SCALE 6.2.1.

Two separate methods for uncertainty and sensitivity analysis can be employed for continuous energy (CE) calculations with TSUNAMI-3D, the Iterated Fission Probability (IFP) method and the Contribution-Linked eigenvalue sensitivity/Uncertainty estimation via Tracklength importance Characterisation) (CLUTCH) method. Both methods have the capability of calculating eigenvalue sensitivity coefficients. However, the CLUTCH method is preferred due to its faster runtime and the use of lower computational memory [21]. In this study, the CLUTCH method was used. The CLUTCH method is described in Section 3.5.3.

In multigroup mode, TSUNAMI-3D can be used to calculation the sensitivity coefficients and propagate the uncertainty in the multiplication factor using General Perturbation Theory. However, TSUNAMI-3D in SCALE 6.2.1 version cannot treat double heterogeneous systems, and therefore was not used in this study. For details on the method, see [11]

3.6.4 SAMS

SAMS is the acronym for Sensitivity Analysis Module in SCALE. In the CE treatment using TSUNAMI-3D, SAMS is used to provide edits of sensitivity and uncertainty results. The sensitivity coefficients computed in CE mode are stored in a multigroup sensitivity data file.

3.6.5 Sampler

Sampler is a module in SCALE 6.2.1 code package for statistical uncertainty analysis using other functional modules within the SCALE 6.2.1 code package. It is a module that statistically samples the input data and analyses the output distributions for the response specified, and in that way performs general uncertainty analysis for SCALE 6.2.1 sequences, as described already.

Sampler has the capability of treating uncertainties from two sources, nuclear data and input parameters. Two of the input parameters are temperature and simple dimension specifications [11].

Sampler generates uncertainties by repeating passes in between computational sequences. Each pass is repeated with a random perturbed sample of the uncertainty quantities requested. See Section 3.5.

According to the SCALE 6.2.1 manual [11], Sampler can perform most general uncertainty calculations on most MG computational sequences of SCALE 6.2.1, but cannot perform uncertainty analysis calculations on continuous energy (CE) computational sequences. Hence in this study, Sampler is used for statistical uncertainty analysis for the MG SCALE 6.2.1 sequences.

CHAPTER 4 RESEARCH METHODOLOGY

4.1 Introduction

This chapter discusses the methodology that was used to generate models and analyse results. There were four main parts to the calculations. These were criticality calculations, self-shielding studies, collapsing of cross sections to obtain group constants and the uncertainty and sensitivity studies.

4.2 Criticality Studies

The MHTGR-350 reactor models that were used in this section of the study are the fresh fuel blocks and supercells, developed using KENO-VI and NEWT (modules of the SCALE 6.2.1 code package). The general description of both the MHTGR-350 fresh fuel block and supercell are outlined in Chapter 2, as well as the benchmark specifications that were used to develop these models.

4.2.1 Tools Used

The computer tools used in developing the models are KENO-VI and NEWT.

As mentioned already in Chapter 3, KENO-VI is a 3D Monte Carlo transport code, which is part of SCALE 6.2.1 code package. KENO-VI can either be used in multigroup or continuous energy mode, for this study it is used using both modes. KENO-VI can calculate many quantities such as the multiplication factor, neutron fluxes and reaction rates. In this study KENO-VI is used for multiplication factor calculations as well as the transport solver for TSUNAMI-3D.

As also already mentioned in Chapter 3, NEWT is a 2D multigroup discrete-ordinates transport code, which is also part of SCALE 6.2.1 code package. The Extended Step characteristic approach (described in Section 3.3.3) is the differencing scheme employed by NEWT to solve the transport equation. In this study NEWT is used for multiplication factor calculations, cross section collapsing as well as the transport solver for Sampler.

4.2.2 Models used

The calculations of the MHTGR-350 fresh fuel block models used in this study were obtained from [18]. A description of the fresh fuel block was given in Section 2.3.3. All benchmark specifications that were used to develop the MHTGR-350 fresh fuel blocks are outlined in Section 2.3.

The TRISO fuel particles in the fuel compact were modelled using a cuboidal lattice. This was achieved by creating a layer of 128 particles in a square lattice in the radial plane with a pitch of 0.091 cm, see Figure 18 (a). All TRISO fuel particles were contained within the cylindrical fuel compact region, i.e. no TRISO fuel particle was clipped by the outer boundary of the cylindrical fuel compact. 50 layers of these radial lattices, with each having a height of 0.09856 cm, where then stacked one on top of the other to form the fuel compact. In total, 6400 fuel particles were modelled in the fuel compact. The BP's where also subject to this lattice treatment, however using different dimensions and quantity, see Figure 18 (b).

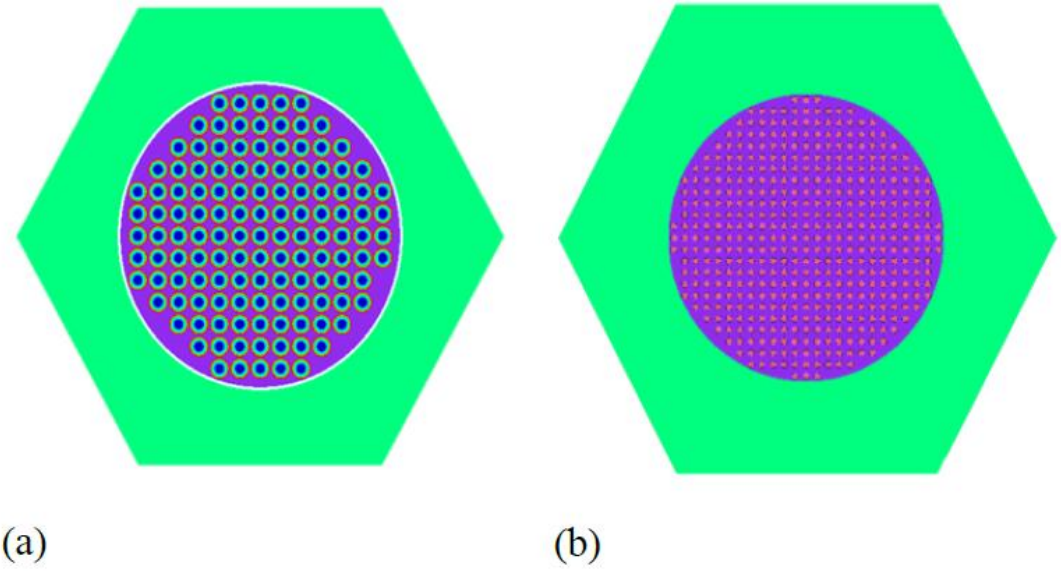


Figure 18: Cross Sectional view of the uniformly distributed (a) TRISO fuel particles in the fuel compact and (b) BP's in the BP compact

Source: [21]

The simplified MHTGR-350 supercell model, which consists of a centred MHTGR-350 fresh fuel block of the hexagonal cell surrounded by the lumped reflector blocks on the one side and lumped depleted fuel blocks on the other side, as already outlined in Chapter 2, was developed for KENO-VI and NEWT calculations. Appendix A provides a line by line description of the KENO-VI and NEWT input files that were used to develop the MHTGR-350 supercell models. Appendix B provides the KENO-VI MG input file of the MHTGR-350 supercell.

KENO-VI MHTGR-350 supercell models were developed in continuous energy (CE) and multigroup (MG) calculation schemes. For CE calculations, the centred fresh fuel block of the MHTGR-350 supercell consisting of the TRISO fuel particles and BPs in the respective compacts were modelled in the same manner as that for the fuel block, and was described above. For the equivalent MG calculations, the DOUBLEHET cell data was specified for the fuel, to consider the double heterogeneous structure of the of the TRISO fuel particles in the

fuel compact. However, since the BP does not contain fissionable or fissile material, it could not be modelled using the DOUBLEHET formulation and the cuboidal lattice modelling for the BP's was retained. Results of these models using ENDF/B-VII.0 and ENDF/B-VII.I nuclear data libraries are discussed in Section 5.2.2. To facilitate comparision with NEWT models, a further model was developed in which the BPs were modelled as a homogenous mixture. This was also a specification of the benchmark [3].

To specify the DOUBLEHET cell data for the TRISO particles, the TRISO fuel particle structure, isotope composition and dimensions of each coated layer of the fuel particles were specified, as well as the volume packing fraction of the fuel particles in the fuel compact. See Appendix A and B for specifications of the DOUBLEHET cell data.

The NEWT (which is an MG calculations scheme) MHTGR-350 supercell models were modelled as the KENO-VI MG models (i.e. the DOUBLEHET cell data was specified for TRISO fuel particles in the fuel compact). However, the BP's in the BP compact were modelled homogeneously, since as mentioned above, the DOUBLEHET treatment requires fissionable or fissile material, and this was not present in the BP definition. A lattice structure could not be used to model the BPs, since NEWT is a two-dimensional code. The results for NEWT models using both ENDF/B-VII.0 and ENDF/B-VII.I libraries are discussed in Section 5.2.3

A comparison of the multiplication factor k KENO-VI MG and NEWT results is made in Section 5.2.4.

The benchmark specifications (i.e. materials, dimensions, number densities, etc.) that were used to develop both the MHTGR-350 fresh fuel block and supercell models used in this study are outlined in Chapter 2.

Figure 19 shows the MHTGR-350 supercell model obtained from a KENO-VI calculation. This supercell model corresponds directly with the IAEA benchmark definition of Exercise I-2c.

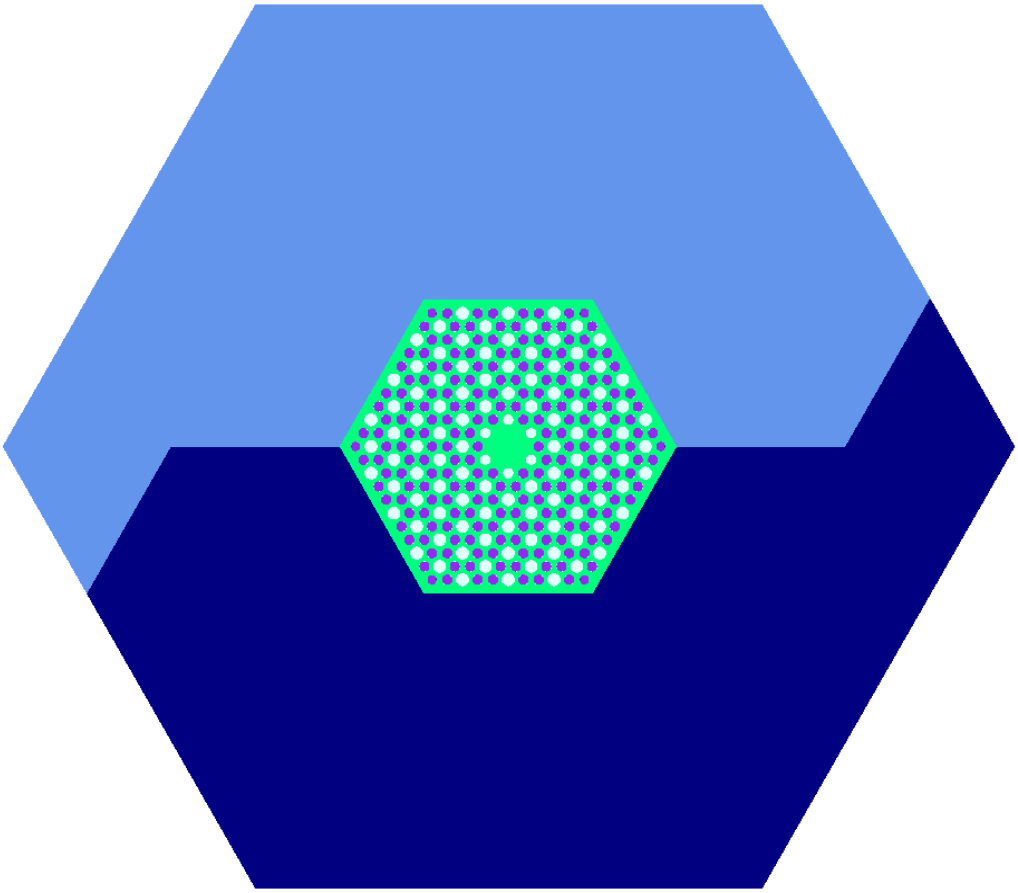


Figure 19: KENO-VI model of the MHTGR-350 supercell

Source: [obtained from KENO-VI]

4.2.3 Convergence Criteria

The convergence criteria of the multiplication factor k results used was based on the number of neutron generations to be run which was set to 600 (i.e. GEN=600 in the input file), the number of neutron per generation which was set to 50000 (i.e. NPG=50000 in the input file) and the number of generation to be skipped was set to 60 (NSK=60 in the input file), these were specified in a way such that the Shannon entropy of the fission source distribution and the multiplication factor were converged, referenced from [15].

4.3 Self Shielding

As mentioned in Section 3.2.4, the nuclear data in the ENDF/B-VII.0 and ENDF/B-VII.1 must be collapsed into 238 or 256 energy groups for use in the lattice physics code NEWT. However, in collapsing the data, the neutron flux is used as the weighting flux. In the presence of

resonances, the neutron flux will show dips in its structure as a function of energy, and this will therefore influence the calculation of the collapsed group constants. This effect is termed “self-shielding”.

With reference to Figure 20, one can observe different types of unit cells in the MHTGR-350 fresh fuel block, Figure 20 c). The unit cells with the yellow, blue and green centres are the fuel compacts, coolant channels and burnable poisons respectively, with each element embedded in the graphite matrix. The grey unit cells are composed completely of the matrix graphite.

It is therefore clear that the flux in these different unit will be different, and therefore in principle different values for the self-shielded values will be obtained in these different unit cells.

The simplest way to proceed with the calculation is to calculate the self-shielded values for the fuel unit cell, and to use these values for the coolant unit cell and the matrix graphite unit cells. Due to the strong absorbing nature of the burnable poisons, this approximation is not expected to work well for the burnable poisons.

It was therefore considered important to test the effect of the approximation, at least on the graphite in the coolant channels and the matrix graphite unit cells.

However, an added level of complexity arises because the fuel compacts contain coated particles. This gives rise to the double heterogeneity. The first level of heterogeneity is the coated particles in the compact matrix, and the second level of heterogeneity is the fuel compacts unit cells, burnable poison unit cells, coolant channel unit cells and the matrix graphite unit cells forming the hexagonal lattice structure in the fuel block as shown in Figure 20 c).

The resonance self-shielding calculation is carried out by calling XSProc. XSProc uses the DOUBLEHET cell description to address the double heterogeneity. First the coated particle with its matrix graphite shown in Figure 20 a) is treated as a unit cubic cell in an infinite cubic lattice, for which flux is calculated and a subsequent set of cross sections for the materials in the cubic cell is calculated. In this calculation, the compact material has been effectively homogenised. (The unit cell consists of the coated particle and its surrounding graphite matrix). A second calculation is then performed in considering the compact, the hexagonal graphite matrix and the helium gap between the compact and the graphite matrix as the solution space as shown in Figure 20 b). The material for the compact is however the homogenised data obtained from the first calculation. The collapsed data arising from this second calculation will then be self-shielded values for the compact as a single unit, the helium in the gap, and the graphite outside the gap. i.e. three cross-sections values are calculated and passed to the lattice calculation (i.e. NEWT).

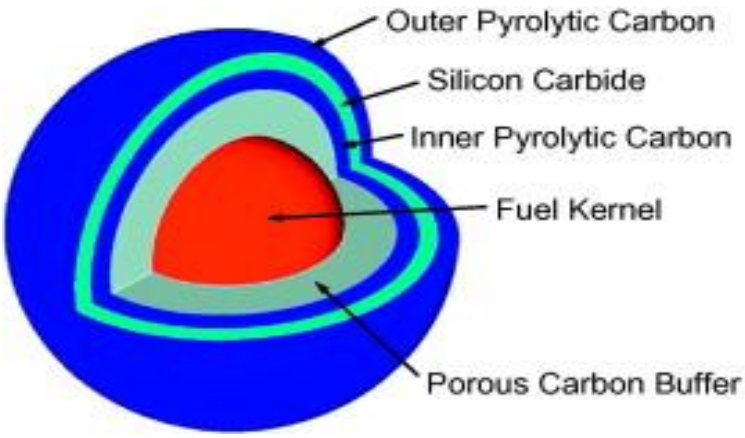
In principle, each unit cell of the fuel block shown in Figure 6 can be processed using XSProc. However, XSProc requires that the compact must have fissile or fissionable material. This therefore complicates the calculation when considering the coolant unit cells, the burnable poisons unit cells and the matrix graphite unit cells.

To test the effect of including self-shielding, two calculations were performed for both the MHTGR-350 fresh fuel block and the supercell.

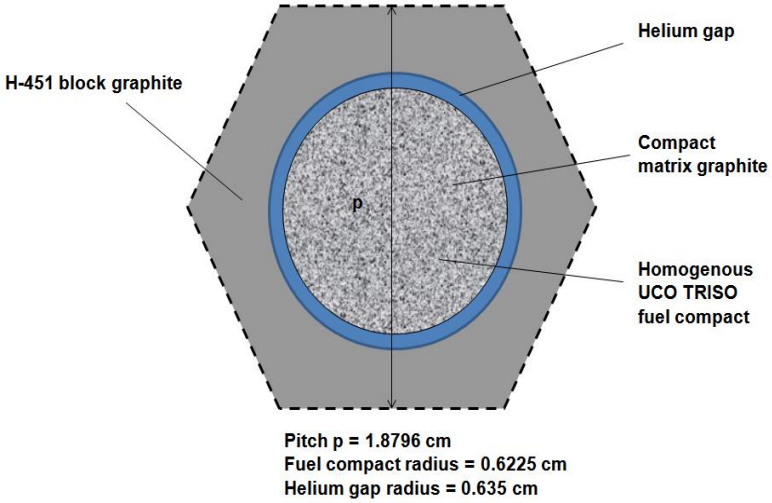
In the first model, only the fuel compact was subject to the self-shielding treatment. The graphite in the coolant channels, the graphite unit cells and the burnable poisons unit cells were not treated. In the second model, the fuel compact was still subjected to self-shielding as in the first model. However, the graphite and helium of the coolant channels were assigned the self-shielded material numbers of the matrix graphite and helium of the fuel unit cell. The graphite matrix unit cells were not self-shielded.

It was beyond the scope of the study to consider the self-shielding effects of the graphite matrix unit cells and the burnable poison unit cells.

a)



b)



c)

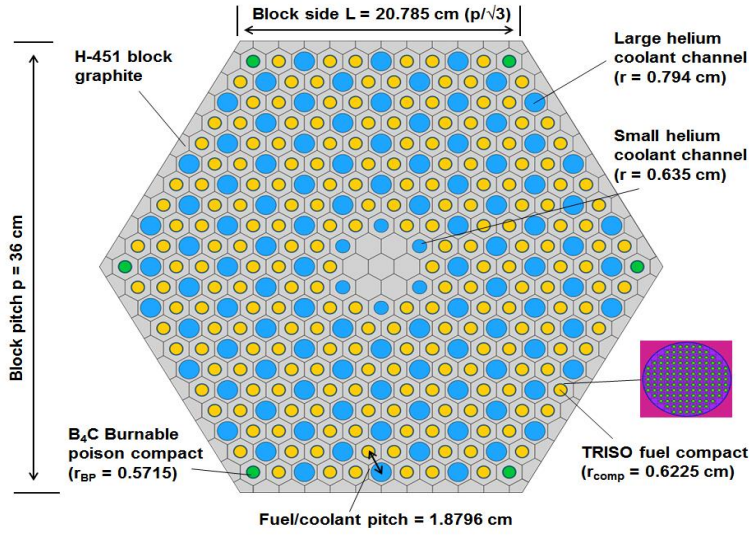


Figure 20: a) TRISO fuel particle, b) fuel compact and c) the MHTGR-350 fresh fuel block

Source [3]

4.4 Cross Section Collapsing

Collapsing of multigroup cross sections of the MHTGR-350 fresh fuel block and supercell models were obtained with NEWT using the four-group energy structure as shown in Table 8. The few group macroscopic cross sections are total, fission, absorption transport, scattering and capture (Σ_{tot}, Σ_{fiss}, Σ_{abs},Σ_{tr} , Σ_{scatt} and Σ_{cap}) together with Nu* fission for the MHTGR-350 fresh fuel block and supercell models. Section 5.4.1 presents the few group cross sections of the MHTGR-350 supercell models using ENDF/B-VII.0 and ENDF/B-VII.I nuclear data libraries. Section 5.4.2 presents the comparison of the few group cross sections of the MHTGR-350 fresh fuel block and supercell models. The unit used for few group cross sections is cm^{-1}.

Table 8: The four-group energy structure

Energy group	Energy limit
1	0.1 MeV - 20 MeV
2	3 keV -0.1 MeV
3	1.86 eV - 3 keV
4	0 eV - 1.86 eV

The absorption macroscopic cross section is equivalent to the sum of fission and capture macroscopic cross sections

$$\Sigma_{abs} = \Sigma_{fiss} + \Sigma_{cap} \tag{4-1}$$

The total macroscopic cross section is equal to the macroscopic absorption cross section plus the macroscopic scattering cross section given as:

$$\Sigma_{tot} = \Sigma_{abs} + \Sigma_{scatt} \tag{4-2}$$

The transport macroscopic cross section which is used to obtain the diffusion coefficient D, is calculated as [39]:

$$\sum_{tr} = \sum_{abs} + (1-\mu)\sum_{scatt} = \sum_{tot} - \mu\sum_{scatt} \tag{4-3}$$

where:

μ is the average cosine of the scattering angle equivalent to $\frac{2}{3A}$ and A is the atomic mass number of the scattering nuclei. However, this equation was not used since $\sum_{tr}$ was obtained directly from the output file.

The diffusion coefficient D, is given by [40]:

$$D = \frac{1}{3\sum_{tr}} \tag{4-4}$$

Nu* fission is defined as the product of the fission cross section and the number of neutrons produced per fission.

To gain more insight into this behaviour of the 4-group collapsed cross sections and other constants, it is helpful to consider how the collapsed macroscopic cross sections were calculated by NEWT. The 4-group collapsed macroscopic cross sections were calculated using Equation (3-19) which was discussed earlier in Section 3.4. This equation used the 252 group cross sections and the 252 group fluxes at each spatial volume.

The 252 group cross sections were calculated in the self-shielding part of the calculation. This was carried out by calling XSProc as discussed earlier. Only one DOUBLEHET definition was used to define all the fuel compacts. Since XSProc produces the 252-group cross sections, this therefore meant that all the compact unit cells shown in Figure 6 (a), had the same 252 group collapsed cross section data set. Regarding the graphite of the coolant channels, a single material was defined for the graphite and this material was not subjected to self-shielding. Therefore, all the graphite of the coolant channel unit cells had the same 252 group collapsed data set. The effect of not self-shielding the graphite in the coolant channel was discussed in the previous section.

It is also important to note that the 252 group self-shielded cross sections are the same for the MHTGR-350 fresh fuel block and the supercell. This is because the difference between the fresh fuel block and the supercell was only modelled in the NEWT part of the calculation. The material definition of the unit cells of the fuel block and the MHTGR-350 supercell calculations

for the unit cells containing fuel compacts are identical. It is noted that the supercell calculation also contains material specifications for the graphite block and depleted homogenous regions, but these material definitions are not used in calculating the collapsed data set.

4.5 Uncertainty and Sensitivity Analysis Assessment

4.5.1 Computer Tools used

The computational tools for uncertainty and sensitivity analysis used in this study are TSUNAMI-3D and Sampler. Both are part of the SCALE 6.2.1 code system. KENO-VI and NEWT are the

TSUNAMI-3D can be used in MG and CE mode. In this study TSUNAMI-3D was only used in CE mode using the CLUTCH method (the CLUTCH method is described in Section 3.5.5), MG calculations were not performed, because TSUNAMI-3D in SCALE 6.2.1 cannot treat the double heterogeneity of the HTGR unit cell as mentioned in Section 3.6.3.

Sampler is a module that uses statistical treatment to perform general uncertainty analysis for SCALE 6.2.1 sequences. In this study, Sampler was used in MG mode (i.e. Sampler uses NEWT as a transport solver, where NEWT is an MG code).

4.5.2 Models Used

The models used for uncertainty and sensitivity analysis are the MHTGR-350 fresh fuel block and supercell models. For TSUNAMI-3D using the CLUTCH method, the same KENO-VI CE models described in Section 4.2.2 were used (i.e. the TRISO fuel particle in the fuel compact and the BP's in the BP compacts were subject to lattice cell treatment). For Sampler calculations the same NEWT MHTGR-350 fresh fuel block and supercell models described Section 4.2.2 were used (i.e. the TRISO fuel particles were subjected to DOUBLEHET treatment and the BP's in the BP compacts were homogenized. To facilitate comparison of the NEWT and KENO-VI calculations, a KENO-VI MG model was also developed. In this model, the BP was treated as an homogenous mixture, as in the NEWT models.

A line by line description of the input files of the MHTGR-350 supercell models that were developed using TSUNAMI-3D and Sampler is provided in Appendix A.

4.5.3 Convergence criteria

The convergence criteria of the TSUNAMI-3D results using the CLUTCH method is based on providing the spatial mesh definition to perform sensitivity coefficient calculation and the $F^*(r)$ function must be converged over the defined mesh. To analyse the $F^*(r)$ function, the inactive generation (NSK) is used. Since the tallies of the $F^*(r)$ function may begin during the inactive

generation of Monte Carlo calculation, this implies that the convergence of the $F^*(r)$ function does not require the fission source to be converged for its convergence [11]. This mesh covers all fissionable material regions of the MHTGR-350 supercell model, as seen in Figure 21 below.

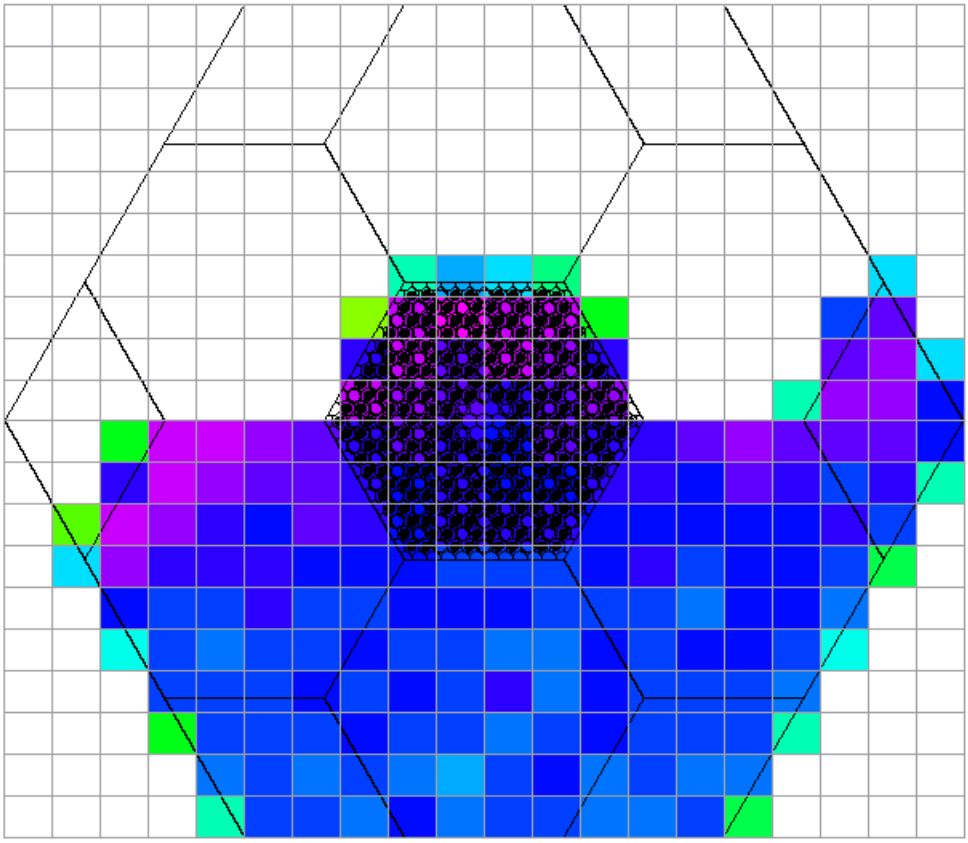


Figure 21: $F^*(r)$ meshes for the MHTGR-350 supercell

Source: (KENO-VI)

The convergence criteria of the Sampler results is based on the number of samples used in a calculation. For more on the convergence of the Sampler results obtained, see Section 5.5.

4.6 Analysing of Results

4.6.1 Criticality Results

After completion of a calculation by either KENO-VI or NEWT, the multiplication factors k were obtained from the output files.

Defining reactivity ρ as [41]

$$\rho = \frac{k-1}{k}$$

the difference in reactivity for two multiplication factors k_1 and k_2 will then be

$$\rho_{diff} = \frac{k_2 - 1}{k_2} - \frac{k_1 - 1}{k_1}$$

When this number is multiplied by 1×10^5, the unit is then termed the “percent mili” (pcm).

It is found that $k_{diff} = k_2 - k_1$ is approximately equal to ρ_{diff}.

Therefore, in this study, all differences are given in terms of the multiplication factors and not the reactivity, in units of pcm.

The models developed were verified by virtual inspection and with comparison of multiplication factors obtained to equivalent benchmark results.

4.6.2 Self-shielding Results

The self-shielding results were analysed in terms of multiplication factors obtained, following the same procedure as explained in Section 4.6.1 above.

4.6.3 Cross Section Collapsing Results

The following percentage difference convention was adopted in evaluating the 4-group collapsed macroscopic cross section (which were obtained from the output file stored in the same directory as the input file):

$\%_{diff} = 100 \times \frac{difference}{average} = 100\left(\frac{\Sigma_2 - \Sigma_1}{(\Sigma_2 + \Sigma_1)/2}\right)$, where $\Sigma_1$and Σ_2 are the two macroscopic cross sections being compared.

4.6.4 Uncertainty and Sensitivity Analysis Results

The following convention was adopted in evaluating the differences of the multiplication factor k and the associated uncertainty:

- Given the two values of multiplication factors, k_1 and k_2 (i.e. from two different calculations) the difference between the two values were analysed as described in Section 4.6.1.

- The statistical error in the multiplication factor k using the Monte Carlo method to calculate k is defined as σk.

- The uncertainty calculated for the multiplication factor k is defined as Δk. In TSUNAMI-3D and Sampler the uncertainty is given as $\frac{\%\Delta k}{k}$.

- With $\frac{\%\Delta k}{k}$ given in the output file as a value C, Δk can be calculated as $\Delta k = \frac{Ck}{100}$. This value can be represented approximately in *pcm* by multiplying by 10^5 as discussed in Section 4.6.1

- The percentage difference between two numbers A and B is defined as:

$$\%_{diff} = 100 \times \frac{difference}{average} = 100\left(\frac{A-B}{(A+B)/2}\right)$$

The results used in this section were obtained from the output files of the TSUNAMI-3D and Sampler calculations.

For TSUNAMI-3D, results that were obtained from the output file of each calculation were the uncertainty in multiplication factor k and top seven contributors to uncertainty in multiplication factors. Each contributor to the uncertainty is known as a nuclide-reaction pair and consists of the specific nuclide and reaction (or parameter) combination [42]. The notation that is used in SCALE to represent the nuclide-reaction pairs for all the cases studied in this work is given in Table 9. The nuclide-reaction pairs are listed in the first column of the table, and the description is given in the second column.

Sensitivity plots were obtained using the sensitivity data file (SDF extension) that is available for plotting together with other text and HTML-formatted output files which are stored in the same directory as the input file once a simulation had completed. These are given for all reaction types in all regions.

For Sampler calculations, results that were obtained from the output file of each calculation were uncertainty in multiplication factor k and uncertainties in macroscopic cross sections.

Table 9: Example of nuclide-reaction pairs applicable to this work

Nuclide-reaction pairs	Description
$^{235}U(\vec{\nu})$ / $^{235}U(\vec{\nu})$	The nuclide-reaction pair for nubar of ^{235}U
$^{238}U(n,\gamma)$ / $^{238}U(n,\gamma)$	The nuclide-reaction pair for radiative capture of ^{235}U
c-graphite elastic / c-graphite elastic	The nuclide-reaction pair for elastic scattering of neutrons in graphite
^{235}U fission / $^{235}U(n,\gamma)$	This is the nuclide-reaction pair for the fission for ^{235}U fission with the radiative capture of ^{235}U
^{235}U fission / ^{235}U fission	This is the nuclide-reaction pair for the fission of ^{235}U

CHAPTER 5 RESULTS AND DISCUSSION

5.1 Introduction

In this chapter results are presented as follows, the first set of calculations that characterize the flux, which are criticality calculations, are shown in Section 5.2. Section 5.3 shows the second set of calculations, which were generation of collapsed cross sections. Uncertainty and sensitivity results were obtained both in terms of the multiplication factor (criticality calculation) and the collapsed cross sections. These could have been presented in Sections 5.2 and 5.3 respectively, however it was decided to report as a separate section, Section 5.4.

The results that are presented were obtained with the KENO-VI, NEWT, TSUNAMI-3D and Sampler, modules of the SCALE 6.2.1 code package. The results presented are for the MHTGR-350 fresh fuel block and supercell models, at hot full power (HFP). A comparison of the models and a discussion thereof are presented.

The results are discussed in terms of the model type (fresh fuel block and supercell), modelling method code (CE and MG), nuclear data (i.e. cross section library) and uncertainties in nuclear data.

The MHTGR-350 fresh fuel block and supercell are different systems; therefore, the multiplication constants were not compared for the two systems.

5.2 Criticality Results

This section presents the criticality (multiplication factor k) results obtained with KENO-VI and NEWT for the MHTGR-350 fresh fuel block and supercell models. The comparisons made with the results generated are in terms of CE vs MG, and the ENDF/B-VII.0 vs ENDF/B-VII.I nuclear data libraries. All calculations were performed at HFP (1200 K).

5.2.1 Criticality Results of the MHTGR-350 Fresh Fuel Block

The calculations of criticality of the MHTGR-350 fresh fuel block, used in this section were obtained from a study already carried out by Sihlangu S.F. [18]. The description of the MHTGR-350 fresh fuel block is presented in Section 2.3.3 and shown in Figure 6(a). Worth noting is that the MHTGR-350 fresh fuel blocks with DOUBLEHET cell data specifications for the TRISO fuel particles in the fuel compacts and homogenized burnable poisons (BP) in the BP compacts are used in this section. The results are discussed in terms of CE and MG, utilizing ENDF/B-VII.0 and ENDF/B-VII.I nuclear data libraries. The multiplication factor k results for the MHTGR-350 fresh fuel block are shown in Table 10 below.

Table 10: Multiplication factor k results of the MHTGR-350 fresh fuel blocks

Nuclear data library	KENO-VI MG [18]	NEWT [18]	Delta
ENDF/B-VII.0	1.04838	1.04885	47 pcm
ENDF/B-VII.I	1.04290	1.04328	38 pcm
	548 pcm	557 pcm	

From Table 10 a difference of 548 pcm and 557 pcm between the two nuclear data libraries is observed for KENO-VI MG and NEWT calculations, respectively. This is due to an update in carbon capture cross section of graphite in the ENDF/B-VII nuclear data library compared to the ENDF/B-VII.0 nuclear data library according to [19], presented in Section 2.5.2. This point is proven in the next section. Another observation that can be made from the table is the difference between KENO-VI and NEWT of 47 pcm and 38 pcm when utilizing ENDF/B-VII.0 and ENDF/B-VII.I nuclear data libraries, respectively. These differences are small, this is because both calculations are MG and use an identical self-shielding calculation (i.e. DOUBLEHET treatment is the same). This small difference also assists in showing that although the discreet ordinate method employed in NEWT is very different from the Monte Carlo method used in KENO-VI, both methods are yielding very similar results in terms of the multiplication factor.

Verification of the MHTGR-350 fresh fuel block models was carried out as follows:

- The MHTGR-350 fresh fuel block model were obtained from [18]. Independent models were also built, and the results agreed within the statistical error. This served to verify the models of [18].
- The dimensions and geometric shapes specified in the input files were further checked to see if they resembled those specified in the benchmark. This was carried out by visual inspection using Fulcrum in SCALE 6.2.1 environment. Fulcrum is a visualization tool of SCALE 6.2.1.

5.2.2 KENO-VI Criticality Results of the MHTGR-350 Supercell Models

Table 11 shows the multiplication factor k values of the KENO-VI MHTGR-350 supercell models obtained using ENDF/B-VII.0 (238-group) and ENDF/B-VII.I (252-group) nuclear data

libraries. The MHTGR-350 supercell models that are used in this section are those that consist of the lattice-cell definition for the fuel particles in the fuel compact as well as for the BPs in the BP compacts, for CE calculations. For MG calculations, the DOUBLEHET cell data was specified for the TRISO fuel particles in the fuel compacts and the lattice-cell definition for the BPs in the BP compacts.

It is observed that the multiplication factor value for the multigroup (MG) calculation underestimates the continuous energy (CE) calculation by -31 pcm and -130 pcm for ENDF/B-VII.0 and ENDF/B-VII.I nuclear data libraries respectively. It must be noted that both KENO-VI MG and KENO-VI CE perform a Monte Carlo calculation for the neutron transport in the MHTGR-350 supercell. In the KENO-VI CE calculation, the CE cross sections are used without the self-shielding treatment. In the KENO-VI MG calculation, the same Monte Carlo calculation is performed, but the DOUBLEHET treatment is utilised to treat the resonance self-shielding of the doubly heterogeneous unit cells containing the fuel compacts in the MHTGR-350 supercell. In the DOUBLEHET treatment of the MG calculation, the self-shielded cross sections are computed in XSPRoc, which calls for both CENTRM and BONAMI. The treatment requires integration over energy in obtaining the self-shielded cross sections, which is not present in the CE calculation. This additional mathematical treatment could therefore be a contributing factor to the difference. The treatment of the self-shielding is discussed further in Section 5.3.

A further contributor could be that in MG mode, the cross sections and other data are taken as constants in each energy group. However, in CE mode, no such constraints are present, and the cross sections can be used in pointwise or analytic form as a function of energy as given in the ENDF/B data files.

A similar approach was also used for the single fuel pebble calculations of the HTR-10 pebble reactor in [20], where the difference between CE and MG calculation was 280 pcm using ENDF/B-VII.I nuclear data library, as presented in Section 2.5.3.

Another observation that can be made from Table 11 is that the multiplication factor calculations utilising ENDF/B-VII.0 nuclear data library are larger than the equivalent ENDF/B-VII.I nuclear data library calculations, with a difference of 508 pcm for CE calculations and 607 pcm for MG calculations. Similar differences are observed for the MHTGR-350 fresh fuel block, discussed in the previous section. This proves the effect of an update in carbon capture cross sections of graphite in the ENDF/B-VII nuclear data library compared to the ENDF/B-VII.0 nuclear data library.

Table 11: Multiplication factor results of the of the KENO-VI MHTGR-350 supercell model

	ENDF/B-VII.0	ENDF/B-VII.1
KENO-VI CE calculation	1.07043±0.00016	1.06535 ± 0.00017
KENO-VI MG calculation	1.07012± 0.00012	1.06405 ± 0.00012
Relative difference	-31 pcm	130 pcm

The results in Table 11 are comparable with those found in the benchmark [3]. It is worth noting that the results provided in the benchmark are for different versions of the SCALE code package and not the SCALE 6.2.1 code package which was used in this study. Comparison of the CE calculation results obtained, and the benchmark results show a difference of 24 pcm and 104 pcm with SCALE 6.1.2 and SCALE 6.2b4 respectively, utilising the ENDF/B-VII.0 nuclear data library. Using the ENDF/B-VII.I nuclear data library shows a difference of 96 pcm for CE calculations when compared with the SCALE 6.2b4 code.

Comparison of obtained MG results to the benchmark results shows a difference of 109 pcm and 125 pcm with SCALE 6.1.2 and SCALE6.2b3 respectively, when utilising the ENDF/B-VII.0 nuclear data library. The ENDF/B-VII.I library shows a difference of 620 pcm with the benchmark calculation using the SCALE 6.2b3 code.

It must be noted that the same MHTGR-350 supercell model benchmark specifications were used in this study. Possible reasons for the differences arise from the following:

1. The SCALE 6.2.1 code package was used in this study, whereas the benchmark presented results from different SCALE versions, viz: SCALE 6.1.2, SCALE 6.2b3 and SCALE 6.2b4 (beta version of SCALE 6.2).
2. GEN=600, NPG=50000 and NSK=60 were used in this study, referenced from [15], whereas in the benchmark GEN=500, NPG=50000 and NSK=50 were used.
3. The use of different optimisation values (e.g. ISN=32 and SZF=0.4 were used in this study as referenced from [15]), since they are not specified in the benchmark.

Verification of the MHTGR-350 supercell models developed was carried out as follows:

- The dimensions and geometric shapes specified in the input files were checked to see if they resembled those specified in the benchmark. This was carried out by visual inspection using Fulcrum in the SCALE 6.2.1 environment (i.e. the MHTGR-350 supercell model

obtained with KENO-VI in Figure 19 is identical to the model in Figure 8 which was obtained from the benchmark).

- Comparison of the multiplication factor k results obtained to the benchmark results as discussed in this section, was also a way of verifying the models.

In the next section, the NEWT calculations of the MHTGR-350 supercell models will be discussed. Since the burnable poisons (BP) were homogenised in these models, the KENO-VI MG models in which the BPs in the BP compacts were homogenised were used for comparison. The isotopic data (i.e. number densities) were taken from the benchmark. The multiplication factors were for ENDF/B-VII.0 and ENDF/B-VII.I nuclear data libraries, respectively.

5.2.3 NEWT Criticality Results of the MHTGR-350 Supercell Models

This section presents the results of the multiplication factor k of the MHTGR-350 supercell models. The MHTGR-350 supercell models that are used in this section consists of the same MG calculation cells that were applied in the previous section for the fuel compacts, but the burnable compacts were homogenised in order to avoid particle structure, according to the benchmark [3]. These calculations are in MG mode (i.e. NEWT is an MG code) developed using ENDF/B-VII.0 and ENDF/B-VII.I nuclear data libraries.

Table 12 below presents NEWT multiplication factor results for the MHTGR-350 supercell model using the ENDF/B-VII.0 and ENDF/B-VII.I nuclear data library. A difference of 617 pcm between the two libraries is observed. This is due to an update in carbon capture cross section of graphite in the ENDF/B-VII nuclear data library as compared to the ENDF/B-VII.0 nuclear data library, as was noted in the previous sections.

Table 12: MHTGR-350 supercell multiplication factor results obtained with NEWT

	ENDF/BVII-0	ENDF/VII.I	Difference
NEWT calculation	1.10106	1.09489	-617 pcm

The results presented in Table 12 above are comparable with those presented in the benchmark [3], with a difference of 23 pcm for the ENDF/B-VII.0 nuclear data library. The results for ENDF/B-VII.I NEWT MHTGR-350 supercell are not presented in the benchmark.

The same method of verification of the NEWT MHTGR-350 supercell models as the method described in the previous section was adopted.

5.2.4 Comparison of the Multiplication Factor Results of the KENO-VI MG and NEWT Models of the MHTGR-350 Supercells

This section presents a final comparison of the multiplication factor k results of the KENO-VI MG and NEWT MHTGR-350 supercell models. The NEWT calculations for the MHTGR-350 supercell models discussed in the previous section consisted of DOUBLEHET specifications for the TRISO fuel particles and homogenized BPs for the BP compacts. Therefore, the KENO-VI MG supercell models that are used for comparison have the same treatment for the TRISO fuel particles and the BPs in the BP compacts. The isotopic data (i.e. number densities) for these models were taken from the benchmark. The results are presented in Table 13, in which the NEWT results presented were obtained from Table 12 in the previous section.

Table 13: KENO-VI MG and NEWT multiplication factor k results of the MHTGR-350 Supercell models

Nuclear Data Library	KENO- MG	NEWT	Delta
ENDF/B-VII.0	1.06325±0.00012	1.10106	3781 pcm
ENDF/B-VII.I	1.05700 ±0.00010	1.09489	3789 pcm

From Table 13 above, an observation that can be made is the significant difference in multiplication results between the KENO-VI MG and NEWT calculations of the MHTGR-350 supercell, 3781 pcm and 3789 pcm for ENDF/B-VII.0 and ENDF/B-VII.1 nuclear data library respectively.

The homogenized regions (graphite and depleted regions) surrounding the MHTGR-350 fresh fuel block on the supercell system seems to be responsible for this significant difference, because the equivalent single MHTGR-350 fresh fuel blocks show a difference of 47 pcm and 38 pcm for ENDF/B-VII.0 and ENDF/B-VII.I nuclear data libraries (see Section 5.2.1). The centre fuel block of the supercell has the same geometric and material definition as the single fresh fuel block, and was given the same self-shielding treatment for both the fuel block and supercell calculations.

A similar trend is observed in the benchmark [3], described in Section 2.5.1, where the difference between the KENO-VI MG and NEWT calculations was 3336 pcm for the MHTGR-350 supercell, while the equivalent MHTGR-350 fresh fuel block was 312 pcm utilising the ENDF/B-VII.0 nuclear data library.

However, it is acknowledged that this an important question since the collapsed cross sections discussed in the next section might change significantly when this question is resolved.

A possible way to find reasons for this difference would be to formulate numerical experiments, in which the units of the supercell were changed, and to test which changes bring about the large changes in the multiplication factor. For example, a first test could be to use only graphite in the cells external to the central fuel block. However, due to the time allocated for the present study, it was decided that these studies would be beyond the scope of the present study and are reserved for future work.

In the models that are discussed above, the DOUBLEHET definition for the TRISO fuel particles was identical for both KENO-VI MG and NEWT calculations under the CELLDATA block. However, additional data blocks (which are optional) were added to the CELLDATA block of the KENO-VI MG calculation, those blocks were the CENTRM DATA and MOREDATA blocks. To see the effect of these blocks, another NEWT model was developed, which contained these blocks (CENTRM DATA and MOREDATA), utilising ENDF/B-VII.0 nuclear data library. the multiplication factor obtained for this model was 1.10113, which showed a difference of 7pcm when compare to the NEWT model without the CENTRM DATA and MORE DATA block. This difference was considered small. A detailed description of the CENTRM DATA and MORE DATA blocks is provided in Appendix A and the input entries of these blocks are shown in Appendix B, which were obtained from [18].

5.3 Self-shielding Studies

In this section, both the NEWT MHTGR-350 fresh fuel block and supercell models were used. The MHTGR-350 fresh fuel block and supercell models used in this section, are those that were described in the previous section, which consist of homogenised BPs in BP compacts. The calculations were performed using the ENDF/B-VII.I nuclear data library, to see the effect of self-shielding on the two systems (MHTGR3-50 fresh fuel block and supercell).

The comparison of the multiplication factor between self-shielded and the non-self-shielded MHTGR-350 fresh fuel block calculations was 7 pcm, which was fairly small. The MHTGR-350 supercells also showed a very small difference of just less than 1 pcm. Non-self-shielded here means that the fuel compact material was subjected to the self-shielding treatment, but the graphite of the coolant channels and of the centre matrix graphite cells were not subjected to the self-shielding treatment.

XSProc when using the default, assumes an infinite array for the unit cell, and the Dancoff factor is automatically calculated. The Dancoff factor accounts for the symmetry of the unit cell

in the lattice. However, the MHTGR-350 fresh fuel block is not an array consisting only of fuel compacts as seen Figure 20 c), there are other type of unit cells in between as discussed in Section 4.3. Proper consideration would require defining the Dancoff factor to account for this change in symmetry rather than using the default calculation.

Another notable point worth making is that the burnable poisons (BPs) were modelled as homogeneous mixtures. Self-shielding treatment for BPs would require more effort than within the scope of this study. However, a parallel study in the author's research group has shown that this can be modelled using the "Trace" method in which trace amounts of ^{238}U are introduced into the BP compact [18].

Furthermore, in the MHTGR-350 supercell, the blocks neighbouring the fresh fuel are homogenised. Therefore, self-shielding could not be carried out since the heterogeneous nature of unit cells must be considered in order to formulate the unit cell structure required for the XSProc calculation.

Given the scope of this study, this could not be adequately addressed. Therefore, since the difference in the multiplication factors for the two models studied were 7 pcm for the MHTGR-350 fresh fuel block and less than 1 pcm for the MHTHR-350 supercell, which were considered to be small, the non-shielded models were used. The full effect of self-shielding would be considered in future studies.

5.4 Collapsed Cross Sections of the MHTGR-350 Supercell

This section presents the collapsed multigroup (MG) cross sections of the MHTGR-350 supercell model obtained with NEWT using the four-group energy structure as outlined in Section 4.4. The NEWT models used to obtain the results in this section are the same models that were used to obtain results in Section 5.2.3 (i.e. DOUBLEHET specifications for the TRISO fuel particles and homogenization for the BP's in the BP compacts). A further comparison of these MG cross sections of the MHTGR-350 supercell is made to equivalent MHTGR-350 fresh fuel block cross sections in Section 5.4.2. In this work, the few group macroscopic cross sections of total, fission, absorption transport, scattering and capture (Σ_{tot}, Σ_{fiss}, Σ_{abs}, Σ_{tr}, Σ_{scatt} and Σ_{cap}) and of Nu* fission are presented in cm^{-1}.

5.4.1 The 4-Group Macroscopic Cross Sections of the NEWT MHTGR-350 Supercell Models

The NEWT 4-group collapsed macroscopic cross sections of the MHTGR-350 supercell models are presented in Table 14 for ENDF/B-VII.0 and ENDF/B-VII.I nuclear data libraries.

Comparison of the 4-group collapsed macroscopic cross sections between the two nuclear data libraries shows that all the percentage differences of the macroscopic cross sections and other constants for all groups are less than one percent, with the largest percentage difference being 0.87% for group 4 of both Nu*fission and fission. It can therefore be concluded that using either ENDF/B-VII.0 or ENDF/B-VII.I nuclear data libraries will not cause a significant change in the macroscopic cross sections and diffusion coefficients. For this reason, only the ENDF/B-VII.I nuclear data library will be used to assess the effect of using supercells instead of a single fuel block on multigroup cross sections of the MHTGR-350 reactor.

Table 14: Collapsed macroscopic cross sections of the MHTGR-350 supercells

Macroscopic cross section Group	ENDF/B-VI.0	ENDF/B-VII.I	(%) difference
Total			
1	0.22169	0.22177	0.03
2	0.34899	0.34878	0.06
3	0.35889	0.35841	0.13
4	0.36924	0.36878	0.13
Fission			
1	0.00007	0.00007	0.16
2	0.00033	0.00033	0.08
3	0.00104	0.00104	0.01
4	0.00551	0.00546	0.87
Nu* fission			
1	0.00018	0.00018	0.20
2	0.00080	0.00080	0.08
3	0.00253	0.00253	0.01
4	0.01343	0.01331	0.87
Absorption			
1	0.00012	0.00012	0.59
2	0.00117	0.00117	0.52
3	0.00589	0.00594	0.77
4	0.00975	0.00969	0.60
Transport			
1	0.17514	0.17534	0.12
2	0.32868	0.32843	0.08
3	0.33854	0.33700	0.46
4	0.35583	0.35521	0.17

5.4.2 Comparison of the 4-group Macroscopic Cross Sections of MHTGR-350 Fresh Fuel Block and Supercell models

Table 15 presents the comparison of the 4-group collapsed macroscopic cross sections of the MHTGR-350 fresh fuel block and supercell obtained using NEWT with the ENDF/B-VII.I nuclear data library.

Table 15: Macroscopic cross section of the MHTGR-350 fresh fuel block and supercell

Macroscopic cross section / Group	Fuel block [17]	Supercell	(%) difference
Total			
1	0.21702	0.22177	2.17
2	0.33356	0.34878	4.46
3	0.34145	0.35841	4.85
4	0.34673	0.36878	6.16
Fission			
1	0.00007	0.00007	-8.25
2	0.00041	0.00033	-21.98
3	0.00126	0.00104	-19.36
4	0.00560	0.00546	-2.54
Nu* fission			
1	0.00019	0.00018	-7.87
2	0.00099	0.00080	-21.98
3	0.00307	0.00253	-19.36
4	0.01365	0.01331	-2.54
Absorption			
1	0.00013	0.00012	-6.23
2	0.00148	0.00117	-22.70
3	0.00716	0.00594	-18.66
4	0.00932	0.00969	3.88
Transport			
1	0.17227	0.17534	1.77
2	0.31413	0.32843	4.45
3	0.32072	0.33700	4.95
4	0.33256	0.35521	6.59
Scattering			
1	0.21689	0.22165	2.17
2	0.33208	0.34761	4.57
3	0.33429	0.35248	5.30
4	0.33741	0.35908	6.22
Capture			
1	0.00005	0.00005	-3.51
2	0.00107	0.00085	-22.98
3	0.00590	0.00490	-18.51
4	0.00372	0.00423	12.80
Diffusion coefficients			
1	1.9350	1.9010	-1.77
2	1.0611	1.0149	-4.45
3	1.0393	0.9891	-4.95
4	1.0023	0.9384	-6.59

From Table 15, it is observed that the fission macroscopic cross sections decrease when moving from the MHTGR-350 fresh fuel block to the supercell, across all four groups. Nu* fission (which is defined as the product of the fission cross section and the number of neutrons produced per fission) follows a similar trend to the fission macroscopic cross section.

It is observed from the table that the Σ_{abs} decreased for groups 1 to 3 and increased for group 4. The capture macroscopic cross section was calculated using Equation (4-1), (i.e. $\Sigma_{abs} = \Sigma_{fiss} + \Sigma_{cap}$) and followed a similar trend to the absorption macroscopic cross section. Worth noting is that the values of the capture macroscopic cross sections were larger than the fission macroscopic cross section for groups 1 to 3 and less for group 4.

The total macroscopic cross section increases from the MHTGR-350 fresh fuel block to the supercell across all four collapsed energy groups and a similar trend is observed for the scattering macroscopic cross section, which was calculated using Equation (4-2) described in Section 4.4. It can be observed that Σ_{scatt} is much larger than Σ_{abs} for both fuel block and supercell systems. With Σ_{scatt} being the biggest contributor to the Σ_{tot} the similarity in the behaviour of Σ_{tot} and Σ_{scatt} is not surprising.

The transport macroscopic cross section which is used to obtain the diffusion coefficient D, is calculated using Equation (4-3). However, this equation was not used since Σ_{tr} was obtained directly from the output file. The diffusion coefficient D, is given by Equation (4-3)

From Table 21, it is also observed that the transport macroscopic cross section increases from the MHTGR-350 fresh fuel block to the supercell.

It is highly unlikely that a definite behaviour for this data can be obtained from looking at the data of Table 15. Therefore, to gain more insight into this behaviour of the 4-group collapsed cross sections and other constants, it is helpful to consider how the collapsed macroscopic cross sections were calculated by NEWT. The 4-group collapsed macroscopic cross sections were calculated using Equation (3-19) which was discussed earlier in Section 3.4.1. This equation used the 252 group cross sections and the 252 group fluxes at each spatial volume.

The collapsed 252 cross sections were calculated in the self-shielding part of the calculation. This was carried out by calling XSProc as discussed earlier. Only one DOUBLEHET definition was used to define all the fuel compacts. Since XSProc produces the 252-group collapsed cross sections, this therefore meant that all the compact unit cells shown in Figure 6 (a) had the same 252 group collapsed cross section data set. Regarding the graphite of the coolant channels, a single material was defined for the graphite and this material was not subject to self-shielding. Therefore, all the graphite of the coolant channel unit cells had the same 252

group collapsed data set. The effect of not self-shielding the graphite in the coolant channel was discussed in Section 5.3.

It is further important to note that the 252 group self-shielded cross sections are the same for the MHTGR-350 fresh fuel block and the supercell. This is because the difference between the fresh fuel block and the supercell was only modelled in the NEWT part of the calculation. The material definition of the unit cells of the fuel block and the MHTGR-350 supercell calculations for the unit cells containing fuel compacts are identical. The supercell calculation also contains material specifications for the graphite block and depleted homogenous regions not present in the fuel block calculation, but these material definitions are not used in calculating the collapsed data set.

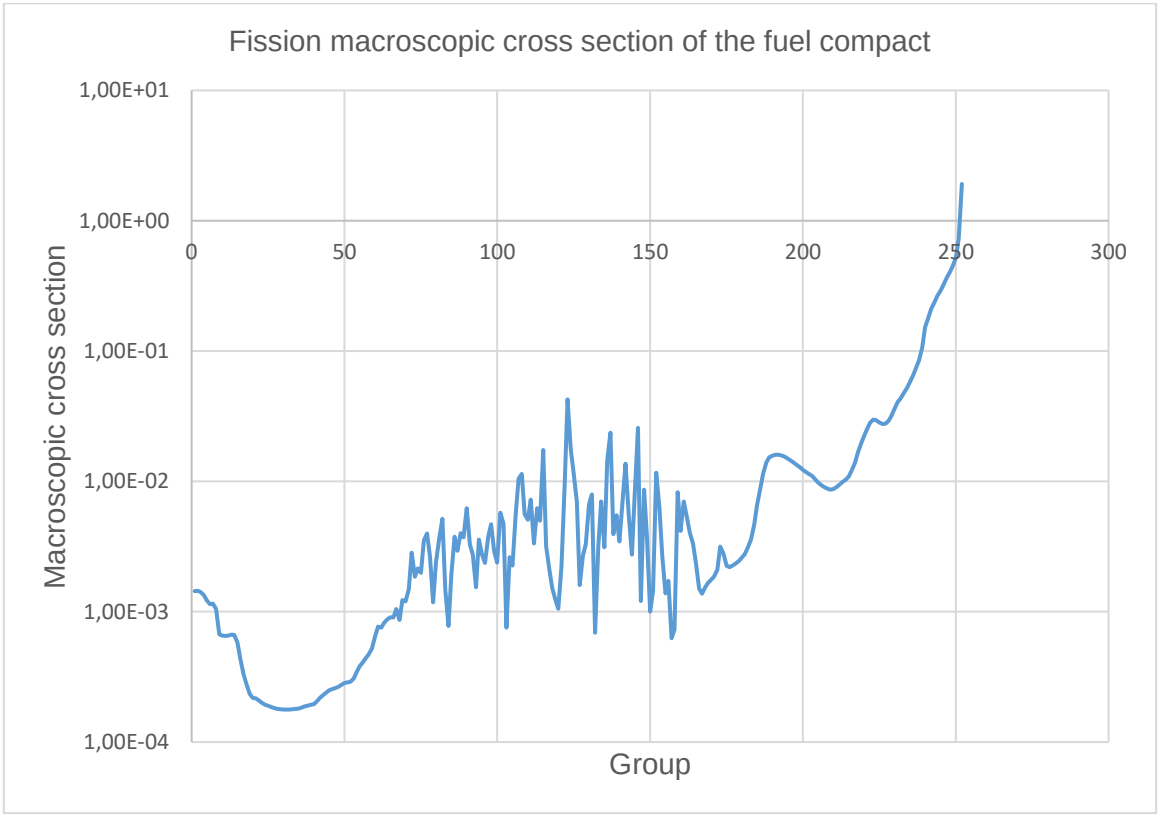


Figure 22: Fission macroscopic cross section data set for the MHTGR-350 fuel

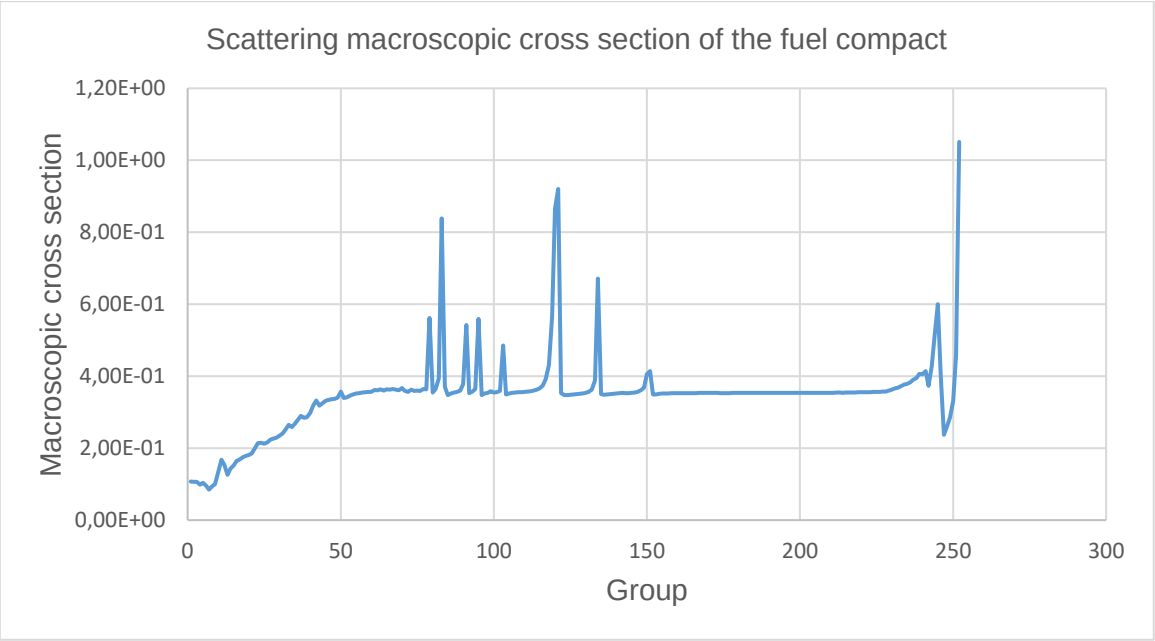


Figure 23: Scattering macroscopic cross section data set for the MHTGR-350 fuel compact

Therefore, in applying Equation (3-19) to obtain the collapsed macroscopic cross sections, the 252 fluxes calculated for each unit cell shown in Figure 24 are the cause of the change in macroscopic cross sections.

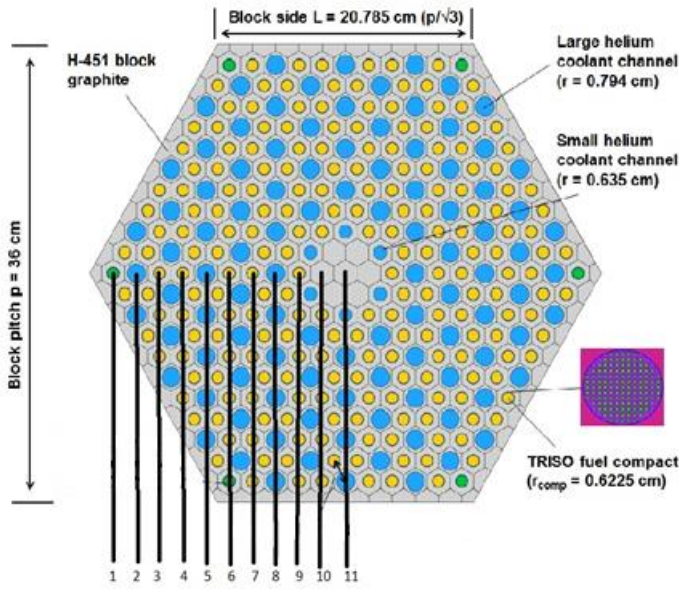


Figure 24: MHTGR-350 fresh fuel block showing unit cell numberings from 1 to 11

Source [3]

For interest, the self-shielded fission and scattering macroscopic cross section data sets for the fuel compact are shown in Figure 22 and 23 respectively, for 252 groups.

Figures 25 and 26 show the collapsed 4-group fluxes for equivalent MHTGR-350 reactor unit cells of the fuel block and supercell at equivalent spatial volumes. With reference to Figure 24 of the MHTGR-350 fresh fuel block, position 1 corresponds to the unit cell with the green centre (the burnable poison compact) and position 11 corresponds to the graphite cell at the centre of the fuel block. The positions 2 to 10 are the unit cells between these two unit cells (position 1 and 11).

It is observed that the flux distributions are different for the two systems (MHTGR-350 fresh fuel block and supercell). This therefore shows why the 4-group collapsed macroscopic cross sections are different between the two systems. It is noted that in these figures for position 11 the relative flux is much lower for the MHTGR-350 fuel block than that of the supercell. At this position, the centre of the block, there is only graphite.

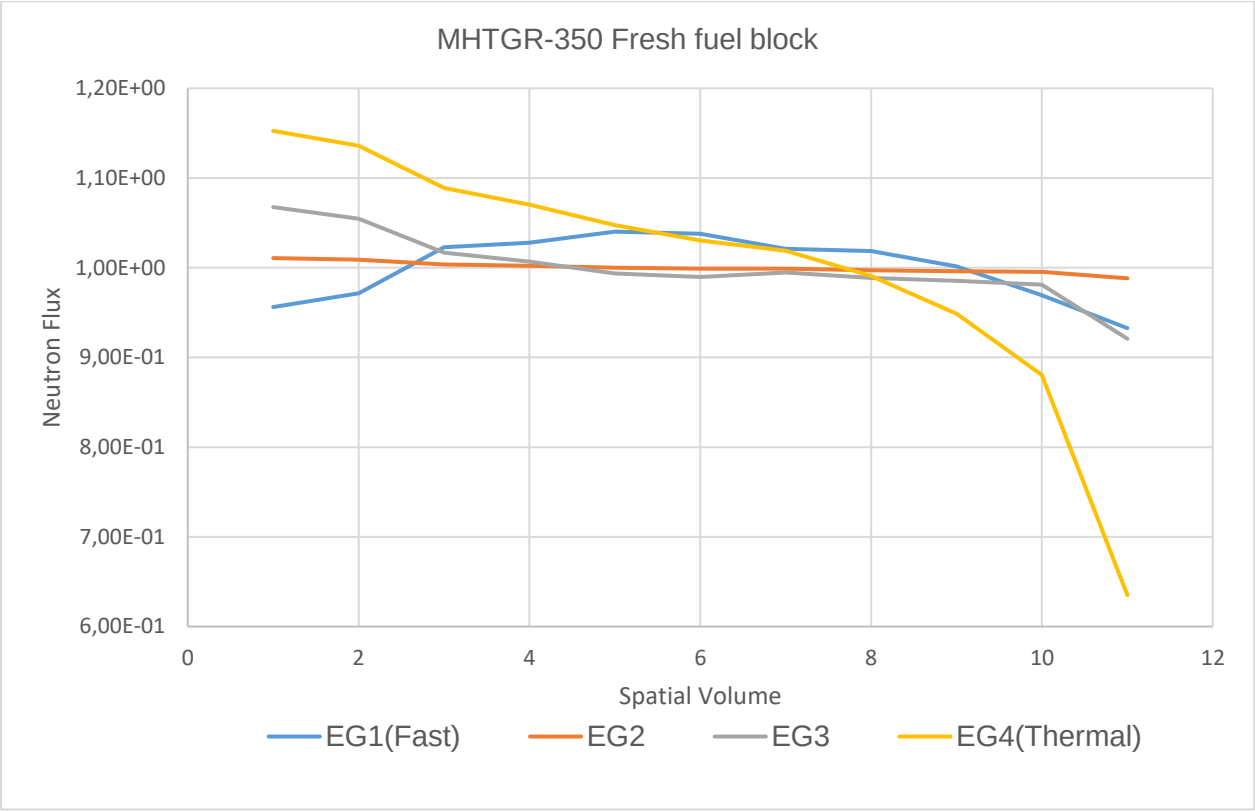


Figure 25: Flux distribution for the MHTGR-350 fresh fuel compact

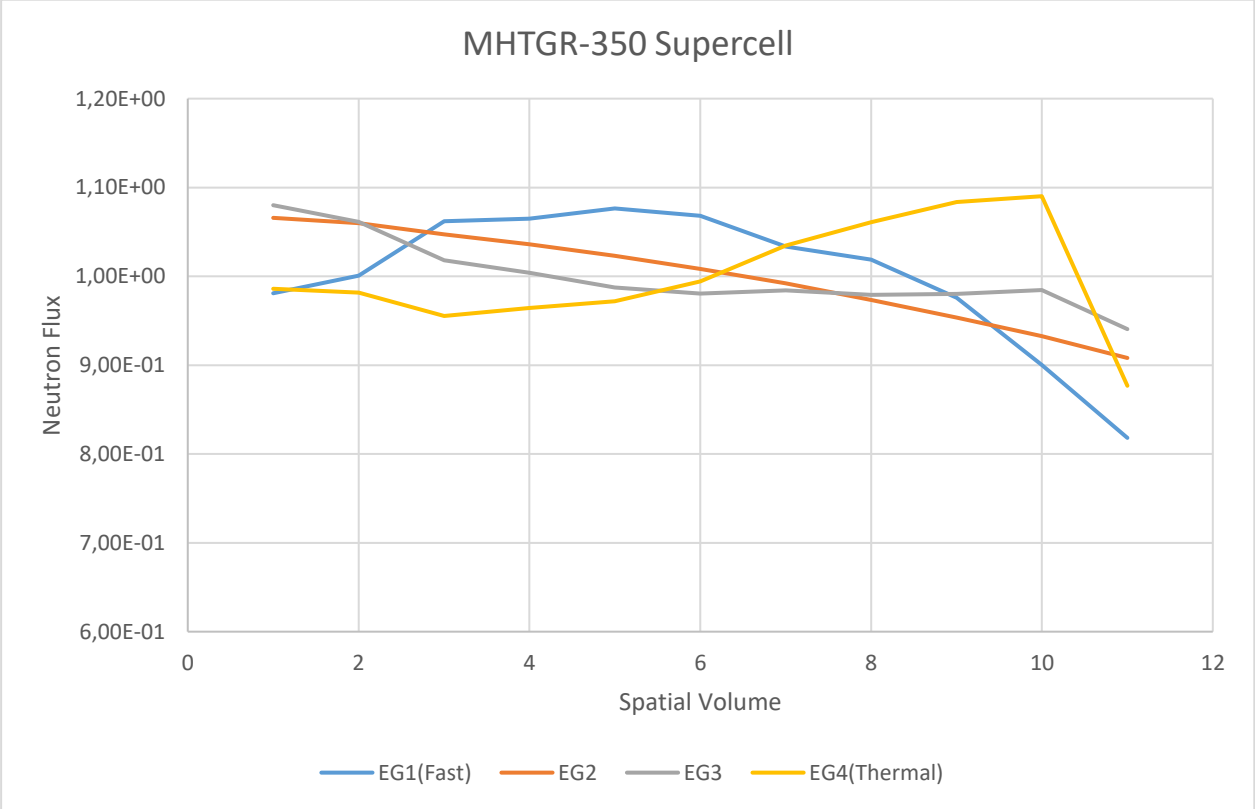


Figure 26: Flux distribution for the MHTGR-350 supercell

It should be noted however that in Equation (3-19) the individual 252 group fluxes are used and not the 4-group fluxes, therefore it is important to observe how these individual fluxes behave. Five energy groups from each broad group were chosen and the results are shown in Figures 27 to 31.

From these figures, it is observed that the fuel block and the supercell fluxes for each group shown are different from each other. However, if one only looks at the fuel block or the supercell spectra, one also notices significant differences between energy groups, for example between EG-142 and 151, and between EG-229 and 245. To further understand this, only the changes between EG-142 and EG-151 were further studied. All the spectra between and including EG-142 and EG-153 are plotted in Figure 29. It can be seen that the spectra for EG-151 and EG-152 are different from the rest. In the fuel block and supercell spectra, the fluxes at positions 3, 4, 6, 7 and 9 are lower than the neighbours in these two groups. From the MHTGR-350 fresh fuel block Figure 24, these are the units which contain fuel. The energy limits that encompass these two groups are 6.5 eV and 6.87 eV. It is known that U-238 has a strong resonance absorber at 6.67 eV [43]. Therefore, these dips in the spectra at positions 3, 4, 6, 7 and 9 are most probably due to the resonance absorption of U-238 in the fuel.

The analysis in terms of Figures 27 to 31 show that the flux has a very close dependence on the behaviour of the cross sections as a function of energy, and this becomes more marked at the resonances. The resulting collapsed cross sections are therefore also closely dependent on the nature of the flux as a function of energy. This is therefore then a clear indication that the environment of the fuel assembly (i.e. whether it is a reflected fuel block or a supercell) must be considered when calculating the collapsed constants.

This complicated behaviour of the flux as function of energy also indicates that a simple interpretation of the data of Table 16 would be difficult.

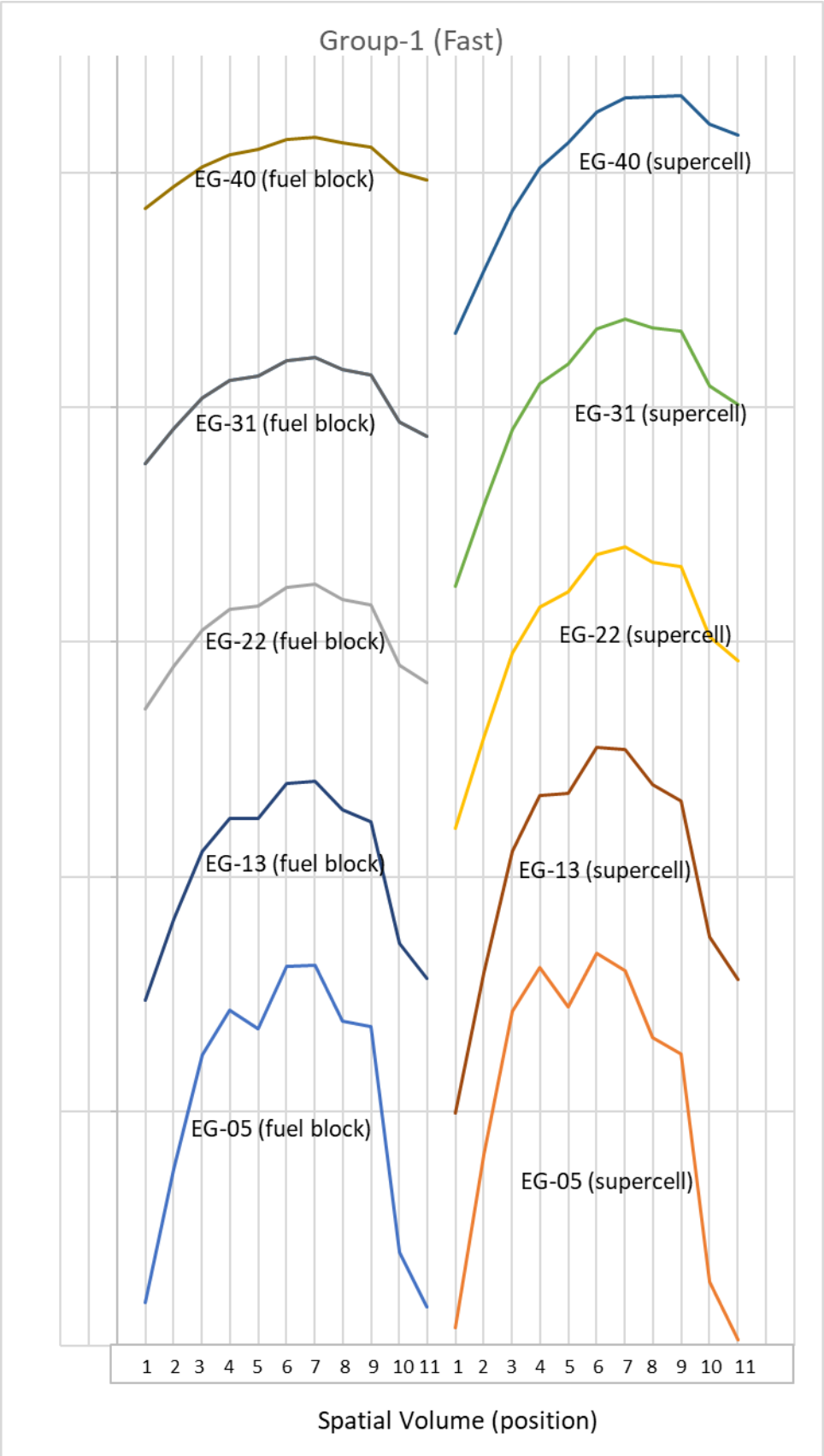


Figure 27: Five individual fluxes from collapsed energy group-1

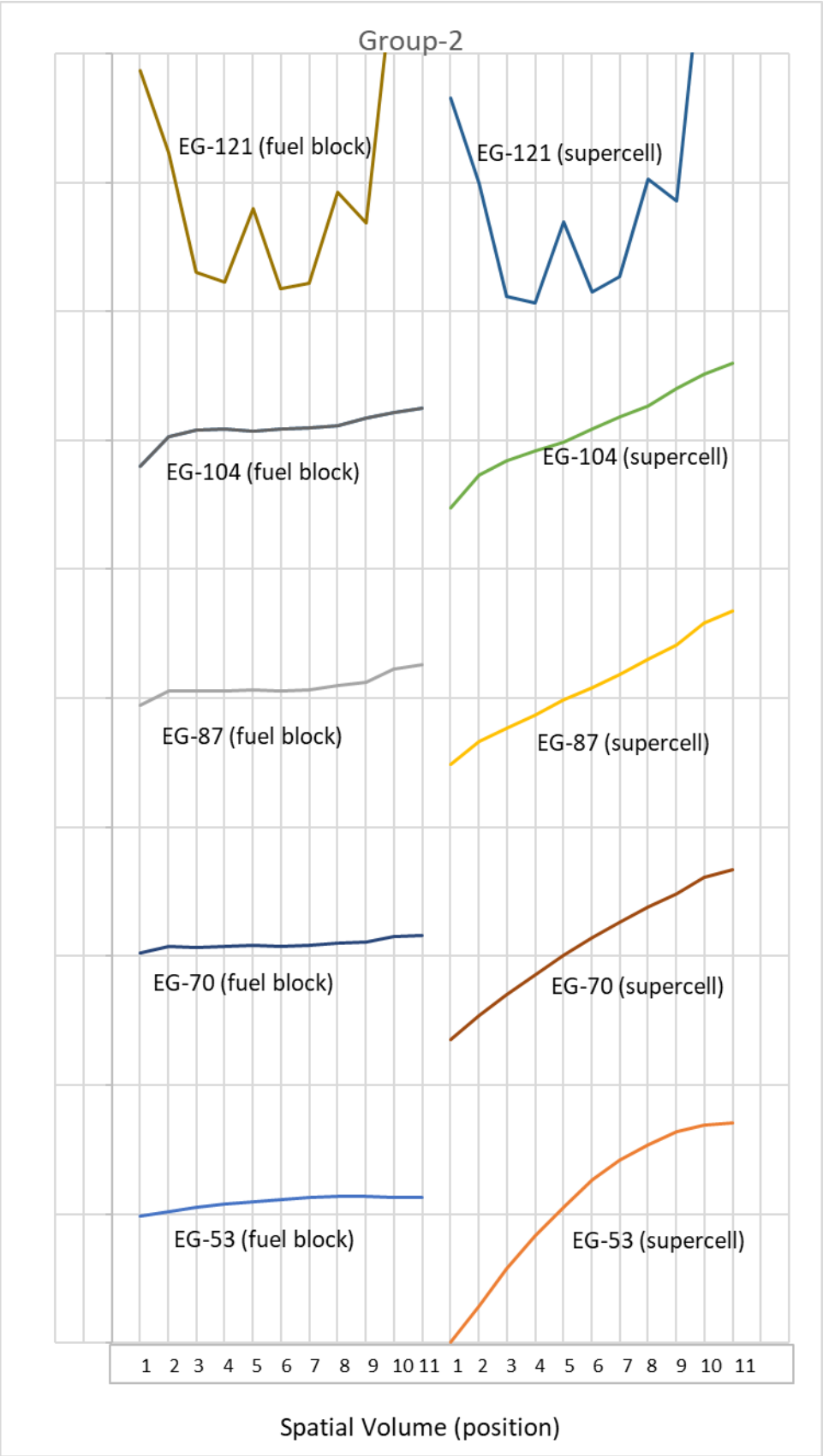


Figure 28: Five individual fluxes from collapsed energy group-2

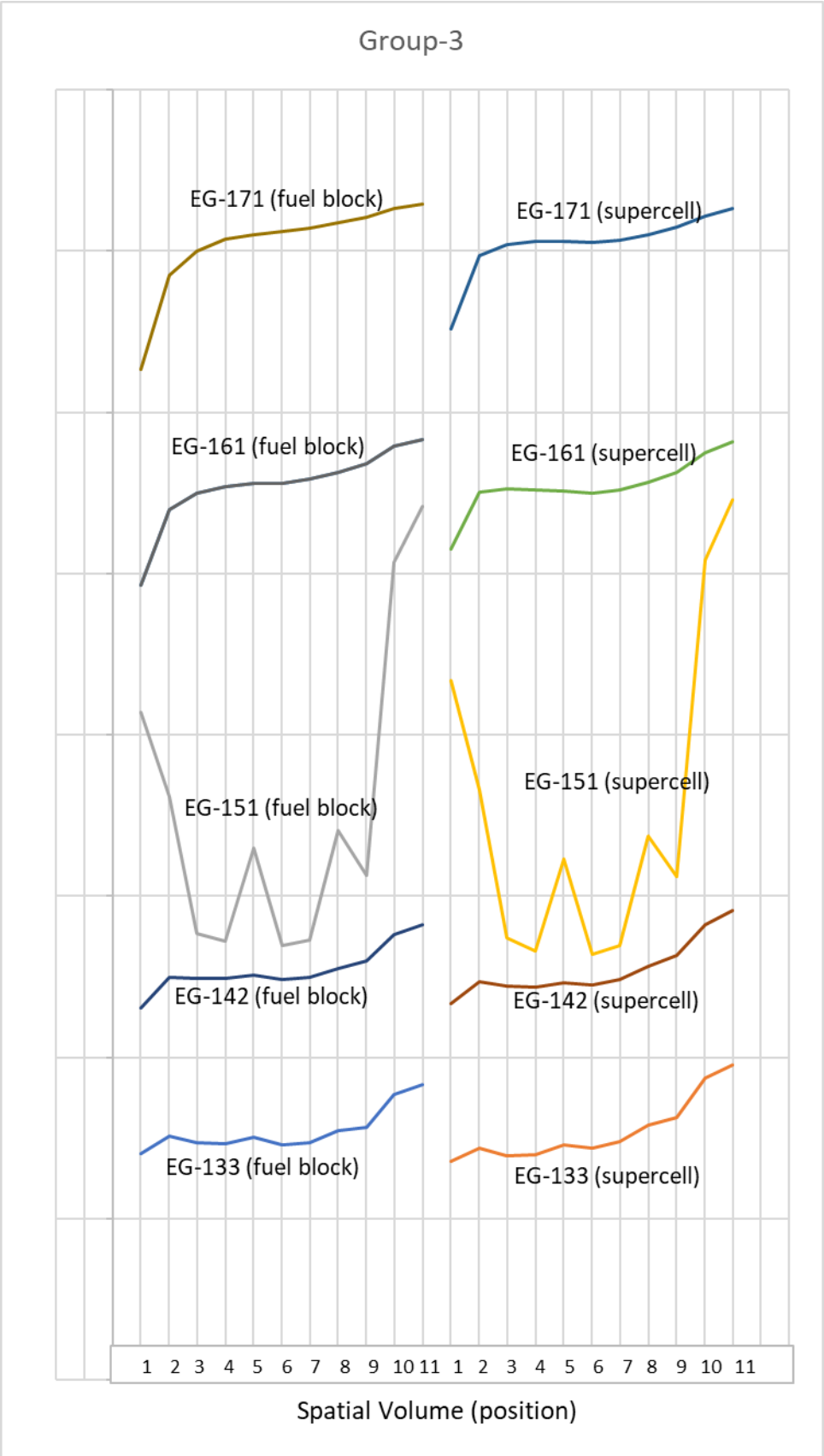


Figure 29: Five Individual fluxes from collapsed energy group-3

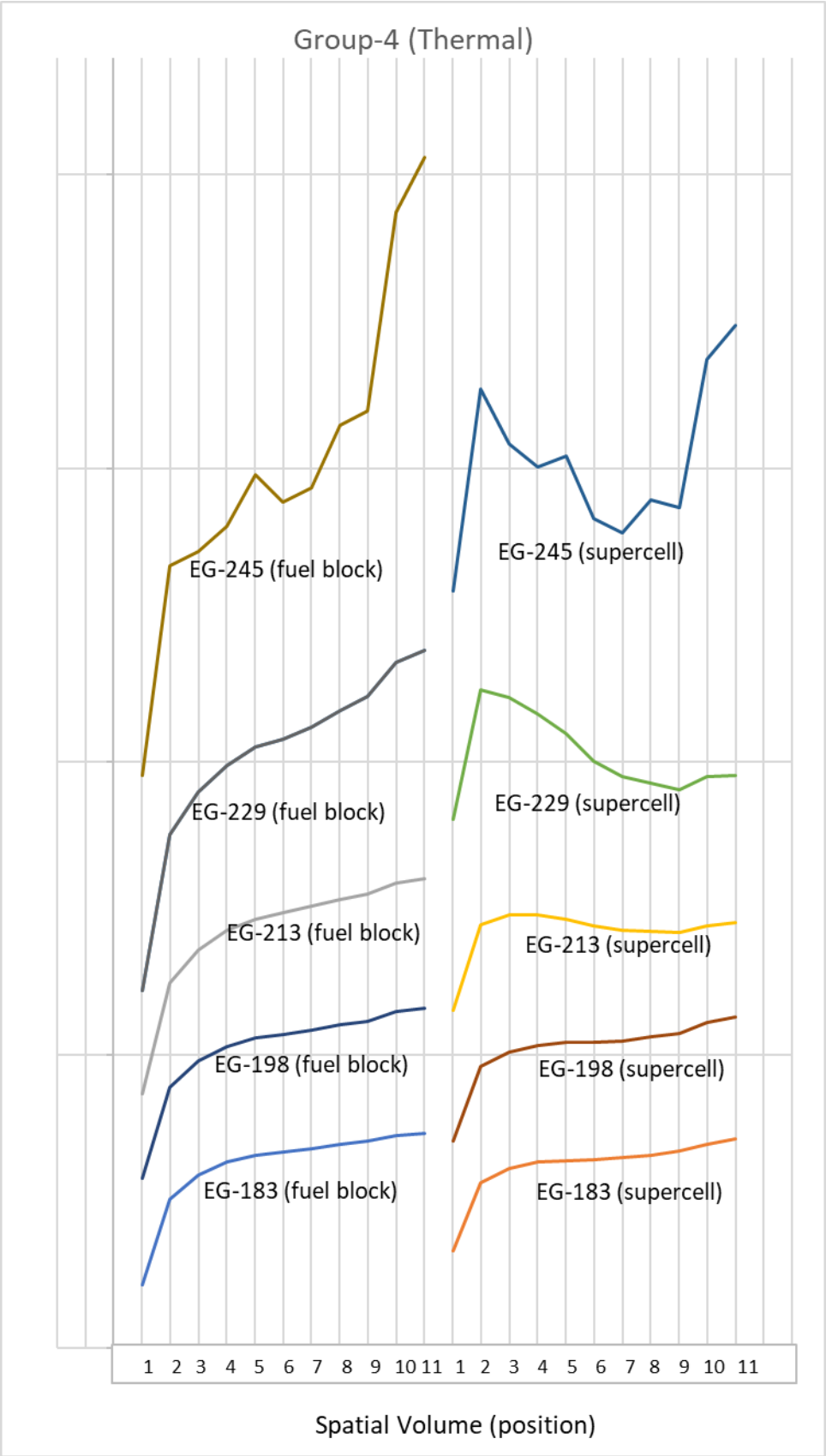


Figure 30: Five individual fluxes from energy group-4

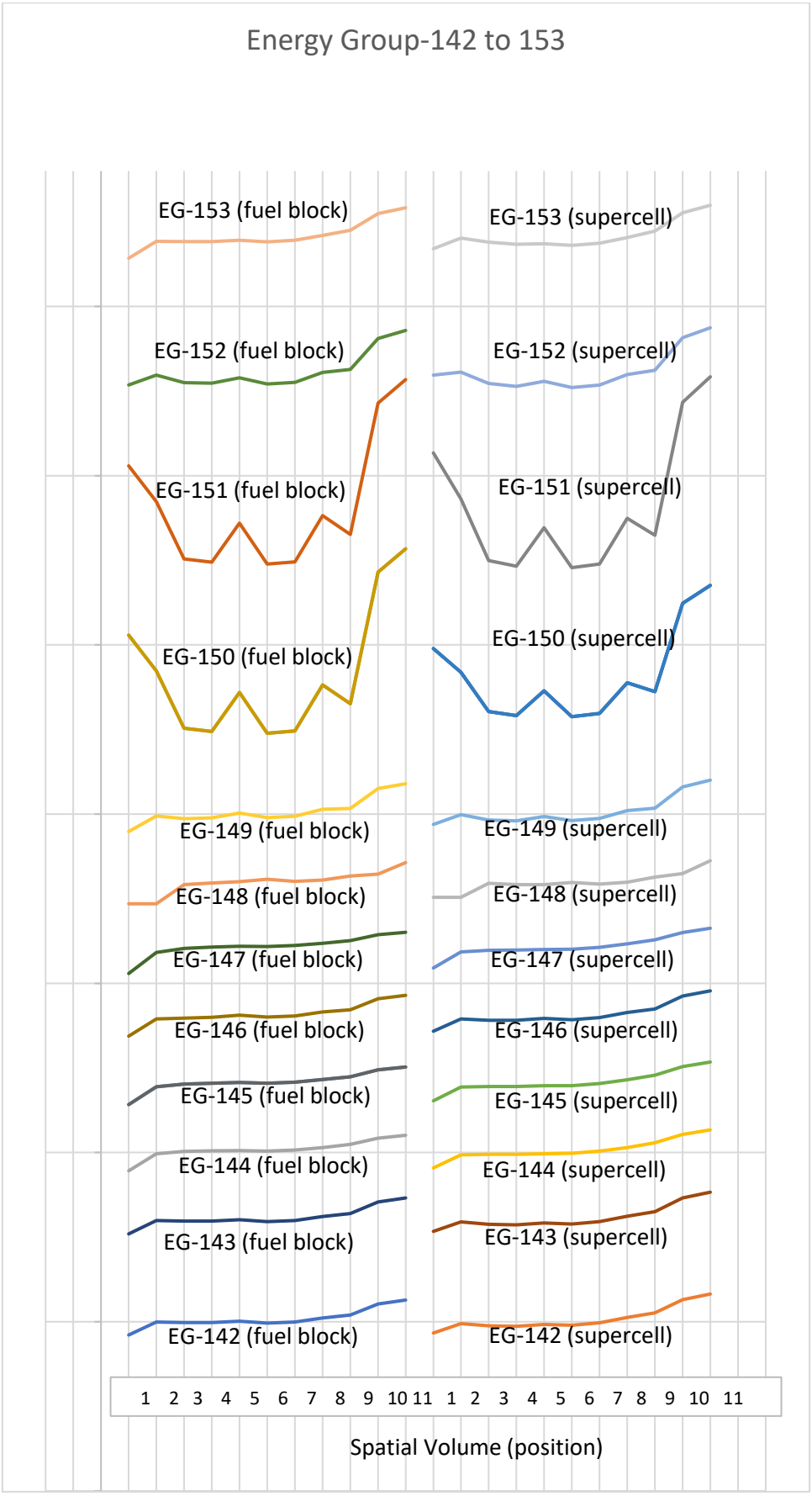


Figure 31: Individual fluxes for energy groups-142 to 153

5.5 Results of Uncertainty and Sensitivity Analysis Assessment

This section presents uncertainty and sensitivity results obtained with TSUNAMI-3D and Sampler of the SCALE 6.2.1 code package. The results of the MHTGR-350 supercell models are presented using ENDF/B-VII.0 and ENDF/B-VII.I nuclear data libraries. The MHTGR-350 supercell results are further compared to the MHTGR-350 fresh fuel block results.

5.5.1 TSUNAMI-3D Results of the MHTGR-350 Supercell Model

Table 16 presents the uncertainty in the multiplication factor k of the MHTGR-350 supercell models using the ENDF/B-VII.0 and ENDF/B-VII.I nuclear data libraries, obtained using TSUNAMI-3D. The models that were used in this section are similar to those that were used for the CE calculations in Section 5.2.1 (i.e. lattice cell treatment for the TRISO fuel particles in the fuel compacts as well as BPs in the BP compacts). The results between the two nuclear data libraries are comparable, with the difference of Δk and $\%\Delta k/k$ being 7 pcm and 0.003, respectively.

Table 16: Uncertainty in multiplication results for the MHTGR-350 supercells

ENDF/B-VII.0		ENDF/B-VII.I	
Uncertainty calculated for multiplication factor k (Δk)	Uncertainty ($\%\Delta k/k$)	Uncertainty calculated for multiplication factor k (Δk)	Uncertainty ($\%\Delta k/k$)
478 pcm	0.447	471 pcm	0.444

Tables 17 and 18 present the top seven nuclide-reaction pair contributors to the multiplication factor k uncertainty of the MHTGR-350 supercells obtained using ENDF/B-VII.0 and ENDF/B-VII.I nuclear data libraries. The descriptions of the terms appearing in this table were given in Section 3.3.2 and Section 4.6

The order of first four uncertainty contributors is consistent between the two nuclear data libraries, but from the fifth to the seventh contributors, the nuclide-–reaction pairs are not the same, as can be observed. This clearly is caused by the homogenised regions (depleted and graphite regions) surrounding the fresh fuel block on the MHTGR-350 supercell system (see Figure 8 in Section 2.4), because the order of uncertainty contributors for the MHTGR-350 fresh fuel block is consistent for the top seven contributors. The order of uncertainty contributors for the MHTGR-350 fresh fuel block is explained in next section, Section 5.5.2.

The largest contributor to uncertainty for the MHTGR-350 supercell is due to the covariance of $\bar{\nu}$ (nubar) for ^{235}U (i.e. ^{235}U($\bar{\nu}$)) for both nuclear data libraries. $\bar{\nu}$ (nubar) is the average number of fission neutrons emitted when the nucleus fissions. There are at least three possible sources that can give rise to the uncertainty due to this parameter. The first is due to the uncertainty in the actual nuclear data itself. This uncertainty is propagated through the use of covariance matrix. However, it would be beneficial to study the actual data files, to establish the strength of the uncertainty of nubar in comparison with the other weaker contributions. If it proves to be strong, then it is clear that in order obtain a smaller contribution to the uncertainty from nubar, more accurate data in terms of nubar is required. However, to study the nuclear data files requires the implementation of a suitable code that can extract this data, and this task could not be carried out due to time constraints since the proper use of a code also requires a period for learning on how to use the code.

The second possible source for this contribution could be due to the structure of the energy group boundaries, since the parameter nubar is averaged over each group. This average over the energy groups is however also performed for the other contributors, so it is unlikely that this would be the cause.

The third possible source for the contribution could arise from the treatment of nubar in the transport equation as opposed to the macroscopic cross sections. As can be seen from Equation (3-10), nubar is not dependent on the isotopic number densities as the macroscopic cross sections are. If one had to vary the isotopic number densities, then it is possible that a trend could be observed. However, this would have required a consistent redefinition of the number densities in terms of the benchmark definition, and would have therefore required time to carry this out. Since this would have detracted the study from its original intent, this was not pursued further.

It is further observed that the percentage difference between respective contributors for the first and the second contributors when comparing the ENDF/B-VII.I and ENDF/B-VII.0 nuclear data libraries is in agreement with atleast two decimal places, yielding differences of less than one percent. This is small, and the effect can be neglected. However, for the third contributor, the sensitivity of $\%\Delta k$ is increased by 7.41%. The third contributor is graphite (n,γ)/graphite (n,γ). Worth noting is that the ENDF/B-VII.I nuclear data library has been updated in the carbon capture cross section when compared to the ENDF/B-VII.0 nuclear data library, as mentioned in previous sections. Figure 32 presents the sensitivity plot of the third contributor, graphite (n,γ)/graphite (n,γ) reactions for the two nuclear data libraries as a function of incident neutron energy. It can be seen that the ENDF/B-VII.I nuclear data library shows more sensitivity per unit lethargy to graphite in the thermal range as compared to ENDF/B-VII.0 nuclear data library.

Table 17: Top seven contributors to uncertainty in multiplication factor for MHTGR-350 supercell using ENDF/B-VII.0

Rank	Nuclide-reaction pair	Uncertainty ($\%\Delta k/k$)
1	$^{235}U(\bar{\nu})$/ $^{235}U(\bar{\nu})$	0.26
2	$^{238}U(n,\gamma)$/ $^{238}U(n,\gamma)$	0.18
3	graphite (n,γ)/graphite (n,γ)	0.13
4	$^{235}U(n,\gamma)$/ $^{235}U(n,\gamma)$	0.12
5	$^{239}Pu(n,\gamma)$ / $^{239}Pu(n,\gamma)$	0.10
6	^{239}Pu fission / $^{239}Pu(n,\gamma)$	0.09
7	Graphite elastic/graphite elastic	0.09

Table 18: Top seven contributors to uncertainty in multiplication factor for MHTGR-350 supercell using ENDF/B-VII.I

Rank	Nuclide-reaction pair	Uncertainty ($\%\Delta k/k$)
1	$^{235}U(\bar{\nu})$/ $^{235}U(\bar{\nu})$	0.26
2	$^{238}U(n,\gamma)$/ $^{238}U(n,\gamma)$	0.18
3	graphite (n,γ)/graphite (n,γ)	0.14
4	$^{235}U(n,\gamma)$/ $^{235}U(n,\gamma)$	0.12
5	Graphite elastic/graphite elastic	0.11
6	$^{239}Pu(n,\gamma)$ / $^{239}Pu(n,\gamma)$	0.10
7	^{239}Pu fission / $^{239}Pu(n,\gamma)$	0.09

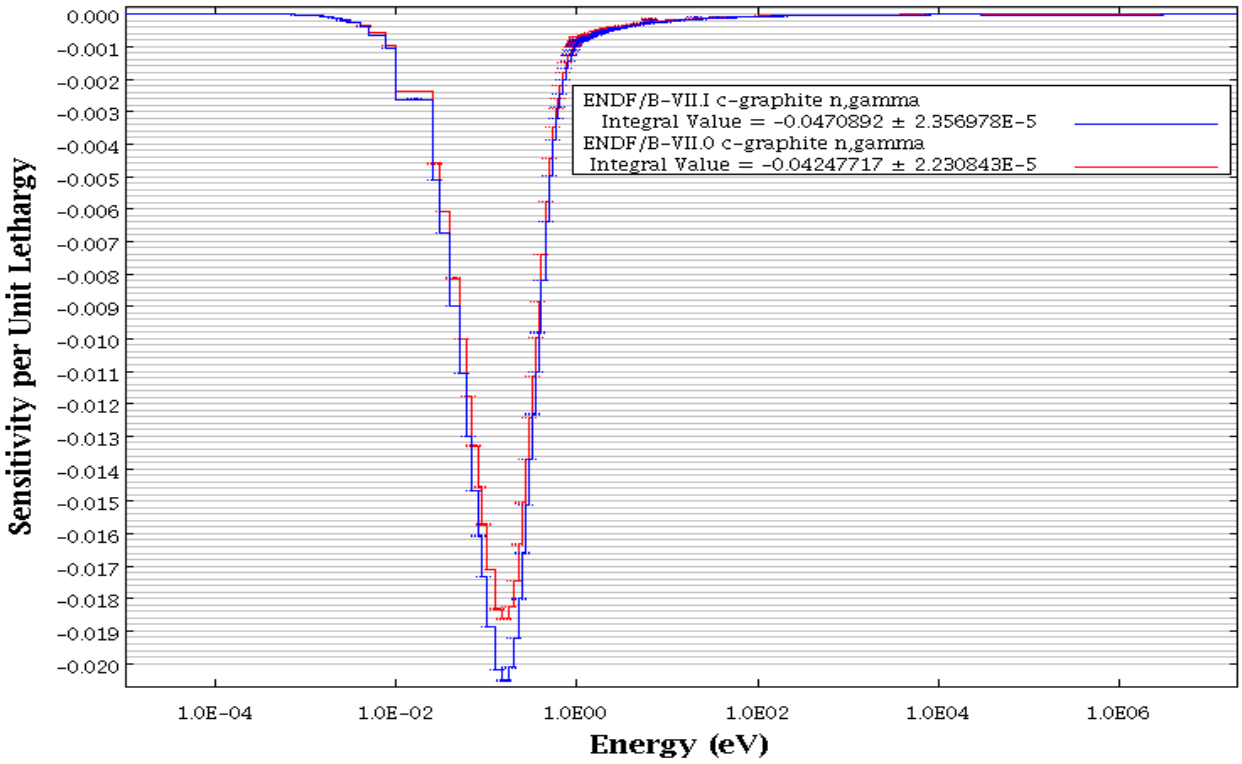


Figure 32: Sensitivity plot of graphite (n,γ)/graphite (n,γ) reactions

5.5.2 TSUNAMI-3D Results of the MHTGR-350 Fresh Fuel Block

The results for the MHTGR-350 fresh fuel block are reviewed in this section to facilitate the comparison between the MHTGR-350 fresh fuel block and supercell models. The MHTGR-350 models used in this section are equivalent to the supercell models used in the previous section, in terms of TRISO fuel particles and BP designs (DOUBLEHET treatment and lattice-cell definition, respectively). These results were obtained from the study performed by Sihlangu S.F [18].

The results between the two nuclear data libraries for the MHTGR-350 fresh fuel blocks are shown in Table 19 and are comparable, with the difference of Δk and $\%\Delta k/k$ being 7 pcm and 0.009 respectively.

Table 19: Uncertainty in multiplication factor k results for the MHTGR-350 fresh fuel blocks

ENDF/B-VII.0		ENDF/B-VII.I	
Uncertainty calculated for multiplication factor k (Δk)	Uncertainty ($\%\Delta k/k$)	Uncertainty calculated for multiplication factor k (Δk)	Uncertainty ($\%\Delta k/k$)
531 pcm	0.498	538 pcm	0.507

Table 20 below presents the top seven contributors to uncertainty for the MHTGR-350 fuel block.

Table 20: Top seven contributors to uncertainty in multiplication factor k for MHTGR-350 fresh fuel blocks

Rank	Reaction	Uncertainty ($\%\Delta k/k$)		
	Nuclide/nuclide reaction	ENDF/B-VII.0	ENDF/B-VII.1	$\%_{diff}$
1	$^{235}U(\nu)$/ $^{235}U(\bar{\nu})$	0.36	0.36	0.01
2	$^{238}U(n,\gamma)$/ $^{238}U(n,\gamma)$	0.20	0.20	0.10
3	$^{235}U(n,\gamma)$/ $^{235}U(n,\gamma)$	0.18	0.18	0.09
4	Graphite elastic/graphite elastic	0.13	0.16	24.62
5	^{235}U fission/ $^{235}U(n,\gamma)$	0.12	0.12	0.02
6	^{235}U fission/ ^{235}U fission	0.11	0.11	0.14
7	^{238}U elastic/ ^{238}U elastic	0.06	0.16	0.76

5.5.3 Comparison of TSUNAMI-3D Results of the MHTGR-350 Fresh Fuel Block and Supercell

Table 21 presents a comparison of the uncertainty in the multiplication factor k of the MHTGR-350 fresh fuel blocks and supercells using ENDF/B-VII.0 and ENDF/B-VII.I nuclear data libraries (data in the table obtained from Tables 16 and 19). For ENDF/B-VII.0 the uncertainty propagated changes by 53 pcm for Δk and 0.051 for $\%\Delta k/k$. For ENDF/B-VII.1 the uncertainty propagated changes by 67 pcm for Δk and 0.063 for $\%\Delta k/k$. Since the actual uncertainty propagated is in the interval (478 pcm, 531 pcm) for ENDF/B-VII.0 and (471 pcm, 538 pcm) for ENDF/B-VII.I nuclear data library, the difference when considering the fuel block or the supercell can be considered to be small. It is between 10 to 13% of that due to the uncertainty due to the

nuclear data, this is due to increase of uncertainty of the neutron multiplicity , of U-235 in the ENDF/B-VII.I nuclear data library, this according to a study described in Section 2.6.5 [22]. Furthermore, the effect of changing the library does not influence the uncertainty propagated using the uncertainties in the nuclear data when one models the MHTHR-350 fresh fuel block or the supercell.

Table 21: Uncertainty in multiplication factor results for the MHTGR-350 fresh fuel block and supercell

	ENDF/B-VII.0		ENDF/B-VII.I	
	Uncertainty calculated for multiplication factor k (Δk)	Uncertainty ($\%\Delta k/k$)	Uncertainty calculated for multiplication factor k (Δk)	Uncertainty ($\%\Delta k/k$)
SC	478 pcm	0.447	471 pcm	0.444
FB [17]	531 pcm	0.498	538 pcm	0.507

The order of the top seven uncertainty contributors to the multiplication factor is considered next.

From Table 20 in the previous section, it is observed that the order of uncertainty contributors is consistent for the MHTGR-350 fresh fuel block system, when either the ENDF/B-VII.0 or the ENDF/B-VII.I nuclear data library is used. This proves that the change in the order of uncertainty contributors that was observed for the MHTGR-350 supercell between the two nuclear data libraries is due to the homogenised regions surrounding the fresh fuel block in the MHTGR-350 supercell.

From the same table, it can further be observed that the percentage differences between the two nuclear libraries for respective contributors are less than 1%, except for the fourth contributor, the graphite elastic/graphite elastic reactions. This once again shows the effect of an update in carbon capture cross section on the ENDF/B-VII.I compared to the ENDF/V-II.0 nuclear data library.

Table 22 shows a comparison of the order of the uncertainty contributors for the MHTGR-350 fresh fuel block and the supercell. The percentage differences between these two systems for respective contributors are also given, using the ENDF/B-VII.0 nuclear data library. Table 23 shows similar data for ENDF/B-VII.I. From the two tables, it can be observed that the first and second nuclide/nuclide reaction contributors are the same. However, from the third contributor

the order is no longer consistent (the rank is not the same) for each nuclear data library and Pu-239 appears only in the MHTGR-350 supercell systems.

In order to understand this, one observes that:

- The relative amount of graphite in the supercell increases compared to that of the fuel block
- The relative amount of uranium decreases in the supercell compared to that of the fuel block
- ^{239}Pu is present in the supercell only

One therefore notices that all the contributions related to U-235 and U-238 decrease from the fuel block to supercell calculations, and the contributions related to graphite increase. The notable exception is the graphite elastic/graphite elastic, which decreases for the ENDF/B-VII.I comparison.

The sensitivity plot of Figures 33 and 34 (obtained from ENDF/B-VII.I nuclear data library) show this behaviour as well for selected contributors.

Table 22: Comparison of the order sensitivity coefficients of the ENDF/B-VII.0 nuclear data library

Reaction contributor	Rank	MHTGR-350 FRESH FUEL BLOCK [18]	Rank	Supercell	%DIFF
235U($\bar{\nu}$)/ 235U($\bar{\nu}$)	1	0.36	1	0.26	32.13
238U(n,γ)/ 238U(n,γ)	2	0.20	2	0.18	8.36
235U(n,γ)/ 235U(n,γ)	3	0.18	4	0.12	35.51
Graphite elastic/graphite elastic	4	0.13	7	0.92	141.64
235U fission/ 235U(n,γ)	5	0.12	8	0.09	30.95
235U fission/ 235U fission	6	0.11	9	0.08	34.24
238U elastic/ 238U elastic	7	0.06	14	0.04	29.92
graphite (n,γ)/graphite (n,γ)	10	0.02	3	0.13	145.60
239Pu(n,γ) / 239Pu(n,γ)			5	0.10	
239Pu fission / 239Pu(n,γ)			6	0.09	

Table 23: Comparison or the order sensitivity coefficients of the ENDF/B-VII.I nuclear data library

Reaction contributor	Rank	FRESH FUEL BLOCK [18]	Rank	Supercell	%DIFF
$^{235}U(\bar{\nu})$/ $^{235}U(\bar{\nu})$	1	0.36	1	0.26	38.28
$^{238}U(n,\gamma)$/ $^{238}U(n,\gamma)$	2	0.20	2	0.18	7.81
$^{235}U(n,\gamma)$/ $^{235}U(n,\gamma)$	3	0.18	4	0.12	35.72
Graphite elastic/graphite elastic	4	0.16	5	0.11	40.84
^{235}U fission/ $^{235}U(n,\gamma)$	5	0.12	8	0.09	31.16
^{235}U fission/ ^{235}U fission	6	0.11	9	0.08	34.42
^{238}U elastic/ ^{238}U elastic	7	0.06	14	0.04	25.69
graphite (n,γ)/graphite (n,γ)	10	0.03	3	0.14	138.92
$^{239}Pu(n,\gamma)$ / $^{239}Pu(n,\gamma)$			5	0.10	
^{239}Pu fission / $^{239}Pu(n,\gamma)$			6	0.09	

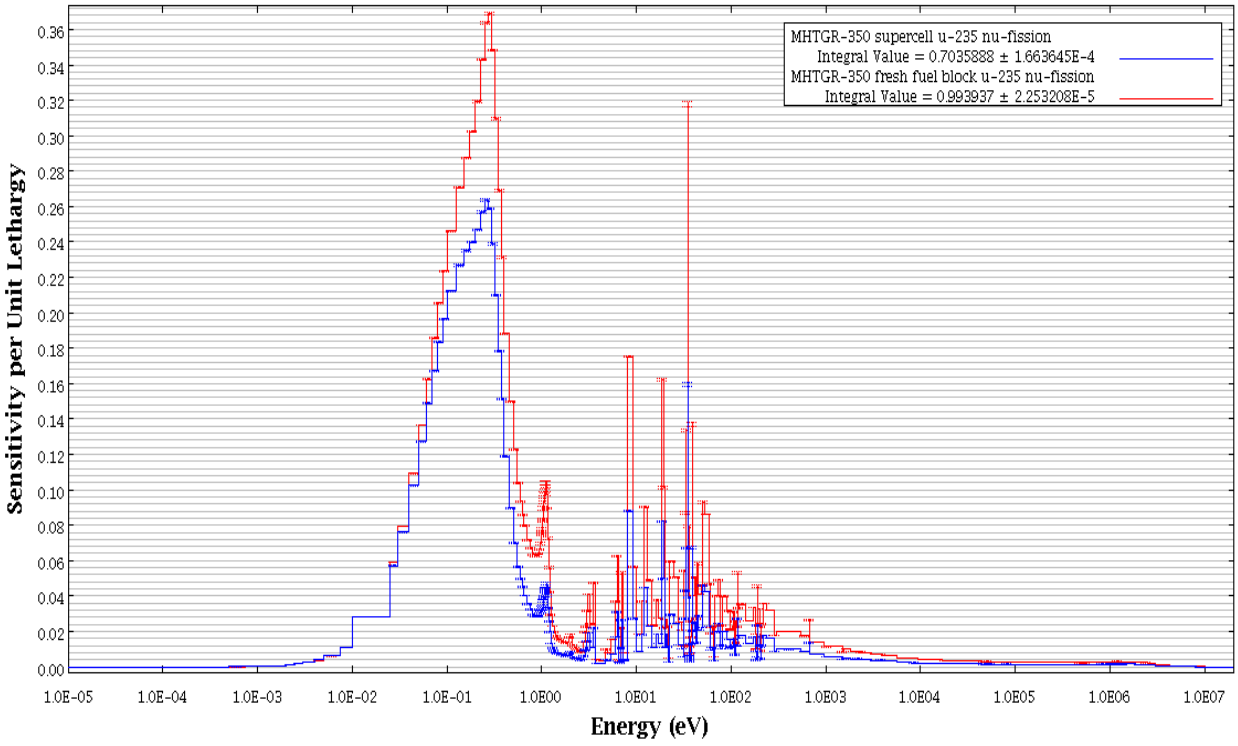


Figure 33: sensitivity plot for $^{235}U(\bar{\nu})$/ $^{235}U(\bar{\nu})$ reactions

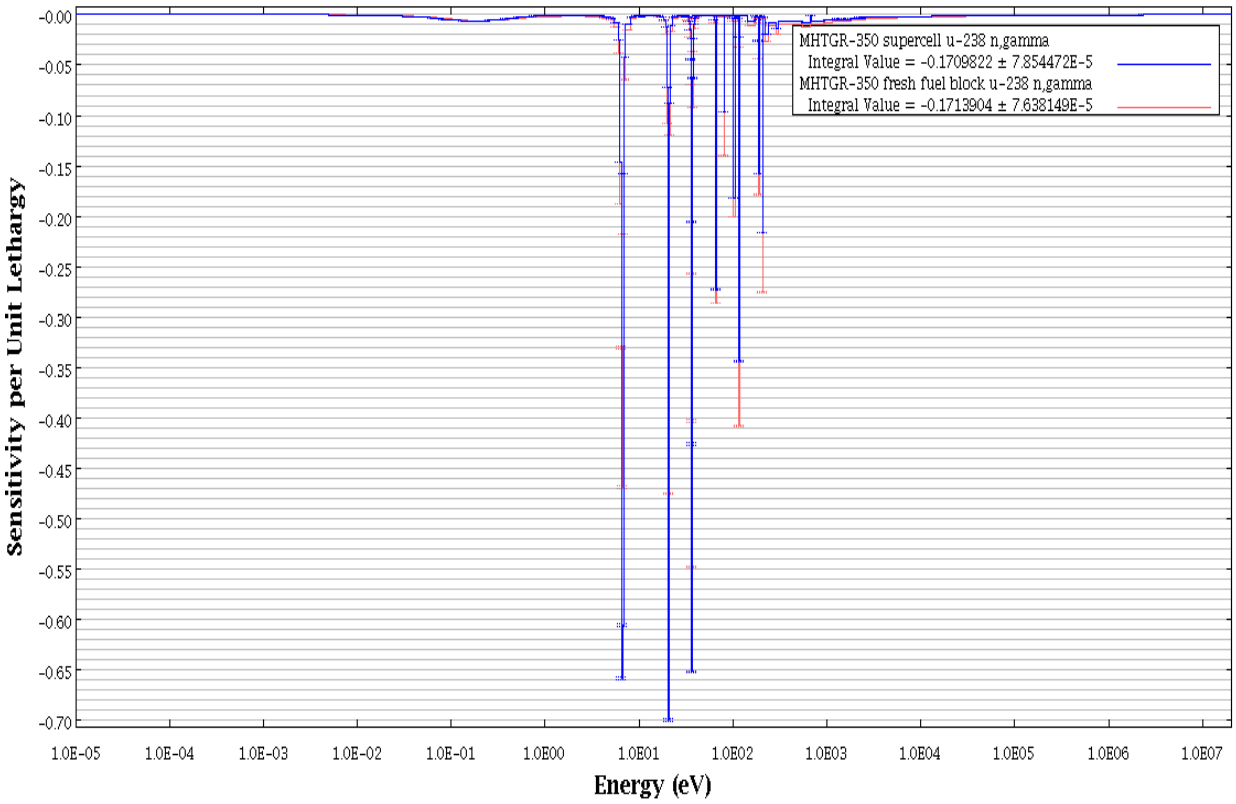


Figure 34: Sensitivity plot for ^{238}U(n,γ)/ ^{238}U(n,γ) reactions

5.5.4 Sampler Results of the MHTGR-350 Fresh Fuel Block and Supercell Models

Table 24 presents the multiplication factor k and its uncertainty for the MHTGR-350 fresh fuel block and supercell models using the ENDF/B-VII.1 nuclear data library, obtained from Sampler for 590 samples. The MHTGR-350 fresh fuel block and supercell models used in this section are similar to the NEWT models used in Section 5.2.3 (i.e. DOUBLEHET treatment for the TRISO fuel particles in the fuel compacts and homogenized BP's in the BP compacts). The multiplication factor k is different from the one reported in Section 5.2.3 since only one sample was used in that section.

Table 24: Uncertainty in multiplication factor results for the MHTGR-350 fresh fuel block and supercell

Fresh fuel block [18]			Supercell		
Multiplication factor k	Uncertainty calculated for multiplication factor k (Δk)	Uncertainty ($\%\Delta k/k$)	Multiplication factor k	Uncertainty calculated for multiplication factor k (Δk)	Uncertainty ($\%\Delta k/k$)
1.04532	529 pcm	0.506	1.09500	482 pcm	0.440

5.5.5 Comparison of TSUNAMI-3D and Sampler Results

The difference between TSUNAMI-3D and Sampler calculations presented above is 9 pcm for Δk. $\%\Delta k/k$ does not show any difference. The ENDF/B-VII.I nuclear data library was used in the Sampler calculation for the MHTGR-350 supercell and the ENDF/B-VII.0 nuclear data library was not used, due to reasons outlined in Section 5.4.

5.5.6 Uncertainty in the Macroscopic Cross Sections

The uncertainties in the 4-group macroscopic cross sections due to the uncertainties in the nuclear data were propagated using Sampler. 590 samples were used for the MHTGR-350 fresh fuel block and 817 for the supercell. Uncertainties for both the fuel block and the supercell were propagated. Running averages of the multiplication factor (k-eff), fission macroscopic cross section for energy group-4 (thermal group) and total macroscopic cross sections for the four collapsed energy groups are shown in Figures 35 to 40. The running average is explained using an example. Given 590 samples, the running average at 300 would be taken using data from samples 1 to 300. The running average of sample 301 would be taken from samples 1 to 301, and so on. Each running average would also have a standard deviation calculated with it.

For all the fuel block running averages shown, by visual inspection, the results can be considered to be converged after 400 samples. The same can be observed for the supercell results except for the total macroscopic cross section of energy group-1. In this case convergence can be considered to start at 550 samples. Spectra for the other cross sections and energy groups available as edits in the output files were also examined although they are not shown here. To be consistent with the total macroscopic cross section of energy group-1, convergence of these other cross sections could also be considered to start at 550 samples. Therefore, running 590 samples for the fresh fuel block was not considered to be a problem.

In Table 25, the average taken at 590 samples is shown for various cross sections, with Nu* fission and the diffusion coefficients shown in rows seven and eight, for the MHTGR-350 fresh fuel block and supercell respectively. The differences between the MHTGR-350 fresh fuel block and the supercell are shown in column six of the respective row.

The standard deviations as a function of the number of samples used are shown in Figures 35 to 40. For all the cases shown, the standard deviation can be considered to be converged after 400 samples. It is noted that the standard deviation of a parameter (such as Σ_{tot}) is the uncertainty due to the nuclear data uncertainties.

The uncertainties propagated using Sampler due to the nuclear data uncertainties are shown in columns four and five for the MHTGR-350 fresh fuel block and supercell respectively. These uncertainties were the standard deviations calculated with 590 samples. In all cases the uncertainties calculated for both systems were close to each other with the averages shown in column seven. However, the uncertainties for the total, transport and scattering macroscopic cross sections together with the diffusion coefficients were much larger than those due to absorption and fission macroscopic cross sections together with Nu* fission. However, the total, transport and scattering macroscopic cross sections were also much larger than the absorption and fission macroscopic cross sections. Therefore, this observation on the uncertainties correlates with the actual values.

For the total, transport, absorption and scattering macroscopic cross sections, the uncertainties due to the nuclear data uncertainties are approximately the same across the groups. For the fission macroscopic cross sections, the uncertainty due to the nuclear data uncertainties in the fourth collapsed group is larger than that due to the other three groups. For the diffusion coefficient the first group has a larger uncertainty due to nuclear data uncertainties than the other three groups. Finally, for Nu* fission, the fourth group has a largest uncertainty due to nuclear data uncertainties, while groups one and two are small and group three is in between.

Column eight shows the ratio of the error arising from the model used (fresh fuel block and supercell) to that of the uncertainties due to nuclear data. For the total, transport, scatter macroscopic cross sections and the diffusion coefficients, the ratio lies in the range 1.4 to 2.5 for the energy group-1. For group-4 the range is between 12.0 and 13. For absorption and fission macroscopic cross sections together with Nu*fission, the ratios are much larger for groups two and three.

Another way of looking at the difference is by evaluating the quantity $\%\Delta\Sigma/\Sigma$. This quantity is shown in Table 26. Columns two and three represent the uncertainties due to nuclear data for the MHTGR-350 fresh fuel block and supercell. Column four is the percentage difference between the fuel block and the supercell. $\langle\Delta\Sigma\rangle$ used to calculate the data in this column is the average uncertainty in the cross sections, calculated using $\langle\Delta\Sigma\rangle = \frac{\Delta\Sigma_{FB}+\Delta\Sigma_{SC}}{2}$.

A similar trend can be seen as was observed in Table 25. The percentage difference due to the model used is larger than the percentage difference in the uncertainty due to the nuclear data uncertainties.

It is therefore clear that the choice of model selected generates a significantly larger uncertainty for the collapsed constants than that due to the uncertainties propagated by nuclear data uncertainties.

Table 25: Uncertainty in macroscopic cross section of the MGTGR-350 fresh fuel block and supercell

Σ_x Group	Running Average FB [18]	Running Average SC	Standard Deviation FB	Standard Deviation SC	Running Average differences	Standard Deviation Average	Ratio of Running Average and Standard Deviation
Σ_{tot}							
1	0.21719	0.22170	0.00182	0.00183	0.00450	0.00183	2.5
2	0.33372	0.34879	0.00168	0.00174	0.01507	0.00171	8.8
3	0.34157	0.35842	0.00171	0.00180	0.01685	0.00176	9.6
4	0.34676	0.36874	0.00174	0.00185	0.02198	0.00180	12.2
Σ_{tr}							
1	0.17244	0.17524	0.00209	0.00204	0.00280	0.002063	1.4
2	0.31429	0.32844	0.00158	0.00164	0.01415	0.001610	8.8
3	0.32085	0.33701	0.00161	0.00170	0.01616	0.001654	9.8
4	0.33261	0.35520	0.00168	0.00179	0.02259	0.001733	13
Σ_{abs}							
1	0.00013	0.00012	0.00001	0.00001	-0.00001	0.00001	-1.4
2	0.00148	0.00118	0.00001	0.00001	-0.00030	0.00001	-28
3	0.00717	0.00594	0.00002	0.00002	-0.00123	0.00002	-61.4
4	0.00931	0.00969	0.00002	0.00002	0.00039	0.00002	21.2
Σ_{fiss}							
1	0.00007	0.00007	0.000001	0.000001	-0.00001	0.000001	-6.4
2	0.00041	0.00033	0.000001	0.000001	-0.00008	0.000001	60.1
3	0.00126	0.00104	0.000004	0.000003	-0.00022	0.000003	69.6
4	0.00561	0.00546	0.000020	0.000018	-0.00015	0.000019	-8.
Σ_{scatt}							
1	0.21707	0.22158	0.00183	0.00183	0.00451	0.00183	2.5
2	0.33225	0.34762	0.00168	0.00174	0.01537	0.00171	9
3	0.33440	0.35249	0.00171	0.00180	0.01808	0.00175	10.3
4	0.33745	0.35904	0.00173	0.00185	0.02156	0.00179	12.1
Nu* fission							
1	0.00019	0.00018	0.000003	0.000003	-0.000014	0.000003	-5.0
2	0.00099	0.00080	0.000004	0.000003	-0.000197	0.000004	50.8
3	0.00307	0.00253	0.000015	0.000012	-0.000543	0.000014	40.1
4	0.01367	0.01331	0.000072	0.000066	-0.000361	0.000069	-5.2
Diffusion coefficients							
1	1.93331	1.90240	0.02336	0.02217	-0.03091	0.02277	-1.4
2	1.06062	1.01494	0.00533	0.00507	-0.04569	0.00520	-8.8
3	1.03893	0.98912	0.00523	0.00498	-0.04981	0.00510	-9.8
4	1.00219	0.93846	0.00506	0.00472	-0.06372	0.00489	-13

Table 26: Macroscopic cross section uncertainties due to nuclear data uncertainties

Macroscopic cross section Group	$\frac{\%\Delta\Sigma(nuclear\ data)}{\Sigma_{FB}}$ [18]	$\frac{\%\Delta\Sigma(nuclear\ data)}{\Sigma_{SC}}$	$\frac{\%(\Sigma_{sc}-\Sigma_{FB})}{\langle\Delta\Sigma\rangle}$
Σ_{tot}			
1	0.84	0.83	2.05
2	0.50	0.50	4.42
3	0.50	0.50	4.82
4	0.50	0.50	6.14
Σ_{tr}			
1	1.21	1.16	1.61
2	0.50	0.50	4.40
3	0.50	0.50	4.91
4	0.50	0.50	6.57
Σ_{abs}			
1	4.13	4.30	-5.89
2	0.78	0.85	-22.72
3	0.31	0.31	-18.79
4	0.20	0.18	4.05
Σ_{fiss}			
1	1.28	1.25	-8.07
2	0.36	0.37	-21.99
3	0.28	0.28	-19.38
4	0.35	0.32	-2.67
Σ_{scatt}			
1	0.84	0.83	2.06
2	0.50	0.50	4.52
3	0.51	0.51	5.27
4	0.51	0.52	6.20
Nu* fission			
1	1.56	1.53	-7.67
2	0.44	0.43	-22.00
3	0.49	0.48	-19.39
4	0.52	0.50	-2.68
Diffusion coefficients			
1	0.00005	0.00005	-3.51
2	0.00107	0.00085	-22.98
3	0.00590	0.00490	-18.51
4	0.00372	0.00423	12.80
Diffusion coefficients			
1	1.21	1.17	-1.61
2	0.50	0.50	-4.40
3	0.50	0.50	-4.91
4	0.51	0.50	-6.57

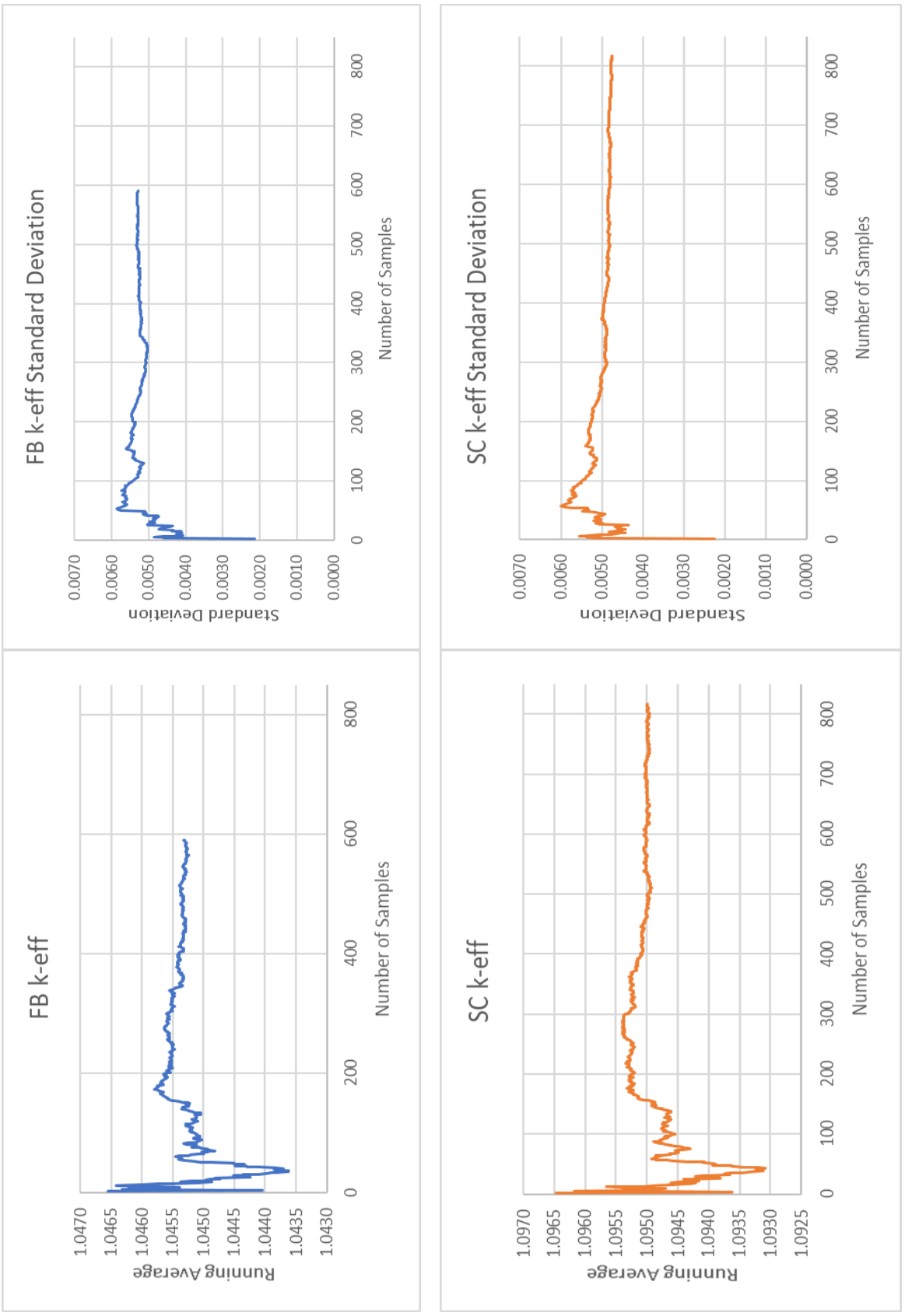


Figure 35: The running average of the multiplication factor and its associated standard deviation

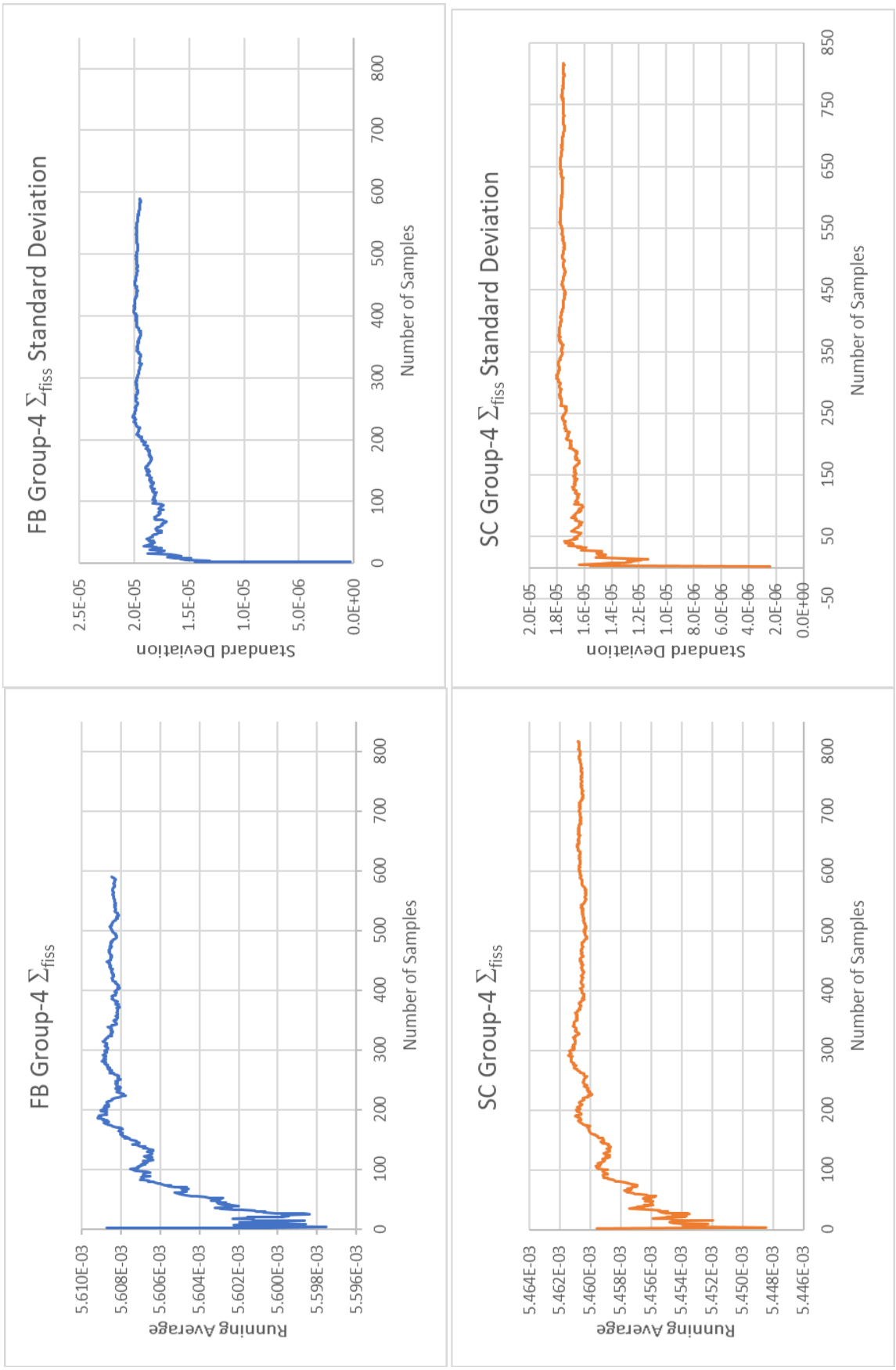


Figure 36: The running average of group-4 Σ_{fiss} and its associated standard deviation

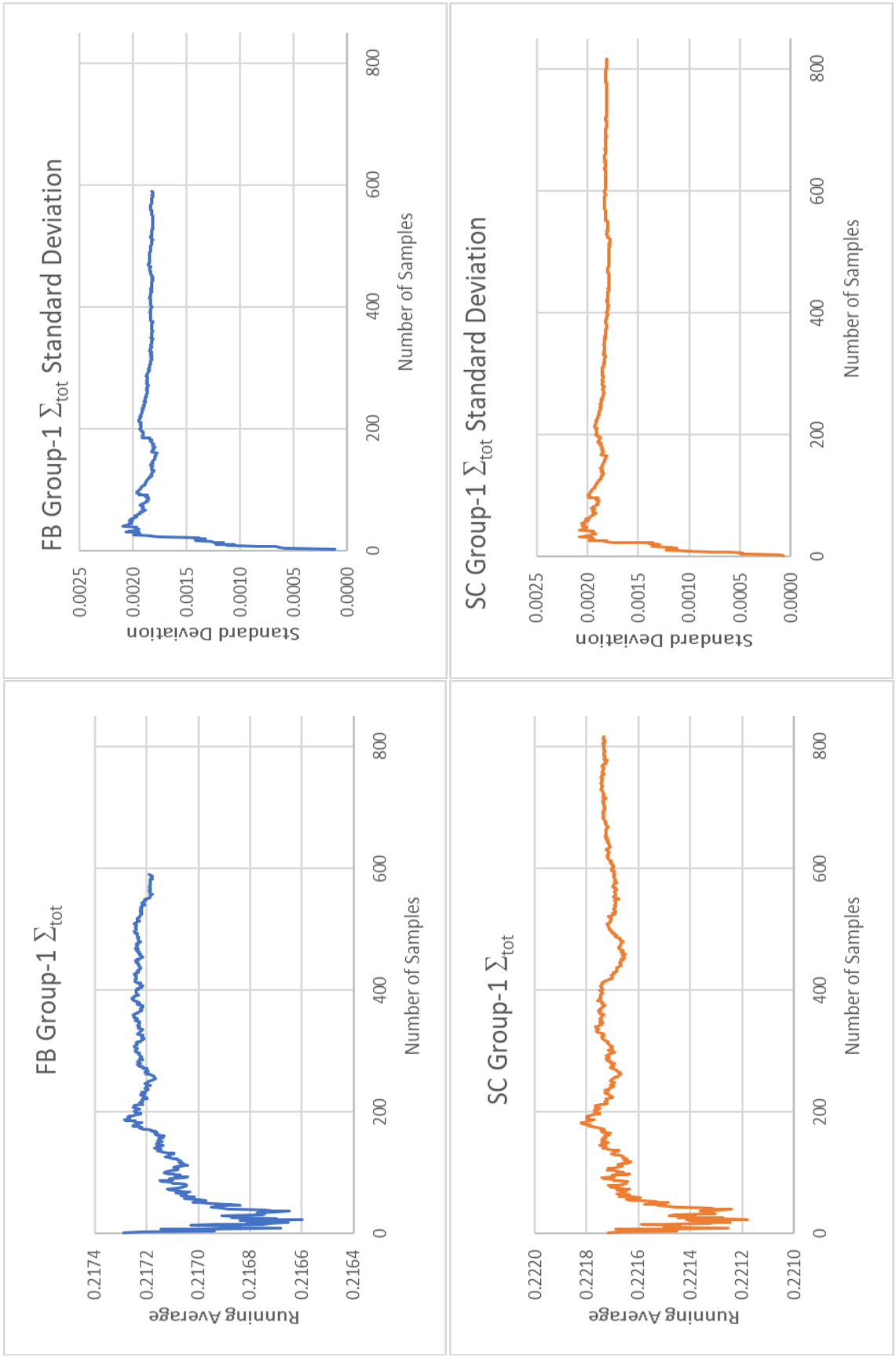


Figure 37: The running average of group-1 Σ_{tot} and its associated standard deviation

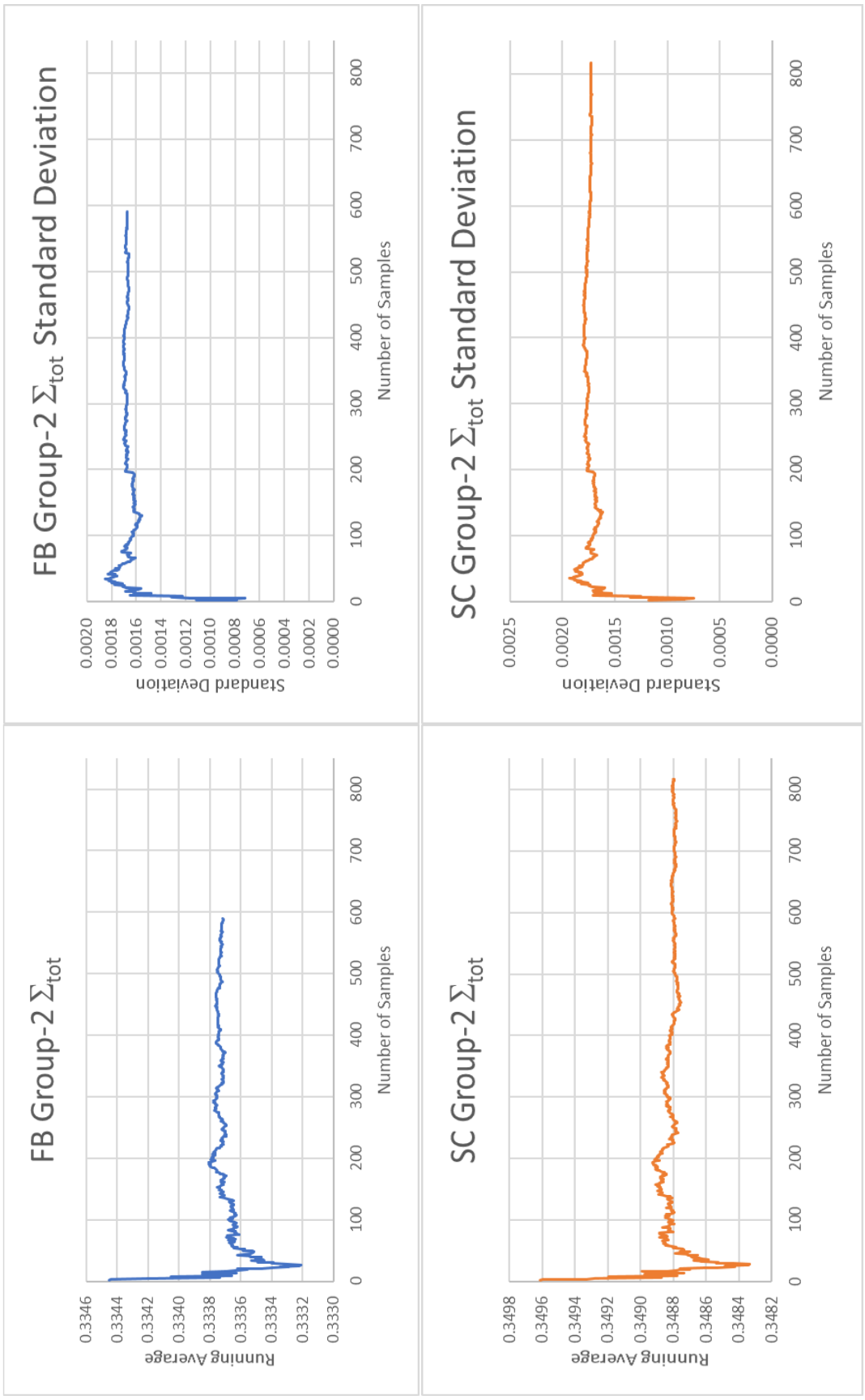


Figure 38: The running average of group-2 Σ_{tot} and its associated standard deviation

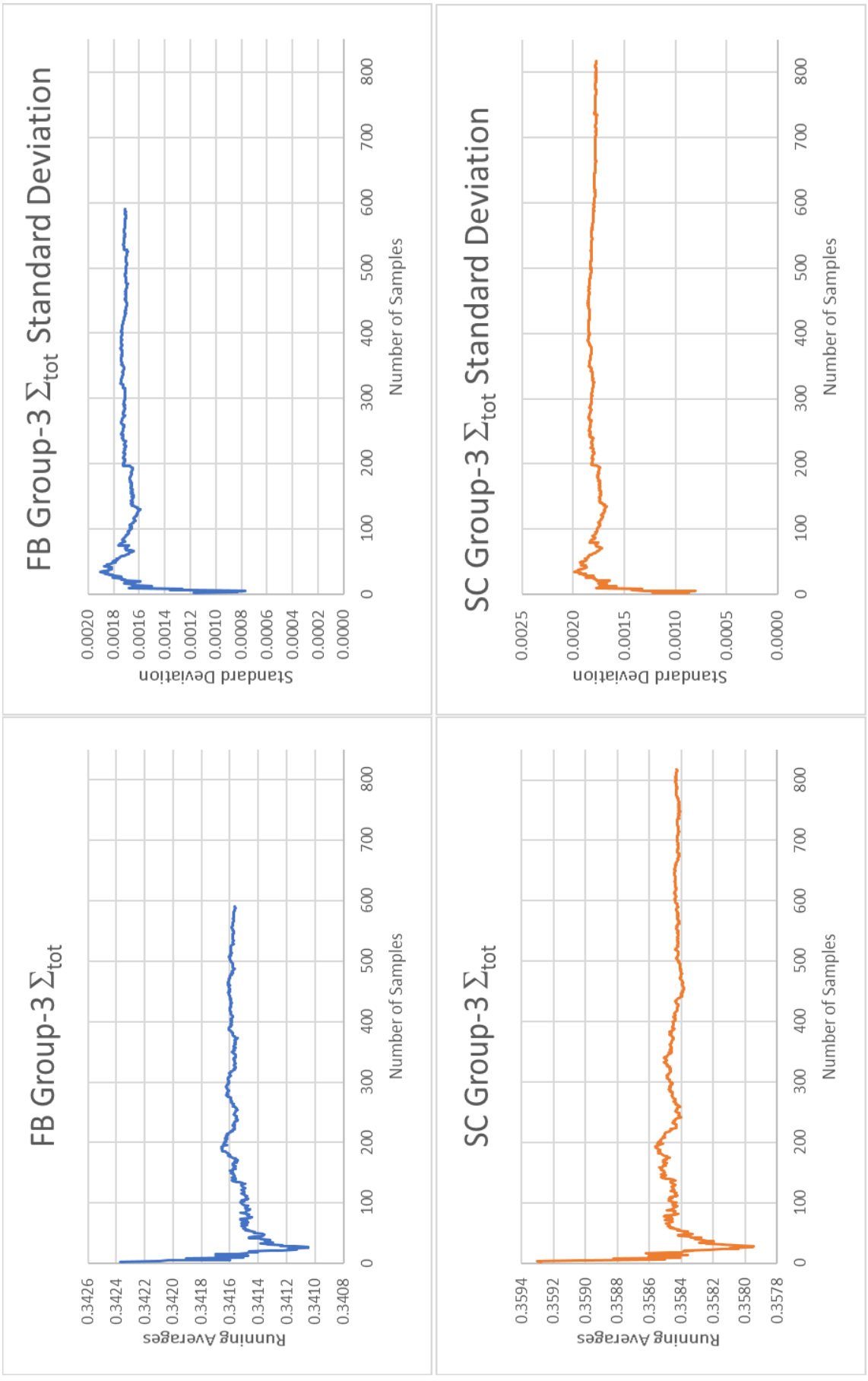


Figure 39: The running average of group-3 Σ_{tot} and its associated standard deviation

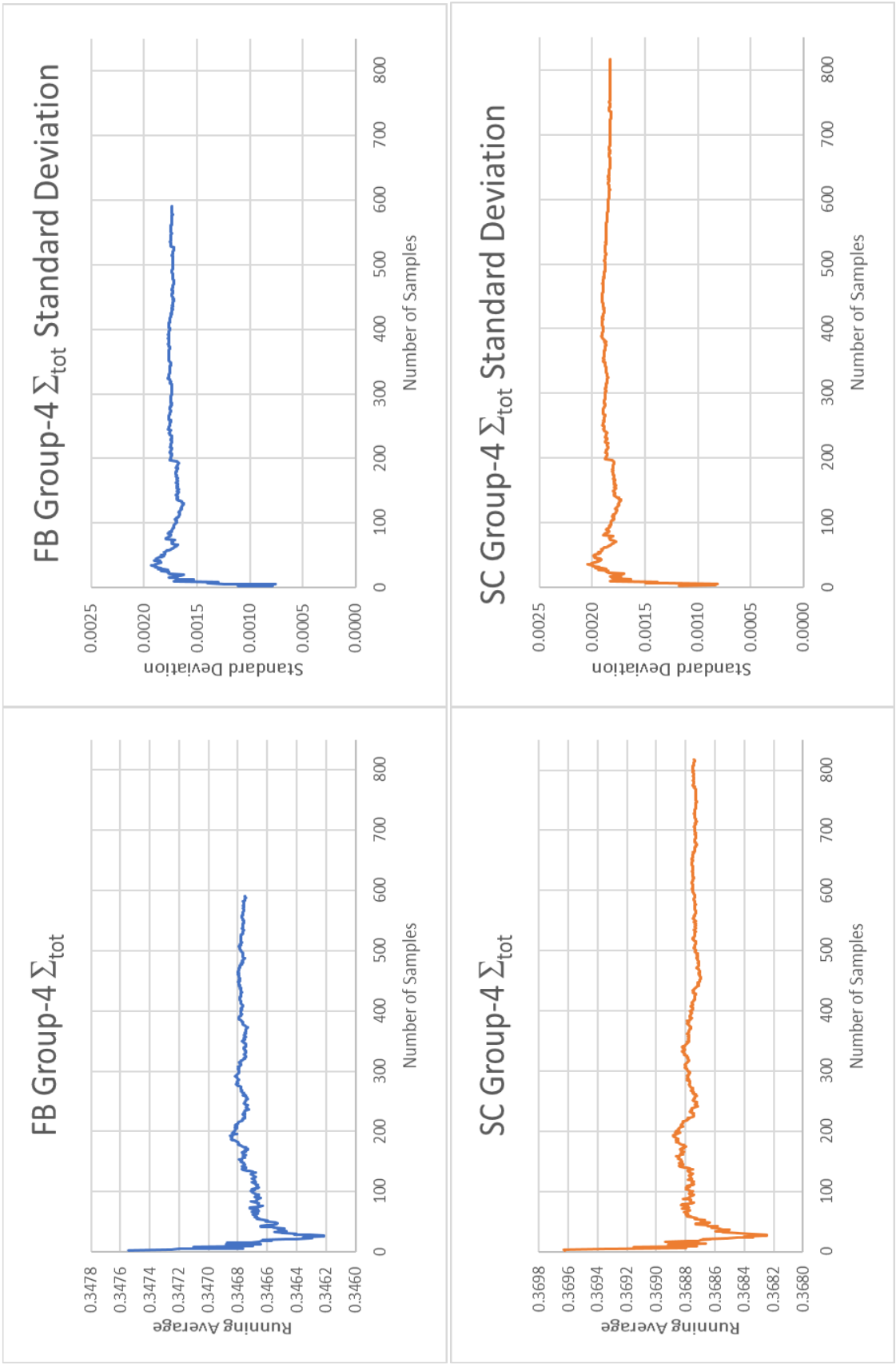


Figure 40: The running average of group 4 Σ_{tot} and its associated standard deviation

5.6 Contributors to Uncertainty in the Multiplication Factor

From the results above, values of 0.498 and 0.507 $\%\Delta k/k$ were obtained for the MHTGR-350 fresh fuel block models utilising ENDF/B-VII.0 and ENDF/B.VII.1 nuclear data libraries, respectively, when considering the uncertainties due to the nuclear data. This amounts to 531 pcm and 538 pcm. For the MHTGR-350 supercell models values of 0.447 and 0.444 $\%\Delta k/k$ were obtained when utilising ENDF/B-VII.0 and ENDF/B.VII.1 nuclear data libraries respectively, which amounts to 478 pcm and 471 pcm respectively. The highest contributor to the uncertainty due to the nuclear data was the $^{235}U(\bar{\nu})$/ $^{235}U(\bar{\nu})$ nuclide-reaction pair for both the MHTGR-350 fresh fuel block and supercell models, with values of 0.36 and 0.26 $\%\Delta k/k$ respectively. This amounts to 375 pcm and 278 pcm respectively.

The multiplication constant for the fuel block and supercell KENO-VI MG models decreases by 548 pcm and 607 pcm respectively for the ENDF/B-VII.0 and ENDF/B.VII.I nuclear data libraries. It is noted that this is about the same magnitude due to the nuclear data uncertainties. It was shown that the effect of an update in carbon capture cross section in the ENDF/B-VII.I nuclear data library compared to ENDF/B-VII.0 was the reason for this change in eigenvalue results, when comparing the results for both nuclear data libraries.

The least contributor to the uncertainty in the multiplication factor considered in this study was observed for the comparison of KENO-VI CE and MG calculations, with differences in the multiplication factor of less than 140 pcm for both nuclear data libraries.

A change in the modelling code (i.e. KENO-VI MG compared to NEWT MG) yielded changes in the multiplication factor of 3781 pcm and 3789 pcm for ENDF/B-VII.0 and ENDF/B-VII.1 respectively. Another participant of the benchmark also reported a large difference. The input models were carefully reviewed to ensure that the self-shielding treatment was the same for both the KENO-VI MG and NEWT MG calculations. Since the fuel block did not show such large differences, this difference is most likely due to the introduction of the neighbouring cells of the supercell structure. It was not possible to investigate this fully, and a set of numerical experiments are proposed which were listed in Section 5.2.4.

CHAPTER 6 CONCLUSION AND RECOMMENDATIONS

6.1 CONCLUSION

The MHTGR-350 supercell models were successfully developed utilising the KENO-VI, NEWT, TSUNAMI-3D and Sampler modules of the SCALE 6.2.1 code package at hot full power (1200 K). All these models were verified as explained in the Chapter 5. Investigations were carried out in terms of criticality, the effect of self-shielding, behaviour of multigroup cross sections and uncertainty and sensitivity assessments on the MHTGR-350 fresh fuel block and supercell models.

Models were investigated with continuous energy (CE) and multigroup (MG) mode for KENO-VI and in multigroup (MG) mode for NEWT. A decrease by 31 pm and 130 pcm in the multiplication factor *k* between the CE and MG KENO-VI calculations using ENDVB/V-II.0 and the ENDF/B-VII.I nuclear data library was found. Comparing the NEWT calculation with the equivalent KENO-VI MG calculation (i.e. discrete ordinates method and Monte Carlo method), an increase of 3781 pcm and 3789 pcm for ENDF/B-VII.0 and ENDF/B-VII.1 nuclear data libraries respectively were observed in the multiplication factor *k*.

In all the MHTGR-350 supercell models, the ENDF/B-VII.0 and ENDF/B-VII.I nuclear data libraries were utilised. It was found that the effect of an update in carbon capture cross section in the ENDF/B-VII.I nuclear data library increases the difference in eigenvalue results between the two libraries.

The 4-group collapsed macroscopic cross sections (Σ) of the MHTGR-350 supercell were successfully obtained from NEWT calculations. It was found that the percentage difference of the collapsed Σ between the two nuclear data libraries was significantly low. The 4-group collapsed macroscopic cross sections were also obtained for the fuel block, since the neighbouring environment of the fuel block in the supercell is different to that when only the fuel block is modelled with reflective boundaries. All the 4-group collapsed cross sections showed significant changes in the values between the MHTGR-350 fresh fuel block and the supercell.

Using this information, it is therefore necessary to investigate the remaining groups constants such as the diffusion constants. These constants can then be used in a nodal calculation, and the difference in the multiplication factor and the power and flux profiles can be studied in terms of the influence of the neighbouring environment of the fuel block.

MHTGR-350 supercell models were also successfully developed using CE TSUNAMI-3D and Sampler, for uncertainty and sensitivity analysis assessments. The uncertainties due to the

nuclear data uncertainties for the models considered using ENDF/B-VII.I was 0.44 in $\%\Delta k/k$ and in the range (471 pcm, 482 pcm) in Δk. The highest contributor to the uncertainty was $^{235}U(\bar{\nu})$/ $^{235}U(\bar{\nu})$, with a value of 0.26 in $\%\Delta k/k$.

The uncertainties in the collapsed cross sections due to the nuclear data were also calculated. It was found that the uncertainty (obtained using the difference) in the collapsed cross sections due to modelling using the fuel block or the supercell was significantly larger than the uncertainty due to the nuclear data uncertainties. This therefore implies that careful consideration must be given to the environment of the fuel block when calculating collapsed constants.

6.2 Recommendations

In calculating the multigroup cross sections, the homogenised BPs were not subject to self-shielding. Furthermore, the blocks surrounding the fresh fuel block on the supercell are homogenised, therefore self-shielding as performed by XSProc in this study could not be applied to them. Therefore, it is recommended that the MHTHR-350 supercell must be modelled with all its heterogeneity, as in Figure 7 (i.e. no homogenised regions) for further assessments.

The next step in the modelling would be to use a nodal core solver to solve for the multiplication factor and the flux profiles. The remaining collapsed constants, together with their uncertainties such as the assembly discontinuity factors, must therefore also be generated.

The difference between the KENO-VI MG and the NEWT calculations must be further investigated. This difference was also found by other workers in this field, and is therefore a known question. Resolution of this question will therefore be of interest to others as well. A possible way to investigate this question further would be to carry out numerical experiments, proceeding in steps from one state to the next, so that the parameter or modelling procedure at which the high change in the multiplication factor occurs can be identified and possible remedied.

The current IAEA CRP on HTGR uncertainties will come to a close in 2019. However, there is still much more work to be carried out in terms of propagating the uncertainties of the HTGR systems. It therefore recommended that the work carried out in this study be continued, with the next steps being the propagation of the uncertainties to the full core model, and subsequent coupling with the thermal fluids calculations. Should another benchmark in this field of research

be started in the future, then with the models and expertise maintained through the NWU participation in this benchmark would be possible.

BIBLIOGRAPHY

[1] P. N. Nkosi and J. Dikgang, “South African Attitutes About Nuclear Power: The Case of Nuclear Energy Expansion,” ERSA, Johannesburg, South AFRICA, 2018.

[2] S. F. Sihlangu, *A Neutronic Model of the PMR200 Prismatic Modular Reactor Using MCNP5,* Potchefstroom: North West University, 2016.

[3] G. Strydom, F. Bostelmann and S. J. Yoon, *Results for Phase I of the IAEA Coordinated Research Project on HTGR Uncertainties,* Idaho Falls: Idaho National Laboratory, 2015.

[4] International Atomic Energy Agency, “Activities of the International Atomic Energy Agency relevant to article IV of the Treaty on the Non-Proliferation of Nuclear weapons,” in *2015 Review Conference of the Parties to the treaty on Non-Proliferation of Nuclear Weapons*, New YORK, 2015.

[5] D. Fischer , “History of the International Atmic agency, the First Forty Years,” IAEA, Vienna, 1997.

[6] M. Methnami, *IAEA High Temperature Gas Cooled Reactor Activities,* Vienna: IAEA, 2010.

[7] F. Reitsma, G. Strydom, F. Bostelman and K. Ivanov, “The IAEA Coordinated Research Program on HTGR uncertaintiy Analysis: Phase I status and Results,” in *Preceedings of HTGR*, Weihai, Chaina, 2014.

[8] M. Lemaire, H. Lee, N. Tak, H. C. Lee and D. Lee, “Multi-physics steady-state analysis of OECD/NEA modular high temperature gas-cooled reactor MHTGR-350,” *Journal of Nuclear Science and Technology,* vol. 54, no. 6, pp. 668-680, 2017.

[9] OECD, “NEA Benchmark of Modular High-Temperature Gas-Cooled Reactor-350MW Core Design Volume I AND II,” OECD, 2018.

[10] A. Pirouzmand and F. Mohammadhasani, “Multi-Group Neutron Cross Sections and Scattering Matrix Calculations Via Monte Carlo Method,” *Journal of Polytechnic,* vol. 18, no. 4, pp. 235-240, 2015.

[11] B. T. Rearden and M. A. Jesse, *SCALE Code System,* Oak Ridge: Oak Ridge National

Laboratory, 2016.

[12] B. Tyobeka , F. Reitsma and K. Ivanov, “HTGR Reactor Physics, Thermal-hydraulics and Depletion Uncertainty Analysis: A Proposed IAEA Coordinated Research Project,” in *International conference on Mathematics and Computational Methods Applied to Nuclear Science and Engineering* , Rio de Janeiro, Brazil, 2011.

[13] R. Li, B. Liu and C. Tang, “Modification in the stress calculation of PyC material properties in TRISO fuel particles under irradiation,” *Jornal of Nuclear Science and Technology,* vol. 54, no. 7, pp. 752-760, 2017.

[14] V. V. Naicker, D. A. Maratele, F. Reitsma, F. Bostelmann and G. Strydom, “QUANTIFICATION OF THE SCALE 6.1 EIGENVALUE UNCERTAINTY DUE TO CROSS SECTION UNCERTAINTIES FOR EXERCISE I-1 OF THE IAEA CRP ON HTGR UNCERTAINTIES,” in *Physor 2016*, Sun Valley,USA, 2016.

[15] D. A. Maratele, *Uncertainty analysis of the fuel compact of the prismatic high temperature gas-cooled reactor test problem using SCALE 6.1,* Potchefstroom: NWU, 2016.

[16] P. Rouxelin, G. Strydom and K. Ivanov, “IAEA CRP on HTGR Uncertaintioes: Comparison of EX. I-2C Nominal Results and Coupling with the PHISICS/RELAP5-3D Core Model for EX. II-1,” in *PHYSOR 2016*, Sun Valley, 2016.

[17] F. Li, K. Ivanov and J. Hou, “Effect of Double Heterogeneity Treatment on Neutronics Modelling of HTGR Unit Cell,” in *2016 International Topical Meeting on High Temperature Reactor Technology (HTR2016)*, Laz Vegas, 2016.

[18] S. F. Sihlangu, *Uncertainty and sensitivity analysis of aspects of the neutronics of a prismatic block-type HTGR,* Potchefstroom: Thesis submited to North West University, 2018.

[19] F. Bostelmann, H. R. Hammer, J. Ortensi, G. Strydom, K. Velkov and W. Zwermann, “Criticality calculations of the Very High Temperature Reactor Critical Assembly benchmark with Serpent and SCALE/KENO-VI,” *Annals of Nuclear Energy,* vol. 90, pp. 343-352, 2016.

[20] F. Bostelmann, M. L. Williams , C. Celik, R. J. Ellis, G. Ilas and B. T. Rearden, “Assessment of SCALE Capabilities for High Temperature Reactor Modelling and Simulation,” *Transctions of the American Nuclear Society,* vol. 119, pp. 1073-1076, 11-15 Novermber

2018.

[21] S. F. Sihlangu, V. V. Naicker , J. Hou and F. Reitsma, “Uncertainty Quantification in the MHTGR-350 Fuel Compact and Block using TSUNAMI-3D Cluch Method and SAMPLER,” in *ANS Best Estimate Plus Uncertainty International Conference (BEPU 2018)*, Lucca, Italy, 2018.

[22] G. Strydom and F. Bostelmann, *Nuclear data uncertainty and sensitivity analysis of the VHTRC benchmark using SCALE,* Idaho: Idaho Nationsl Laboratory, 2017.

[23] G. P. Nyalunga, *Quantifying uncertainties of Aspects of the Neutronics Modelling of the Kozloduy-6 System Using SCALE 6.2.1,* Potchefstroom: North West University (NWU), 2019.

[24] K. Ivanov, M. Avramova, S. Kamerow, I. Kodeli, E. Sartori, E. Ivanov and O. Cabellos , “Benchmark for uncertainty analysis in modelling (UAM) for design, operation and safety analysis of LWRs,” OECD Nuclear Energy Agency, 2013.

[25] W. M. Stacey, Nuclear Reactor Physics, Atlanta: Wiley-VCH Verlag GmbH & Co. KGaH, 2007.

[26] V. Zerkin, “Nuclear Data Services,” International Atomic Energy Agency, 2008. [Online]. Available: https://www-nds.iaea.org. [Accessed 15 October 2019].

[27] X. Yang, S. Xiao, D. Choe and T. Jevremovic, *Neutrocisc Modeling of TRIGA Reactor at the University of Utah Using Agent, KENO6 and MCNP5 Codes,* XUE YANG1, SHANJIE XIAO2, DONGOK CHOE2, TATJANA JEVREMOVIC2: University of Utah.

[28] J. Ortensi, J. J. Cogliati, M. A. Pope, J. D. Bess, R. M. Ferrer, A. Bingham and A. M. Ougouag, “Deterministic Modeling of the High Temperature Test Reactor With DRAGON-HEXPEDIT,” in *Proceedings of HTR 2010*, Prague, Czech Republic, 2010.

[29] F. Leszczynski, D. L. Aldama and A. Trkov, *WIMS-D Library Update,* Vienna: IAEA, 2007.

[30] J. R. Lamarsh and A. J. Baratta, Introduction to Nuclear Engineering Third Edition, Reading, Massachusetts: Addison-Wesley Publishing Company, 1982.

[31] G. Nyalunga , *Developing a fresh core neutronic model at 300 K for a VVER-1000 reactor type using MCNP6,* Potchefstroom: NWU, 2016.

[32] X.-5. M. C. Team, *MCNP-A General Monte Carlo N-Particle Transport Code, Version 5,* Los Alamos: Los Alamos National Laboratory, 2003.

[33] F. B. Brown , *On the Use of Shanon Entropy of Fission Distribution for Assesing Convergence of Monte Carlo Criticality Calculations,* Vancouver, BC, Canada: Physor-2006, 2006.

[34] O. E. Montwedi, “Neutronic simulation of a European Pressurised Reactor,” NWU, Potchefstroom, 2014.

[35] E. L. Redmond, *Multigroup Cross Section Generation Via Monte Carlo Methods,* Cambridge : Mussachusetts Intitute of Technology, 1997.

[36] D. P. Loucks and E. van Beek, *Water Resources Systems Planning and Management: An Introduction to Methods, Models and Applications,* Paris: United Nations Educational Scientific and Cultural Organization (UNESCO), 2005.

[37] J. R. Taylor, *An Introduction to Error Analysis: The Study of Uncertainties in Physical Measurements. Second Edition,* Sausalito, Califonia: University Science Books, 1997.

[38] C. M. Perfetti, “Advanced Monte Carlo Methods For Eigenvalue Sensitivity Coefficient Calculations,” University of Michigan, Michigan, 2012.

[39] B. T. Rearden, L. M. Petrie, D. E. Peplow, K. B. Beckar, D. Wiarda, C. Celik, C. M. Perfetti, A. M. Ibrahim, S. W. D. Hart and M. E. Dunn, “Monte Carlo Capabilities of SCALE Code System,” in *Joint International Conference on Supercomputing in Nuclear Applications and Monte Carlo*, Paris, France, 2013.

[40] F. M. Amer, E. A. Amin and I. I. Bashter, “Generation of Few Energy Group Cross-Sections for some of Gnration-IV reactors,” *Arab Journal of Nuclear Science and Applications,* vol. 50, no. 1, pp. 34-49, 2017.

[41] J. R. Lamarsh, Introduction to Nuclear Engineering, 2nd Eddition, Reading: Addison-Wesley, 1983.

[42] S. Goluoglu, K. Elam, B. T. Rearden, B. L. Broadhead and C. M. Hopper, *SensitivityAnalysis Applied to the Validation of the B-10 Capture Reaction in Nuclear Fuel Casks,* Oak Ridge: Oak Ridge National Laboratory, 2004.

[43] P. Staveloz, F. Poortmans, L. Mewissen and E. Corniles, “Precise Measurement of the Capture Width of the 6.67-eV Neutron Resonance of Uranium-238,” *Nuclear Science and Engineering,* vol. 66, no. 3, pp. 349-353, 2017.

APPENDIX A

Installation and Execution of SCALE 6.2.1 Code Package

This Section provides all procedures followed to install and execute simulations using the SCALE 6.2.1 code package

- **Installation**

The SCALE 6.2.1 code package software for Windows comprises nine discs, numbered 1 to 9. The installation was done following the steps below.

Step 1: Java Visual Machine, also known as Java Runtime Environment (jre-8u171-windows-x64), was downloaded and installed.

Step 2: Disc 1 was inserted into the computer. After double clicking on the SCALE-6.2.1-setup.exe, a loading dialog popped up briefly and once it finished loading, a welcome dialog prompted for the installation to begin.

Step 3: Upon clicking “Next” on the welcome dialog, the installer prompted the license agreement, which was read and all terms and conditions agreed to by clicking on “I agree” to continue with the installation process.

Step 4: After agreeing to the terms and conditions of the license, the installer displayed a dialog to choose the installation location and the path was set by using command C:\SCALE-6.2.1 followed by clicking on “Next”.

Step 5: The choose start menu dialog prompted “Install”, and once clicked on, progress was shown.

Step 6: To install SCALE6.2.1 data, the recommended path inside SCALE 6.2.1 directory was used, C: \SCALE6.2.1. The installer then presented a dialog for available data sets to choose from and all data sets were chosen.

Step 7: A folder was created in C drive, in users as a location for data and all “pak” files from the preceding discs were copied to that folder.

Step 8. The installer was directed to the location of the unpacked files, C: \Users\qol\installer.pak to complete installation.

- **EXECUTION**

Scale was executed by invoking SCALERTE, SCALE Runtime Environment, on the command prompt. For example, SCALE 6.2.1 code package has in it input files of sample problems. As part of testing the code to verify the installation, a folder was created on the desktop, and a sample problem of input file name csas5_7 from sample problems was copied to it and executed by the following commands on the command prompt:

C:\SCALE-6.2.1\bin>scalerte c:\Desktop\sample\csas5_7.inp

After the calculations were completed, the output results were automatically stored in the same directory as the input file, that is in the sample folder which was created on the desktop.

Line by Line Description of the input file

This Section provides all the steps that were followed in building the MHTGR-350 supercell models using KENO-VI, NEWT, TSUNAMI-3D and Sampler

- **KENO-VI Model of the MHTGR-350 Supercell**

The KENO-VI MHTGR-350 supercell model input file used in this study for MG calculations (which is used as reference to other input files, i.e. KENO-VI CE, NEWT, TSUNAMI-3D and Samper) is provided in Appendix B. KENO-VI is a functional module of SCALE 6.2.1 and uses blocks to specify input data in a calculation. The blocks of the input data were used to model the MHTGR-350 and were entered in the form:

Read xxx

Input data

End xxx

Where:
xxx is the keyword for the type of data being entered (e.g. composition, geometry etc.)
Read xxx is used to activate data input.
End xxx is used to terminate data for xxx.

The input of the KENO-VI model of the MHTGR-350 supercell model was built as follows:

=csas6

The csas6 is a control module that provides guidance for calculations to be performed. It

invokes the processor of KENO-VI data to read and check the data of KENO-VI. After checking the KENO-VI data, the csas6 executes the XSProc to process the material input and makes available a temperature and resonance-corrected cross section set for the problem being analysed.

The KENO-VI MHTGR-350 supercell

This is the title of the problem at hand.

v7-238 or v7.1-252n

This specifies the version of nuclear data library which was used. To be noted, v7-238 indicates that the ENDF/B-VII.O nuclear data library was used and the 238 multigroup energy scheme was used. Similarly, v7.1-252n indicates that the ENDF/B-VII.I nuclear data library and 252 multigroup energy scheme were used for a calculation.

Composition block

This block is the material composition block, represented by the keyword comp, in which the nuclides, number densities and temperatures of the MHTGR-350 supercell are specified. Table A1 below shows how the composition of each mixture was assigned.

Table A1: Assignment of material composition mixtures

Material composition	Mixture number	Material composition	Mixture number
Fuel kernel	1	Coolant channel	15
Porous carbon	2	H-451 block graphite	16
IPyC	3	BP kernel	19
SiC	4	BP buffer	20
OPyC	5	BP graphite	21
Fuel graphite matrix	6	Depleted fuel region	22
Fuel compact gap	10	Reflector block graphite region	23
Graphite	11		

All the nuclides, their number densities and temperatures used are outlined in Section 2.3 and 2.4.

Parameters block

This block is the parameter block, represented by the keyword param. It was used to read the parameters which control the number of cycles a calculation may run for, and when a calculation could terminate. It also determined which output files were to be generated after completion of a simulation. An example of a requested output for the MHTGR-350 supercell model is the multiplication factor. The values of the number of generations to be run (GEN), number of neutrons per generation (NPG), and number of generations to be skipped when collecting results (NSK) are specified in a way such that the Shannon entropy of the fission source distribution and the multiplication factor are converged. The following values were set" GEN=600, NPG=50000 and NSK=60 (referenced from [15]).

Cell data block

The cell data block was used to specify the unit cell type, DOUBLEHET. The DOUBLEHET unit cell type was used to specify the TRISO coated particle structure, isotope composition and dimensions of each coated layer. The volume packing fraction (vf) of TRISO coated particles in the fuel compact, and also the matrix labels in which the TRISO coated particles were embedded were also specified in this block. The geometry and arrangement of materials of the DOUBLEHET unit cell are shown in Figure A1.

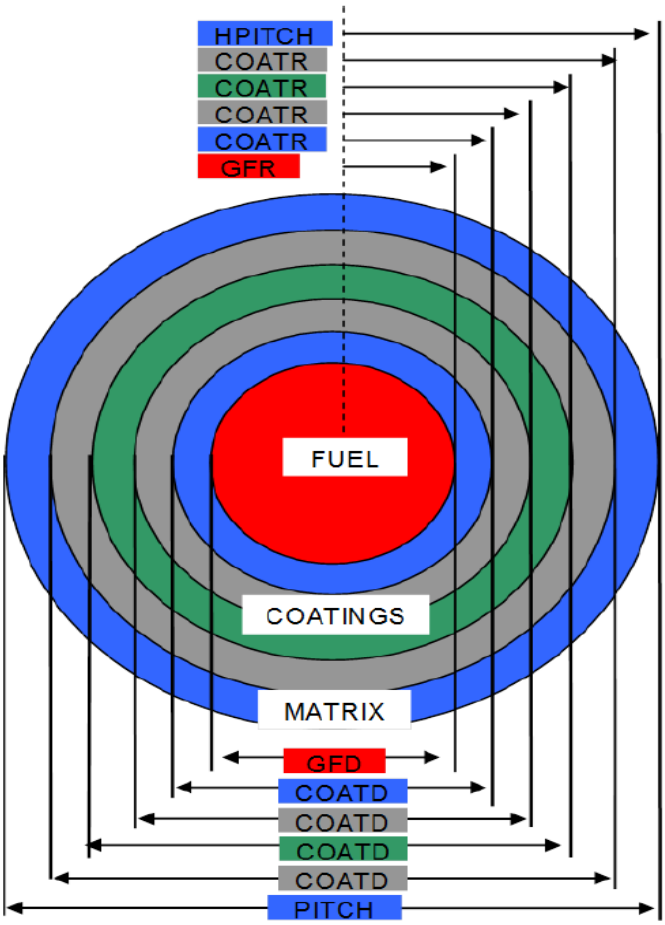


Figure A1 : DOUBLEHET unit cell material arrangement and geometry

Source: [11]

Table A2 shows how the DOUBLEHET unit cell type definitions were used to specify the geometry and arrangement of materials of the TRISO coated particles in the MHTGR-350 supercell.

Table A2: Definition of TRISO coated particles using the DOUBLEHET definition

	DOUBLEHET definition	Dimension [cm]
Fuel kernel outer radius	GFD	0.20125
Porous carbon buffer outer radius	COATR	0.03125
IPyC outer radius	COATR	0.03525
SiC outer radius	COATR	0.03875
OPyC outer radius	COATR	0.01275
Unit cell pitch	PITCH	0.9398

The composition belonging to GFP was identified as 1, the composition in the porous carbon buffer outer radius (COARR) was 2, the composition in the COATR (IPyC) was 3, the composition in the COATR (SiC) was 4, the composition in the COATR (OPyC) was 5 and the composition in HPITCH was 6. This was consistent with the labelling described above.

Also specified in the cell data block was the CENTRM data. CENTRM data contain the order of angular quadrature, ISN=32, spatial mesh factor, SZF=0.4 and number of scattering angles, SCT= 2, which are used for cross section processing. The values for ISN, SZF and SCT were assigned with reference to [15].

The cell data block is required for MG calculations. Therefore, it was only included in the MG calculations and not the CE calculations of the MHTGR-350 supercell models.

The CENTRM DATA parameter data block is an optional block which defines input parameter values for the CENTRM module. The parameter IXPRT and NPRT were specified to control the amount of information to be printed on the output file. IXPRT was set to 1 (to print more information on the output file), and the NPRT was set to 2 (to print both 1-D and 2-D cross section). Another parameter that was also specified in this block was ISN, which was set to 32 (default value for spheres), which defines the order of angular quadrature.

An optional sub block, the “more data” sub block was added to the cell data block. Parameters specified in this sub block allow certain default options to be modified for individual cell calculations. In this sub block, the parameter SZF was specified. This parameter was used to adjust the spatial mesh size (a value between zero and one yields a finer mesh). The value was set to 0.40, with reference to [18].

Geometry block

The geometry block is represented by the keyword geom. It is used to define different units and arrays that constitute the formation of the MHTGR-350 supercell model. A unit may consist of one or more material regions with its own local coordinate system. An array, also called a lattice, is constructed by stacking the units [28]. The nuclides that are contained in each unit were specified by using mixture numbers assigned to them in the material composition block.

From Appendix A, global unit 4000 was used to describe the outermost geometry boundary of the MHTGR-350 supercell, which is the rotated hexaprism (rhexaprism). The pitch was 54cm and the height was 4.9280 cm starting from zero cm 4000 identifies the rhexprism. The volume of the MHTGR-350 supercell model consists of rhexaprism blocks of the fresh fuel blocks,

depleted fuel and graphite, as shown in Figure 8. An array (array 1) was used to describe and place these rhexaprisms inside the rhexaprism 40, which is the outer boundary of the MHTGR-350 supercell. A more detailed description of the array 1 will be given in the array block.

Unit 1000 was used to represent the fresh fuel block, which is a rhexaprism of pitch 18 cm and a height of 4.9280cm starting from zero. Array 2 placed in rhexaprism 10 was used to describe the unit cells in the fresh fuel block, which includes large and small coolant channels, graphite blocks, burnable poison and fuel compacts.

Unit 2 was used to represent the large coolant channel, which consists of a cylinder with radius 0.6350cm that is inside a hexaprism of pitch 0.9398cm with the same height as the fresh fuel block. Media 10 and 11 (mixture numbers) were used to specify the materials in the cylinder and the hexaprism respectively. With respect to the material composition block mixture 10 is helium and mixture 11 is graphite. Unit 3 was used to represent the small coolant channel with a cylinder of radius of 0.6350cm but otherwise the same as unit 2.

Unit 4 was used to represent the graphite block that is in a shape of a hexaprism with a pitch of 0.9398cm.

Unit 6 was used to represent the burnable poison compact, which consists of a cylinder of radius 0.5715cm inside a graphite hexaprism of pitch 0.9398cm. Array 36 was defined and placed in cylinder 10 of unit 6. Array 36 (which contains B_4C particles) will be further described in the array block.

Unit 7 was used to represent the fuel compact, which consists of a cylinder of radius 0.6225cm inside a graphite hexaprism of the same pitch as unit 6. The fuel mixture defined as DOUBLEHET was placed inside cylinder 10 of unit 7.

Unit 35 and 37 were used to define the TRISO and burnable poison particles respectively. In unit 35, the following definitions were made: sphere 10 to be the fuel kernel, sphere 20 to be porous carbon, sphere 30 to be IPyC, sphere 40 to be SiC and sphere 50 to be OPyC, which constitutes a TRISO particle. A further definition to define cuboid 20 of length 0.0455cm was made. The cuboid was used to house the TRISO particle which was used to form an array inside cylinder 10 of unit 7. The dimensions of each sphere were used as outlined in Table 2 Similarly, definitions were made for the burnable poison particles using dimensions in Table 2 and mixture numbers from the material composition block for unit 37.

Unit 2000 was set to be an empty rhexaprism cell by setting its media to be zero. This was done to achieve the shape of the outermost boundary (rhexaprism) of the supercell system.

Units 3000 and 5000 were used to represent the graphite reflector region and depleted region respectively.

Boundary block

The boundary block was represented by the keyword BOUND. The boundary condition of the MHTGR-350 supercell was set to be reflective (all = mirror). In this way the supercell was modelled as an infinite array of supercells.

Array block

The array block is represented by the keyword ARA. ARA=X, and X is the reference number of the array. This block was used to specify the type and size of the constructed array, and to position the units that were defined in thegeometry block. This was done to represent the described geometry in a 3D lattice. Four arrays were constructed for the MHTGR-350 supercell model: ARA=1, ARA=2, ARA=34 and ARA=36. The array orientation data in all the four arrays was set to fill. By Setting the orientation data to fill, the data is entered by stringing in unit numbers from X=1, Y=1, Z=1 varying with X, then Y, followed by Z. This was done to fill the array. To specify the number of units used in an array, number of units in X-direction (NUX), number of units in Y-direction (NUY)and number of units in Z-direction (NUZ) were used.

Array 1 (ARA=1) was used to stack the different blocks (i.e. the fresh fuel block, graphite blocks and depleted blocks) that constitute the MHTGHR-350 supercell. The type of array was set to be rhexagonal (rotated hexagon), since it is an array of rotated hexagonal blocks.

Array 2 (ARA=2) was used to arrange all units in the fresh fuel block. The type of array was set to be shexagonal. This was done to stack the units so that the faces (of the units) perpendicular to the X-axis met.

Array 34 was poisoned in cylinder 10 of unit 7, to capture the arrangement of TRISO particles. The type of array was set to cuboidal.

Array 36 was positioned in cylinder 10 of unit 6, to capture the arrangement of the B_4C particles. The type of array was set to cuboidal.

This concludes the procedure followed in modelling the MHTGR-350 supercells using either the 238 multigroup or 252 multigroup cross section library with KENO-VI. For the continuous energy (CE) scheme, similar structures were set up and the version of nuclear data v7-238 was replaced with ce_v7 for the ENDF/B-VII.0 CE cross sections and v-7.1-252n with ce_v7.1 for the ENDF/B-VII.I CE cross sections. For CE calculations the cell data block and DOUBLEHET

treatment was omitted, since it was already mentioned that both apply only to MG calculations. To account for the DOUBLEHET treatment of the fuel, Array 34 (which contains TRISO particles) was constructed and placed inside cylinder 10 of unit 7.

- **NEWT Model of the MHTGR-350 Model**

To develop the NEWT model of the MHTGR-350 supercell, the following changes and additions were made to the KENO-VI MG structure setup already described in this section.

T-NEWT (TRITON)

The control module of KENO-VI, CSAS6 was replaced by T-NEWT, T-NEWT is the control module of NEWT calculations.

The NEWT model of the MHTGR-350 supercell

This is the title of the problem.

Composition block

The burnable poison (BP) definition was changed from the heterogeneous to the homogeneous definition. This was achieved by omitting the BP buffer (mixture 20) and BP graphite (mixture 21). Homogenisation of the BP compacts definition was done in accordance with the benchmark.

Geometry block

The geometry is the same as that of the KENO-VI geometry. It was explained in Section 3.11.2.2 that NEWT is capable of modelling 2D systems, hence the third dimension (z-axis) specifications were omitted. The benchmark provided the following recommendations for the definition of the grid structure: the fuel compact unit cells to consist of a 4 × 4 grid and all other compacts to consist of 2 × 2 grid [3]. However, in this study the global unit of the MHTGR-350 supercell consisted of a 16 ×16 grid. Within this global unit, 4 × 4 grids for the fresh fuel block (unit 1000), homogenised depleted block and homogenised graphite blocks were defined. In the fresh fuel block, the unit cells and all other compacts consisted of a 2 × 2 grid.

The BP definition of a lattice, which was achieved by construction of array 36 in the MHTGR-350 supercell KENO-VI MG calculation, was changed to a homogenisation definition. This was done by replacing array 36 by homogenised BP's (mixture 19) in the cylinder of the same radius, which was within a graphite (mixture 16) hexaprism.

The number of units in the Z-direction (NUZ) were omitted, to change from a 3D system to a 2D system.

Array block

Since NEWT is a 2D discrete-ordinates transport code, only the number of units in the X and Y directions were set and the number of units in the Z direction were omitted for all units, to change from a three-dimensional (3D) system to a 2D system. For example Array 1 from the description of KENO-VI MG model, which shows the arrangement of the fresh fuel block, depleted fuel blocks and graphite blocks were constructed with NUX and NUY with NUZ omitted.

Array 36 was omitted to account for the homogenisation of the BP compacts, by defining all material of the BP compacts as a single mixture.

Parameter block

Table A3 presents a summary of data parameters that were added to the parameter block

Table A3: Additions that were made to the parameter block

Parameter data added	Function
Echo=yes	Generates output at each outer iteration during the iteration phase of execution
PRTMXSEC=YES	to print the mixture macroscopic cross sections in the output
PRTHMMIX=YES	to print the homogenised mixture macroscopic cross sections in the output
PRTXSEC=YES	To print microscopic cross sections
PRTBROAD=YES	To print broad cross sections in the output
DRAWIT=YES	To create postscript files showing the grid structure and material definition determined from the input
PRTFLUX=YES	To create a postscript plot file showing the distribution of flux for each energy group
TIMED=YES	To turn on the printing of the iteration timing and CPU use data

Materials block

The materials block was used to specify material data and the order of scattering that was used in the calculation. Mixtures 10, 11, 15, 16, 18, 27, 38, 23 and 22 were each assigned the order

for scattering P_n=2. This was done in accordance with the benchmark [3].

Collapse block

The collapsed block was added. This block contains the collapsed (broad) group assignment from the input group structure. Both nuclear data libraries were used. In this study the original group structure (238-group or 252-group) was collapsed to four group structures. For ENDF/B-VII.0, the 238-group structure was collapsed as follows: The first 44 groups were collapsed to the first broad group (20MeV-0.1MeV), the second 71 groups into second broad group (0.1MeV-30eV), the third 46 groups into the third broad group (30Ev-1.86Ev) and the remaining 77 into the fourth group (1.86Ev -0).

Homogenisation block

The homogenisation block is characterised by the keyword homog. This block was used to create homogenised cross sections using the energy structure that is defined in the collapse block. The homogenised mixture identity (121 fuel) and the list of mixtures (mixtures 10, 11, 15, 16, 18, 19, and 29 of the fuel) to be homogenised for collapsed multigroup constants were specified in this block.

The homogenised mixture can be defined for a single geometric unit or multiple units. One of the edits in the output file when using the homogenisation block is the flux in that unit or multiple unit. Therefore, the flux in two adjacent units can be obtained separately if each unit is defined by a different homogenised mixture. In this way the self-shielding studies were performed on the MHTGR-350 supercell and fresh fuel block, where an individual unit cell was considered a spatial volume.

The other blocks not described in this section retain the same set up as those described in KENO-VI MG model for the respective nuclear data library.

This concludes the procedure followed in the development of the NEWT model of the MHTGR-350 supercell using the ENDF/B-VII.0 (238 multigroup cross section library). To conclude the procedure for the ENDF/B-VII.I (252 group cross section library), v7-238 was replaced by v7.1-252n, the second collapsed group was changed to 84 groups and the third collapsed group to 47 groups to suit the 252 group.

- **TSUNAMI-3D Model of the MHTGR-350 Model**

To develop the TSUNAMI-3D model, the following changes and additional data were made to the KENO-VI CE model development already described.

TSUNAMI-3D-K6

TSUNAMI-3D-K6 is the control module that was used to guide the sequence of calculations that were performed using TSUNAMI-3D.

TSUNAMI-3D model of the MHTGR-350 supercell

This is the title of the problem at hand.

Cross section library

All TSUNAMI-3D calculations were executed using the continuous energy (CE) mode, for the EBDF/B-VII.0 and ENDF/B-VII.I nuclear data libraries. To specify the version of nuclear data library, either ce_v7 for ENDF/B-VII.0 or ce_v7.1 ENDF/B-VII.I nuclear data library were specified for each simulation.

Parameter block

CET=1 was used to specify the continuous energy (CE) sensitivity method used, which is the CLUTCH method described in Section 3.12.1. Furthermore, CET=1 creates a grid geometry for the weighting function, $F^*(r)$ mesh. This mesh covers all fissionable material regions of the MHTGR-350 supercell, as seen in Figure 20 in Section 4.5. CFP=20, as suggested in the SCALE 6.2.1 manual [11], was used to specify the number of latent generations for calculating $F^*(r)$. CDG=1, was used to specify the identity of the $F^*(r)$ spatial grid. FST=YES, was used to print the $F^*(r)$ grid values in a .3DMAP file, shown in Figure 20. DBR=1 was used to perform Doppler broadening on one dimensional (1D) cross sections (the Doppler broadening phenomenon is described in Section 3.2.3). This option recalculates the collision probabilities after Doppler broadening with regard to temperature to ensure consistency.

GridGeometry block

This block was used to specify the spatial grid for the $F^*(r)$ mesh in the X-, Y-, and Z-directions. XLINEAR was used to generate x-y $F^*(r)$ meshes from minimum X- position to the maximum X-position. Similarly, YLINEAR and ZLINEAR were used for Y- and Z-positions respectively.

The remaining blocks that are not described retain the same setup as those described in KENO-VI MG model, except for the cell data block, which was omitted, since it was stated that it only applies to an MG calculation.

Two models of the TSUNAMI-3D MHTGR-350 supercell were obtained using ENDF/B-VII.0 and

ENDF/B-VII.I nuclear data libraries.

- **Sampler Model of the MHTGR-350 Supercell**

As explained in Section 3.6.4, Sampler is a module for statistical uncertainty analysis with SCALE 6.2.1 sequences, hence it uses sequences for statistical sampling. With NEWT used as the neutronic solver, the following additions and changes were made to the input file of the NEWT MHTGR- 350 supercell already explained in this section to convert it to a Sampler calculation:

=sampler

This is the control module that was used to guide the sequence of calculation performed by Sampler in modelling the MHTGR-350 supercells. Hence, T-NEWT from the NEWT input file was omitted.

Parameters block

The parameters block identifies the base cross sections used for building perturbed cross sections. The main workflow and output parameters of Sampler were controlled in this block by specifying the following: the nuclear data library, the number of samples to be calculated and whether to perform cross section perturbation or not. Table A4 summarises the nuclear data that was specified in the parameters block:

Table A4: Data specified in the parameters block

Library=xn238v7	this was used to specify the nuclear data library used in performing a calculation, in this case it was the ENDF/B-VII.0 library.
N_sample=1000	This was used to specify the number of samples for nuclear data perturbations.
Perturb_xs=yes	This was used to perform cross section perturbations.
Print_data=yes	This option was used to print data per sample value in the main output
Print_corr=yes	This was used to print correlation matrices in the main output
Print_cov=yes	This was used to print the covariance matrices in the main output
Print_chi2= yes	This was used to print the chi-square normality test in the main output

Case block

A Sampler calculation may contain one or multiple cases. This block is used to specify the number of cases and sequence of the calculation. In this study, a single case was run per calculation. The following data was used in this block:

Sequence=t-newt was used to specify that the NEWT input file is used as a sequence in this Sampler calculation. Hence the MHTGR-350 NEWT input file explained in Section 4.3.2 was integrated into this Sampler calculation. However, the nuclear data specification of the NEWT input file library was changed to match the library described in the parameters block (i.e. from the form v7-238 to xn238v7 for ENDF/B-VII.0 and v7.1-252 to xn252v7.1 for the ENDF/B-VII.I nuclear data library.

The title of the problem was also specified in this block: Sampler model of the MHTGR-350 supercell, which is an optional choice.

Response block

Responses are extracted from any case executed with Sampler. A Sampler response can be a time-dependent series or a single number, which is assigned a name. The response block was defined in a way to result in the extraction of k-effective including the uncertainty.

Two models of the MHTGR-350 supercells were developed using this setup, by changing the nuclear data library versions, using the xn238v7 which is based on the ENDF/B-VII.0 and xn252v7.1 based on the ENDF/B-VII.I nuclear data library.

APPENDIX B

KENO-VI input file

```
=csas6
The KENO-VI MHTGR-350 supercell
V7-238
read comp
' fuel
  u-235        1 0 3.6676e-3 1200       end
  u-238        1 0 1.9742e-2 1200       end
  o-16         1 0 3.5114e-2 1200        end
  c-graphite   1 0 1.1705e-2 1200       end
```

```
' Porous Carbon
  c-graphite   2 0 5.2646e-2 1200      end
' IPyC
  c-graphite   3 0 9.5263e-2 1200      end
' SiC
  c-graphite   4 0 4.7883e-2 1200     end
  si-28        4 0 4.4159e-2 1200        end
  si-29        4 0 2.2433e-3 1200        end
  si-30        4 0 1.4805e-3 1200        end
' OPyC
  c-graphite   5 0 9.5263e-2 1200      end
' Fuel Graphite Matrix
  c-graphite   6 0 7.2701e-2 1200      end
' Fuel compact Gap
  he-4         10 0 2.46e-05 1200         end
  c-graphite  11 0 0.0928   1200       end
' Coolant channels
  he-4         15 0 2.46e-05 1200        end
' Block graphite
  c-graphite  16 0 0.0928   1200         end
' BP Kernel
  b-10         19 0 2.1400e-02 1200       end
  b-11         19 0 8.6300e-02 1200       end
  u-238        19 0 1.0000e-12 1200       end
  c-graphite  19 0 2.6900e-02 1200        end
'BP Buffer
  c-graphite  20 0 5.0200e-02 1200        end
' BP PyC
  c-graphite  21 0 9.3800e-02 1200        end
' BP matix
  c-graphite  29 0 7.2701e-2 1200          end
  c-graphite  37 0 0.0928   1200            end
'  depleted region
H-1         22 0  1.0174E-11 1200        end
He-4        22 0  4.8356E-06 1200        end
B-10        22 0  6.6179E-28 1200        end
B-11        22 0  9.1294E-20 1200        end
C-graphite 22 0  6.9359E-02 1200    end
N-14        22 0  1.1437E-15 1200        end
O-16        22 0  3.4381E-04 1200        end
Si-28       22 0  6.4819E-04 1200         end
Si-29       22 0  3.2928E-05 1200         end
Si-30       22 0  2.1732E-05 1200         end
Kr-83       22 0  6.2255E-08 1200         end
Zr-91       22 0  6.9367E-07 1200         end
```

```
Zr-93      22 0  8.6442E-07 1200        end
Zr-94      22 0  9.2196E-07 1200        end
Zr-95      22 0  8.0991E-08 1200        end
Zr-96      22 0  9.3065E-07 1200        end
Nb-93      22 0  5.4954E-14 1200        end
Nb-95      22 0  4.4501E-08 1200        end
Mo-95      22 0  7.7378E-07 1200        end
Mo-97      22 0  6.7966E-07 1200        end
Mo-98      22 0  9.1913E-07 1200        end
Mo-99      22 0  3.8419E-09 1200        end
Mo-100     22 0  1.0236E-06 1200        end
Tc-99      22 0  8.5469E-07 1200        end
Ru-100     22 0  1.2082E-07 1200        end
Ru-101     22 0  8.3103E-07 1200        end
Ru-102     22 0  8.2728E-07 1200        end
Ru-103     22 0  4.5748E-08 1200        end
Ru-104     22 0  5.2966E-07 1200        end
Ru-106     22 0  1.5154E-07 1200        end
Rh-103     22 0  4.4004E-07 1200        end
Rh-105     22 0  1.1382E-09 1200        end
Pd-105     22 0  3.6784E-07 1200        end
Pd-107     22 0  1.9336E-07 1200        end
Pd-108     22 0  1.2803E-07 1200        end
 Ag-109    22 0  6.9654E-08 1200        end
Cd-113     22 0  1.7453E-10 1200        end
 In-115    22 0  1.4151E-09 1200        end
Sb-126     22 0  1.3844E-11 1200        end
I-127      22 0  3.7479E-08 1200        end
I-129      22 0  1.2345E-07 1200        end
I-135      22 0  4.0156E-10 1200        end
Xe-131     22 0  3.4937E-07 1200        end
Xe-133     22 0  8.1610E-09 1200        end
Xe-135     22 0  3.0374E-10 1200        end
Cs-133     22 0  9.1492E-07 1200        end
Cs-134     22 0  1.1453E-07 1200        end
Cs-135     22 0  5.4225E-07 1200        end
Cs-137     22 0  9.7835E-07 1200         end
Ba-140     22 0  1.6807E-08 1200         end
La-139     22 0  9.7876E-07 1200         end
Ce-141     22 0  4.0385E-08 1200         end
Ce-142     22 0  8.8921E-07 1200         end
Ce-143     22 0  1.6053E-09 1200        end
Ce-144     22 0  2.8611E-07 1200         end
Pr-141     22 0  8.4172E-07 1200         end
Pr-143     22 0  1.5842E-08 1200         end
```

```
Nd-143     22 0  7.0924E-07 1200        end
Nd-144     22 0  6.4641E-07 1200        end
Nd-145     22 0  5.1870E-07 1200        end
Nd-146     22 0  5.1685E-07 1200        end
Nd-147     22 0  5.3346E-09 1200        end
Nd-148     22 0  2.6984E-07 1200        end
Pm-147     22 0  1.3156E-07 1200        end
Pm-148     22 0  9.0799E-10 1200       end
Pm-149     22 0  8.5754E-10 1200        end
Sm-147     22 0  5.0618E-08 1200        end
Sm-149     22 0  4.3684E-09 1200        end
Sm-150     22 0  2.0234E-07 1200        end
Sm-151     22 0  1.8420E-08 1200        end
Sm-152     22 0  6.5111E-08 1200        end
Sm-153     22 0  6.1520E-10 1200        end
Eu-151     22 0  2.4498E-11 1200        end
Eu-153     22 0  7.9950E-08 1200        end
Eu-154     22 0  1.8657E-08 1200        end
Eu-155     22 0  3.8997E-09 1200        end
Eu-156     22 0  2.0699E-09 1200        end
Gd-152     22 0  7.9225E-13 1200        end
Gd-154     22 0  1.2559E-09 1200        end
Gd-155     22 0  1.0069E-10 1200         end
Gd-156     22 0  3.7784E-08 1200         end
Gd-157     22 0  2.2117E-10 1200         end
Gd-158     22 0  9.9975E-09 1200         end
Gd-160     22 0  6.2518E-10 1200         end
U-234      22 0  6.6749E-10 1200          end
U-235      22 0  2.2142E-05 1200          end
U-236      22 0  2.6869E-06 1200          end
U-238      22 0  1.8238E-04 1200         end
Np-237     22 0  2.6466E-07 1200         end
Pu-238     22 0  8.9788E-08 1200          end
Pu-239     22 0  2.6484E-06 1200          end
Pu-240     22 0  6.6258E-07 1200          end
Pu-241     22 0  9.3451E-07 1200          end
 Pu-242     22 0  2.4145E-07 1200          end
 Am-241     22 0  2.6070E-08 1200          end
 Am-242     22 0  6.9754E-11 1200          end
 Am-243     22 0  4.9165E-08 1200          end
 Cm-242     22 0  8.8262E-09 1200          end
 Cm-243     22 0  1.9221E-10 1200          end
 Cm-244     22 0  1.4647E-08 1200          end
 'reflector block graphite
       c-graphite   23 0 9.2756E-2 1200          end
```

```
b-10        23 0 2.7600E-8 1200              end
end comp

read param
       gen=600 npg=50000 nsk=60
       xs1=yes  fdn=yes flx=yes
end param

read celldata
doublehet  right              _bdy=white                fuelmix=18 end
gfr=0.02125          1     coatr=0.03125    2       coatr=0.03525       3      coatr=0.03875 4          coatr=0.04275          5
matrix=6                     vf=0.35 end grain
rod triangpitch right_        bdy=white                        hpitch=0.9398    11          fuelr=0.6225
gapr=0.6350          10      fuelh=4.928          end

centrm data
ixprt=1 isn=32 nprt=2
end centrm
moredata
szf=0.40
end moredata
end celldata

read geom
global unit 4000
        rhexprism 40 54.0   4.9280 0.0
      '   media 4 1 40
        array 1  40  place 3 3 1   3*0.0
        boundary 40

unit 1000
rhexprism 10   18.0     4.928  0.0
array 2  10  place 13 13 1  0.0  0.0  0.0
boundary   10
unit  2
‘com='large helium coolant channel'
cylinder 10 0.7940      4.928  0.0
hexprism 20 0.9398      4.928  0.0
media 15 1 10
media 16 1 20 -10
boundary 20
unit   3
com='small helium coolant channel'
cylinder 10 0.6350      4.928  0.0
hexprism 20 0.9398      4.928  0.0
```

```
media 15 1 10
media 16 1 20 -10
boundary 20
unit  4
com='graphite block'
hexprism 10 0.9398     4.928  0.0
media 16 1 10
boundary 10
unit  5
com='graphite block'
hexprism 10 0.9398     4.928  0.0
media 0 1 10
boundary 10
unit  6
com='BURNABLE POISON'
cylinder 10  0.5715     4.928  0.0
media 38 1 10
hexprism  20  0.9398     4.928  0.0
media 37 1 20 -10
boundary 20
unit 7
cylinder 10  0.6225   4.928  0.0
media 18 1 10
cylinder 20 0.6350    4.928  0.0
media 10 1 20 -10
hexprism  30  0.9398  4.928  0.0
media 11 1 30 -20
boundary 30
unit  2000
com='EMPTY CELL'
rhexprism 20 18 4.9280 0.0
media 0 1 20
boundary 20
unit  3000
rhexprism 30 18 4.9280 0.0
media 23 1 30
boundary 30
unit  5000
rhexprism 10   18.0     4.928  0.0
media  22 1 10
boundary   10
end geom

read bnds
        body=40
```

```
        all=mirror
end bnds

read ara
     ara=1      typ=rhexagonal    nux=5      nuy=5      nuz=1     fill
         2000 5000 5000 5000 2000
         2000 5000 5000 5000 5000
         3000 3000 1000 3000 5000
         2000 3000 3000 3000 2000
         2000 2000 2000 2000 2000
End fill
ara=2          typ=shexagonal          nux=25          nuy=25          nuz=1          fill
       5 5 5 5 5 5 4 4 4 4 4 4 4 4 4 4 4 4 4 5 5 5 5 5 5
        5 5 5 5 5 4 4 4 4 4 4 4 4 4 4 4 4 4 4 4 5 5 5 5 5
       5 5 5 5 5 4 4 6 7 2 7 7 2 7 7 2 7 6 4 4 5 5 5 5 5
        5 5 5 5 4 4 7 2 7 7 2 7 7 2 7 7 2 7 4 4 5 5 5 5 5
       5 5 5 5 4 4 2 7 7 2 7 7 2 7 7 2 7 7 2 4 4 5 5 5 5
        5 5 5 4 4 7 7 2 7 7 2 7 7 2 7 7 2 7 7 4 4 5 5 5 5
       5 5 5 4 4 7 2 7 7 2 7 7 2 7 7 2 7 7 2 7 4 4 5 5 5
        5 5 4 4 2 7 7 2 7 7 2 7 7 2 7 7 2 7 7 2 4 4 5 5 5
       5 5 4 4 7 7 2 7 7 2 7 7 2 7 7 2 7 7 2 7 7 4 4 5 5
        5 4 4 7 2 7 7 2 7 7 2 7 7 2 7 7 2 7 7 2 7 4 4 5 5
       5 4 4 2 7 7 2 7 7 2 7 7 3 7 7 2 7 7 2 7 7 2 4 4 5
        4 4 7 7 2 7 7 2 7 7 3 4 4 3 7 7 2 7 7 2 7 7 4 4 5
       4 4 6 2 7 7 2 7 7 2 7 4 4 4 7 2 7 7 2 7 7 2 6 4 4
        4 4 7 7 2 7 7 2 7 7 3 4 4 3 7 7 2 7 7 2 7 7 4 4 5
       5 4 4 2 7 7 2 7 7 2 7 7 3 7 7 2 7 7 2 7 7 2 4 4 5
        5 4 4 7 2 7 7 2 7 7 2 7 7 2 7 7 2 7 7 2 7 4 4 5 5
       5 5 4 4 7 7 2 7 7 2 7 7 2 7 7 2 7 7 2 7 7 4 4 5 5
        5 5 4 4 2 7 7 2 7 7 2 7 7 2 7 7 2 7 7 2 4 4 5 5 5
       5 5 5 4 4 7 2 7 7 2 7 7 2 7 7 2 7 7 2 7 4 4 5 5 5
        5 5 5 4 4 7 7 2 7 7 2 7 7 2 7 7 2 7 7 4 4 5 5 5 5
       5 5 5 5 4 4 2 7 7 2 7 7 2 7 7 2 7 7 2 4 4 5 5 5 5
        5 5 5 5 4 4 7 2 7 7 2 7 7 2 7 7 2 7 4 4 5 5 5 5 5
       5 5 5 5 5 4 4 6 7 2 7 7 2 7 7 2 7 6 4 4 5 5 5 5 5
        5 5 5 5 5 4 4 4 4 4 4 4 4 4 4 4 4 4 5 5 5 5 5 5 5
       5 5 5 5 5 5 4 4 4 4 4 4 4 4 4 4 4 4 5 5 5 5 5 5 5
end fill
end ara
end data
end
```